Performance Evaluation of Nanofluid (Al_2O_3-H_2O & Al_2O_3-H_2O, ethylene glycol) Based Parabolic Concentrating Solar Collector

Thesis submitted in partial fulfillment of the requirements for

the award of degree of

Master of Engineering

in

Thermal Engineering

Submitted By

Ketan Ajay

(Roll No. 801383015)

Under the supervision of

Mr. Kundan Lal

(Assistant Professor)

(MED, Thapar University)

DEPARTMENT OF MECHANICAL ENGINEERING

THAPAR UNIVERSITY

PATIALA – 147004

July, 2015

CERTIFICATION

I, Ketan Ajay, declare that this thesis report entitled ***"Performance evaluation of nanofluid (Al_2O_3-H_2O & Al_2O_3-H_2O, ethylene glycol) based parabolic concentrating solar collector"***. Submitted towards fulfillment of the requirements for the award of Master's Degree in Thermal Engineering, in Mechanical Engineering Department of Thapar University, Patiala, is entirely my own work. This document has not been submitted for any degree in any other institution

Date 14/July/2015
Place Patiala

Ketan Ajay
801383015
Thapar University, Patiala

This is to certify that above statement made by the candidate is correct and true to the best of my knowledge.

Mr. Kundan Lal
(Assistant Professor)
Mechanical Engineering Department
Thapar University, Patiala

Countersigned by

Dr. S.K. Mohapatra
Sr. Professor and Head
Mechanical Engineering Department
Thapar University, Patiala

Dr. S.S. Bhatia
Dean of Academic Affairs
Thapar University, Patiala

AKNOWLEDGEMENT

First of all, I am extremely thankful to my respective guide ***Mr Kundan Lal***, Assistant professor, Mechanical engineering department, Thapar University for his valuable guidance, advice, motivation and positive attitude with which he solved my queries and provide delightful ambiance for learning, exploring and making this thesis possible. It has been a great pleasure and experience to work under his sanctuary.

I am heartily thankful to ***Dr. S.K Mohapatra***, Sr. Professor and Head, Mechanical Engineering department for motivation. I am also extremely thankful to ***Dr. Bonamali Pal***, Professor and Head, School of chemistry and biochemistry, and ***Dr. S.S. Mallick***, Assistant professor, Mechanical engineering department for providing me facility for the completion of my research work.

I would also like to thank my family members who are dearest and precious to me for their love, encouragement, blessings and support in all respects.

Ketan Ajay

ABSTRACT

Solar collectors are efficient devices to trap the immense solar energy. Efficiency of such collector is highly dependent upon, nature of working fluid, intensity of solar energy, design and material of the collector and reflector. Nanoscience application plays a major role in heat transfer related problem. In this proposed thesis work, an attempt has been made to enhance the collector's performance by altering the working fluid, through suspension of the fine sized nanomaterials in the base fluid. α-Al_2O_3 nanoparticle of 20 nm average size is used. Two different base fluid of H_2O (DI) and mixture of $C_2H_6O_2$- H_2O (DI) (40:60 by volume) are used. Four different volumetric concentrations (0.05%, 0.075%, 0.1% and 0.125%) of nanofluid are prepared. Working fluid is made to flow at three different volume flow rate (30 LPH, 50 LPH and 80 LPH. Effect of different working fluid and of different flow rate on collector's overall efficiency is studied through both experimental and CFD analysis. CFD analysis is carried out using ANSYS FLUENT 14.5. Solar flux is modeled using solar load cell and solar ray tracing. Three dimensional temperature contours is obtained and thus outlet temperature is recorded from within. It has been observed that there is improvement in instantaneous efficiency, thermal efficiency and in overall efficiency, when nanofluid is replaced by the water. Also an improvement of about 9.31%, 11.87%, and 13.98% in the collector's overall efficiency is seen, when alumina – water nanofluid of 0.125% vol. conc. is used as compared to water at a flow rate of 30 LPH, 50 LPH and 80 LPH respectively. While, when water-ethylene glycol mixture is replaced by 0.125% vol. conc. Al_2O_3- $C_2H_6O_2$- H_2O (DI) nanofluid, an improvement of about 14.9%, 15.81% and 16.7% is reported at 30 LPH, 50 LPH and 80 LPH respectively. Enhancement in the performance of the collector is seen, when mass flow rate of working fluid is made to increase. It is also observed that, collector's efficiency is higher with water-based nanofluid as compared with ethylene glycol-water mixture based nanofluid of same volumetric conc. Also, there is a close agreement between both experimental and simulated results with a maximum difference of about 11%.

TABLE OF CONTENTS

LIST OF FIGURES

LIST OF TABLES

NOMENCLATURE

Symbols

$A_{aper.}$	Aperture area, m^2
Al_2O_3	Alumina
Al	Aluminium
C_r	Concentration ratio
C_p	Specific heat J/kg-K
C_{pnf}	Specific heat of nanofluid, J/kg-K
C_{bf}	Specific heat of base fluid, J/kg-K
C_{np}	Specific heat of nanoparticle, J/kg-K
CuO	Copper oxide
D_i	Inner diameter of receiver tube, m
D_o	Outer diameter of receiver tube, m
D_{ci}	Inner diameter of glass cover
D_{co}	Outer diameter of glass cover, m
f_v	Volume fraction of nanoparticles in percentage
G_t	Global solar intensity, W/m^2
h_f	Convective heat transfer coefficient, W/m^2-K
k	Thermal conductivity, W/m-K
k_{nf}	Thermal conductivity of nanofluid, W/m-K
k_{bf}	Thermal conductivity of base fluid, W/m-K
k_{np}	Thermal conductivity of nanoparticles, W/m-K
L	Length of collector, m
$\dot{m}$	Mass flow rate, kg/sec
m	Mass.kg
ppm	Parts per million
q_u	Useful heat gain, W
R_b	Bond resistance
R_e	Reynolds number
S	Absorbed heat flux, W/m^2
SiO_2	Silicon dioxide

TiO_2	Titanium oxide
T_m	Mean temperature, ^oC
T_a	Ambient temperature, ^oC
T_{out}	Outlet temperature, ^oC
T_{in}	Inlet temperature, ^oC
T_{max}	Maximum temperature, ^oC
T_{min}	Minimum temperature, ^oC
T_{min}	Minimum temperature,
U_l	Overall los coefficient, W/m^2-K
V_{bf}	Volume of base fluid, m^3
V_{np}	Volume of nanoparticle, m^3
V_{nf}	Volume of nanofluid, m^3
W	Width of collector, m
W_{nf}	Weight of nanofluid, gm
W_{np}	Weight of nanoparticle, gm

Greek symbols

α	Absorptivity of absorber tube
τ	Transmissivity of glass cover of absorber tube
β	Specular reflectivity of concentrated
υ	Kinematic viscosity, m^2/s
μ	Dynamic viscosity, $N\text{-}s/m^2$
μ_{nf}	Dynamic viscosity of nanofluid, $N\text{-}s/m^2$
μ_{bf}	Dynamic viscosity of base fluid, $N\text{-}s/m^2$
ρ	Density, kg/m^3
ρ_{nf}	Density of nanofluid, kg/m^3
P_{bf}	Density of base fluid, kg/m^3
η_{ov}	Overall efficiency
η_{th}	Thermal efficiency
η_i	Instantaneous efficiency
η_{opt}	Optical efficiency

Subscripts

a	Ambient
aper	Aperture
avg	Average
bf	Base fluid
ci	Inner glass cover
co	Outer glass cover
in	Inlet
i	Instantaneous
max	Maximum
min	Minimum
m	Mean
nf	Nanofluid
np	Nanoparticle
out	Outlet
ov	Overall
opt	Optical
r	ratio
v	volume
t	total
th	thermal
u	useful

Abbreviation

BTU	British thermal unit
CSP	Concentrated solar power
CFD	Computational fluid dynamic
CNT	Carbon nanotube
DASC	Direct absorption solar collector
FPSC	Flat plate solar collector
FDM	Finite difference method

HCE	Heat collector element
HTF	Heat transfer fluid
LPH	Liters per hour
MWCNT	Multi wall carbon nanotube
NCSWHS	Nanofluid based concentrating solar water heating systems
PSC	Parabolic solar collector
PVT	Photovoltaic thermal
PTC	Parabolic trough collector
SEM	Scanning electron microscopy
SDS	Sodium dodecyl sulphate
SWCNH	Single wall carbon nanohorns
TEM	Transmission electron microscopy
XRD	X-ray diffraction

CHAPTER-1

INTRODUCTION

1.1 Solar Energy

In this rapid era of modernization and development global warming has become a major threat today. An efficient and effective means have to be sorted out to tackle such hazardous issue which is mainly induced by CO_2, which comes as by- product in a smoke from coal, oil and other conventional fuel fired thermal power plants [1]. Now there is a desire need to find alternative solution which is first of all eco-friendly and is also everlasting. Solar energy is one of the alternative solution. Various types of renewable energy have discovered from time to time like solar energy, wind energy, tidal energy, geothermal energy, ocean thermal energy [2]. The most competent advantage of renewable energy is that they are eco-friendly. In today's era the renewable energy is gaining importance because through them the concept of sustainable development is achieved. Usage of renewable energies is expected to increase at a much higher rate because of following main reasons [3]:

a) World's energy demand is increasing at a much higher rate, due to which conventional fuel reserves are depleting.
b) Due to deteriorating climate conditions.

It has been estimated that earth's upper atmosphere is incident by large amount of solar radiation of value amounting to 174 PW (1PW=1015 W) by the sun.[4] The proficient and the proper utilization of solar energy is progressively more being considered to be the appropriate resolution to solve the comprehensive issue of global warming. Moreover by using the solar energy the concept of sustainable development is also achieved. When this solar energy comes to the earth's surface from the sun it is attenuated by two different causes [5]:

a) Due to earth's atmosphere (6 % by reflection and 16% by the absorption) and
b) Due to clouds (20% by reflection and 3% by absorption).

The energy at rate of 3.8×10^{23} KW is released by the sun, of which only 1.8×10^{14} KW is intercepted by the earth which accounts to 60% of total delivered the sun, as some

of radiations are reflected back into the space and are absorbed by the sun before being coming to earth surface[4]. It has also been discovered that there will be a generation of energy which is 4 times of world's total present generating capacity (about 3000 GW), if 0.1% of energy received at earth surface is converted at an efficiency of 10% [6]. It has also been realized that, with the present rate of energy utilization, reserves of conventional fuels like coal, oil etc will deplete within next two-three decade, besides this the environment will be extensively polluted due to the harmful emissions such as carbon dioxide, nitrogen oxides and other different harmful toxic gases which are released upon their burning.

Solar thermal energy is one of the efficient and very apposite source for heating purposes, using various types of solar energy tapping devices like flat plate solar collectors, concentrating solar collectors and others. The main application of solar energy is for both heating and cooling systems. Solar thermal collector devices are basically used to convert the solar energy to the internal energy of the working fluid flowing in the absorber tube of such collectors. They are also called as heat exchangers. There are basically two of solar collectors: a) concentrating solar collector and b) non concentrating solar collectors

There are basically two typical categories of solar devices, namely a) photovoltaic and b) concentrated solar power (CSP), which utilize solar energy to produce efficient power. Photovoltaic technology is based on photovoltaic effect which includes the solar cells, which tap the solar energy which is incident over a solar panel and electric current is generated. Concentrated solar power employs different method for producing power from the solar energy.

1.2 Solar Collectors

A solar energy is basically a heat exchanger that converts the solar radiation incident over the HCE of the solar collector (heat exchanger) into the thermal energy of the working fluid flowing inside the HCE, which in turn is used for producing power. There are various types of solar collectors available to tap the solar energy. They are basically classified on the basis of maximum possible obtainable temperature in the receiver tube, on this basis the solar collectors are grouped in three categories of low, medium and high temperatures [7]. Widely solar collectors are basically categorized as: a) Non- concentrating collectors e.g.: flat plate collectors, hybrid PVT collectors,

Bifacial collectors and b) Concentrating collectors e.g.: heliostat field collectors, parabolic shaped concentrating collectors, parabolic dish collectors.

1.2.1 Non-concentrating solar collector

Non-concentrating solar collector are those type of solar collector which do not have a concentrator. The sun is directly made to fall over the small area of the absorber. Flat plate solar collector is an example of this type of solar collector which is depicted in the figure 1.1. Flat plate collector is normally fixed so they should be properly installed. This type of collector does not have tracking mechanism.

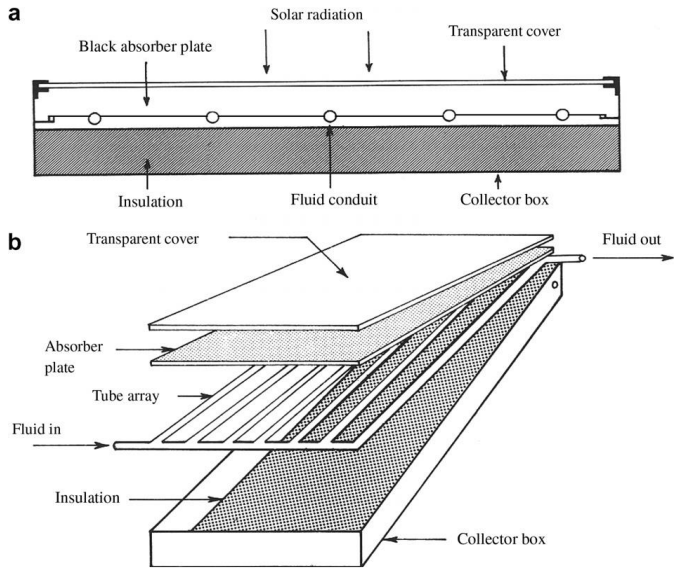

Figure 1.1 pictorial view of flat plate solar collector including components: a) cross-sectional view and b) top view [7]

They basically comprises of a absorber tube which is black coated, glass covers, insulation layer, recuperating tubes carrying the working fluid with them and other required auxiliaries [8]. The solar energy is made incident over the absorber tube which is mainly made up of copper. Glass cover is provided over the top, in order to avoid re-radiation losses. Normally water or other heat transfer fluid is made to circulate within the absorber tube. Max possible temperature obtainable with water as working fluid is up to 100^{o}C. This type of collector is widely used for heating and cooling purpose.

1.2.2 Concentrating solar collector

Solar concentrator is basically a device which concentrates the solar energy onto a smaller surface i.e. absorber tube. Parabolic shaped concentrating solar collector depicted in figure 1.2. The concentration of solar rays is basically done through the usage of suitable refracting elements, which in turns helps in increasing the flux density on the absorber tube. This type of solar collector is capable of producing higher receiver outlet temperature above 350^{o}C.

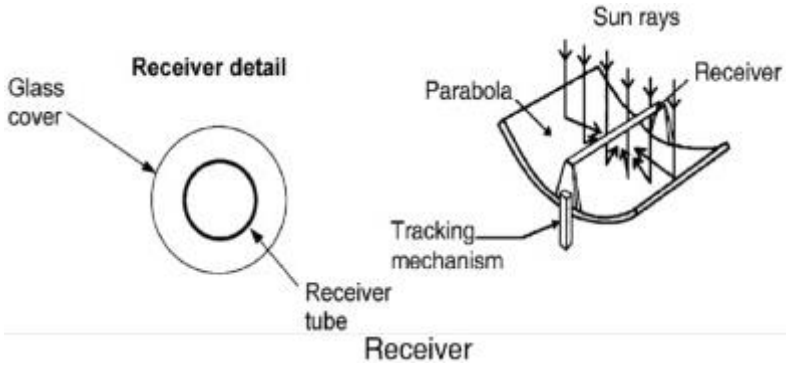

Figure 1.2 Parabolic shaped concentrating solar collector [9].

There is a need of proper tracking mechanism. They are widely used for power generation purposes. Various types of concentrating solar collector are: heliostat field collectors, parabolic shaped concentrating collectors, parabolic dish collectors [9]. However, concentrating solar collector is basically an optical system and hence optical loss terms become quite significant.

1.3 Nanofluid as Working Fluid in Solar Collector

Heat transfer plays a major role in industrial and consumer products. Great problem is faced in heat transfer because of inherent poor thermal conductivity of the fluids. Much advancement has taken place in this era. Starting with dispersion of millimeter or micrometer sized particles in liquids, but major problem of settling of these particles is witnessed. Latest advancement in the field of heat transfer related problems is the usage of nanofluids. The concept and emergence of nanofluids is directly related to trends in miniaturization and nanotechnology [10].

Nanofluid is basically a suspension of fine sized Nanomaterials of size ranging from 1 nm to 100 nm in base fluid like water, ethylene glycol and others [11]. Nanomaterials

of gold, silver, copper, silicon, aluminum and their corresponding oxides are used. Nanofluids are potential heat transfer fluids which have improved thermophysical properties like thermal conductivity, specific heat, dynamic viscosity and density [12].

The usage of nanofluids in the devices like solar collectors as main working medium is very innovative thought. Nanofluid posses high absorption capacity in solar range while in infrared range their emissivity is very low. Besides this nanofluid provides following mention advantages when used in solar based power plants [13]:

a) Nanofluids absorbs heat energy directly, thus avoids intermediate heat transfer steps.
b) Uniform temperature is achieved inside the absorber tube of the solar collector.
c) Enhancement of heat transfer is achieved due to its high thermal conductivity and better heat transfer coefficient as compared with normal working fluid, which in turns improves system efficiency.

Usage of nanofluids as a direct absorption solar collector (DASC) leads to the following main advantages [14]:

a) Variability of the size, shape, material type and volume concentration of the nanoparticles allows for tuning to maximize the spectral absorption of solar energy during the fluid volume.
b) There is improvement in the efficiency of the solar collector, due to enhancement in the thermal conductivity of the fluid.
c) There is an improvement in the surface area due to small size of the particle, which in turns make nanofluid based solar collector attractive for thermo-chemical and photo-catalytic related processes.

1.3.1 Application of nanofluids

As already highlighted that nanofluid is topic of interest and extensive research has been taking place to roll out the possible application of nanofluids due to its improved thermophysical properties. Main application of nanofluids is depicted below [15]:

a) Heat transfer related applications (industrial cooling, nuclear reactors, smart fluids)

b) Automotive applications (nanofluid coolant, nanoparticles in vehicular oils and fuels)
c) Electronic applications (microchip cooling, micro-scale fluidic applications)
d) Biomedical applications (nano-drug delivery, cancer therapeutics, nano-cryosurgery, sensing and imaging, cryopreservation)

1.3.2 Challenges of nanofluids [12]:

a) High cost of Nanomaterials
b) Difficulty in production process
c) Lower specific heat than base fluids
d) Higher viscosity
e) Settling and stability problem
f) Increased pressure drop and pumping power.

1.4 Computational Fluid Dynamics (CFD)

Computational fluid dynamics (CFD) is the computer based simulation technique used for the analysis of system involving fluid flow, heat transfer and chemical reactions. It is widely used simulation technique used for both industrial non-industrial areas of applications such as:

a) Hydrodynamics of ships
b) Power plants
c) Combustion in IC engine
d) Aerodynamic of vehicle and aero craft
e) Turbo-machinery appliances
f) Environmental engineering
g) Hydrology and oceanography
h) Electrical and electronics equipment
i) Biomedical engineering application
j) Environmental engineering

1.4.1 CFD methodology

For the carrying out the CFD simulation, three main elements are involved: a) pre-processor, b) solver and c) post-processor

A. Pre-processor

Various operations involved with pre-processor are:

a) Geometry generation
b) Grid generation (meshing)
c) Selection of physical and chemical model as required
d) Selection of fluid properties or material selection
e) Definition of appropriate boundary condition

B. Solver

When various physical model, material properties and boundary conditions are applied to the meshed geometry, then solver processor is used to solve various governing equation of mass, momentum, energy etc, in order to carry out simulation. Solver performs following basic steps:

a) With the help of simpler functions, unknown flow variables are approximated
b) Approximated simpler functions are then discretized into governing flow equations, with the help of substitution and mathematical manipulations.
c) Solution of the algebraic equation formed is calculated

Generally three techniques are available for discretization such as finite difference method, finite element method and finite volume method.

C. Post-processor

Post processor is used for the display of simulated results. Post processor of CFD codes is available with following different tools:

a) Mesh and geometry display
b) Vector plots
c) Scalar plots
d) Streamline

CHAPTER 2

LITERATURE REVIEW

The literature review shows the detailed discussion about the application of nanofluid in solar collector and various design consideration in solar collectors. Nanofluid exhibits a great potential and a wider scope when applied in a heat transfer related problems. Firstly, literatures based on solar collectors, along with the effect of various parameters like mass flow rate, temperature difference, solar intensity, ambient conditions and design consideration of collector, material of absorber etc. affecting the performance of collector are reviewed. In the later part, the effect of usage of nanofluid like Al_2O_3-H_2O (DI), TiO_2-H_2O (DI), CuO-H_2O (DI),SiO_2-H_2O (DI), Carbon nanotube (CNT) and others as a working fluid in solar collector is highlighted with the help of both experimental and numerical analysis, in which the effect of variation in volume concentration, nanofluids and shape and size of nanoparticles on the thermal performance of collector is studied.

2.1 Research Investigations

Tyagi et al. (2009) [16], performed both experimental and the numerical investigation to evaluate the effect of various different parameters like size of nanoparticles, volume concentration, collector geometry on the performance of the low temperature nanofluid based direct absorption solar collector (DASC). Al_2O_3-H_2O nanofluid was used as a working fluid in solar collector. Different volume concentration ranging from 0.1% to 5 % was taken. From both numerical and experimental analysis it was seen that the efficiency of collector was enhanced with the usage of nanoparticles. It was also concluded that it is not beneficial to use high volume fraction of the nanoparticles, as the efficiency approximately remained constant for the volume fraction higher than 2%. From the nanoparticle size point of view, results showed that efficiency was improved with an increase in size of nanoparticles

Natarajan and Satish (2009) [17], carried out an experimental analysis to study the effect of using nanofluid as working fluid in a solar water heater. Comparison of heat transfer properties was drawn for both water based multiwall carbon nanotube

(MWCNTs) and water. Six different volume fraction of nanofluid were taken (0.2, 0.4, 0.6, 0.8, 1.0 and 1.2). Sodium dodecyl sulphate (SDS) was taken as surfactant for the preparation of nanofluid. Thermal conductivity of the fluids was measured using transient hot wire method. It was concluded that the measured thermal conductivity of nanofluid enhanced with an increase in volume concentration of nanofluid. For a volume concentration of 1% the thermal conductivity increased up to 41% as compared with water .It was also concluded that the efficiency of the solar collector will increase if nanofluids are used as a heat transfer fluid.

Khullar and Tyagi (2010) [18], performed both theoretical and the numerical investigation to roll out positive effects of using nanofluid as working fluid in parabolic shaped concentrating solar collector. Al_2O_3-H_2O nanofluid was used as a working fluid in solar collector. Finite difference method (FDM) was used to obtain the two dimensional temperature fields and thereafter the comparison of optical and thermal efficiencies, mean outlet temperature were drawn for both nanofluid and conventional working fluid like water. Both experimental and numerical analyses have shown that system performance will enhance on using nanofluid as a working fluid and also the absorption characteristics of the system were also enhanced. With the increase in the mass flow rate, increment in the system efficiency was also witnessed.

Otanicar et al. (2010) [19], conducted experimental and the theoretical investigation with different types of nanofluids like carbon nanotubes, graphite and silver, in order to study their effect on the system performance. It was concluded that with the addition of small traces of nanoparticles in a base fluid, leads to remarkable improvement in the efficiency of the solar collector. By using graphite nanoparticles having an average size of 30 nm, performance of the DASC was increased up to 3% as compared with conventional working fluid.

Saini et al. (2010) [20], performed an experiment with nanofluid of single wall carbon nanohorns (SWCNH) dispersed in water to investigate their thermal and optical characteristics in view of their use as working fluid in solar collector device. It was reported that their thermal conductivity was higher as compared with conventional water. Photonic properties of the fluid containing SWCNHs were also

improved too much extent which was confirmed by spectral transmission measurement.

Taylor et al. (2011a) [21], conducted experimental and theoretical investigation to evaluate the performance of nanofluid as working fluid in high flux solar collectors. The result showed that when nanofluid was used as a working fluid in solar collector, an improvement in efficiency of about 10% was seen. It was also reported that with the usage of graphite-therminol VP-1 nanofluid with a volume concentration of 0.01% an improvement in the efficiency was witnessed over conventional working fluid like water.

Taylor et al. (2011b) [22], theoretical and experimental analysis were carried to evaluate the optical characteristics of different nanoparticles like graphite, silver, copper, gold and aluminium suspended both in water and therminol VP-1, in order to chalk out their possible potential utility in direct absorption solar collector (DASC). Modelling techniques were used for the evaluation of optical properties of different nanoparticles. From the conducted research it was revealed that an approximately 95% of the incoming solar radiations were absorbed by the nanofluid (10 ppm) having a thickness greater than10 cm or equal to it.

Mercatelli et al. (2011) [23], experimental investigation was carried out to study both absorption and the scattering properties of carbon nanohorns nanoparticles dispersed in an aqueous solution of water for the usage as a working fluid in solar collector. The different morphologies of carbon nanohorns like: dahlia-like, bud-like, seed-like were taken during the investigation. Surfactant was also used for the preparation of sample. From the scattering results it was revealed that the only small portion of light (less than 5%) was scattered by the single walled carbon nanohorns-water based nanofluid. It means as high as 95% of the incoming solar radiations will be absorbed by the fluid, which in turns improves the system efficiency.

Han et al. (2011) [24], experimental analysis was carried out to evaluate the thermo-physical and optical properties of carbon black aqueous nanofluid used as a working fluid in the solar collector. Carbon black nanofluid was prepared by dispersion of pre-treated carbon black nanopowder in the aqueous solution of water. Four different volume concentration of the nanofluid were taken as 4.4%, 5,5%, 6.6% and 7.7% , while wavelength was varied from 200-2500μm. It was revealed that enhancement in

the photo-thermal properties were seen at high volume concentration. Also with an increment of the volume concentration of the nanofluid, an increment in shear stress, thus viscosity was also seen. But for the same volume concentration a decrement in the shear rate was witnesses with an increment of the temperature. Thermal conductivity of the nanofluid was also increased with an increase in volume concentration. Further it was finally concluded that with the usage of carbon black nanofluid an improvement in the absorption efficiency was also seen.

Saini et al. (2011) [25], experimental analysis was carried out to evaluate the potential usage of single walled carbon nanohorns (SWCNHs) particles suspended in the ethylene glycol as a base fluid for the application as working fluid flowing in the solar collector system. Optical characterization of the single walled carbon nanohorns (SWCNHs) was also presented. From the measured spectral transmission it was concluded that SWCNH has a very important role to play as they enhanced the photonic properties of the fluid, which leads to growth of light extinction level even with small volume concentrations.

Yousefi et al. (2012a) [26], experimental analysis was performed on a flat plate solar collector using Al_2O_3-H_2O nanofluid as a working fluid. Comparison was also drawn between conventional working fluid like water and Al_2O_3-H_2O nanofluid. Two different types of nanofluid consisting of surfactant (TritonX-100) and without surfactant were prepared. Two different volume concentration of nanofluid (0.2% and 0.4%) were used. Nanoparticle 15 nm as a average size was used. Three different mass flow rate of 1liter per min, 2 liter per min and 3 liter per min were taken. It was concluded that with the 0.2% volume concentration of nanofluid, the efficiency of solar was improved by 28.3% as compared with water. With the increment of mass flow rate an improvement in efficiency of solar collector was also witnessed.

Yousefi et al. (2012b) [27], carried out an experimental analysis on flat plate solar collector using multiwall carbon nanotubes-water (MWCNTs-H_2O) nanofluid as a working fluid. Two different types of nanofluid consisting of surfactant and without surfactant were prepared. TritonX-100 was used as a surfactant. Two different volume concentration of nanofluid (0.2% and 0.4%) were used. The average diameter of nanoparticles ranges from 10-30 nm. Three different mass flow rate of 1liter per min, 2 liter per min and 3 liter per min were taken. It was found out that the efficiency of

the solar collector was improved upon usage of nanofluid (without surfactant) as compared with conventional working fluid. With the increment of mass flow rate, collector efficiency was also improved.

Saidur et al. (2012) [28], experimental investigation was performed to evaluate the effect of usage of nanofluid as a working fluid in direct solar collector. Al_2O_3-H_2O nanofluid is used as working fluid. Different size of nanoparticle and different volume concentration of the nanofluid were used during the experimentation. It was found out that optical properties of the nanofluid were independent of the size of the nanoparticle. While linear relationship is developed between volume concentrations of Al_2O_3-H_2O (DI) and extinction coefficient. It was also seen that with the of application of nanofluid in solar collector as a working fluid, an improvement in the efficiency was observed due to improved optical and thermal properties.

Khullar et al. (2012a) [29], environmental impact of nanofluid based concentrating solar water heating system (NCSWHS) was carried out using experimental analysis. Possible application of nanofluid as a working fluid in NCSWHS was also presented. The performance of NCSWHS was found to be better than that of water based solar water heating system. Higher output in terms of greater outlet temperature of the working fluid was also seen with the usage of nanoparticle in base fluid of solar collector as compared with simple base fluid. From the environmental aspects, greater reduction in the CO_2 level and other green houses responsible for global warming was also seen with the usage of nanofluid as a main working fluid in solar collector system.

Khullar et al. (2012b) [30], performed theoretical investigation, to evaluate the effect of nanofluid based concentrating solar collector (NCSC) over conventional water based solar collector. Nanofluid of Al_2O_3-Therminol-VP-1 of volume concentration of 0.05% was used a working fluid in parabolic shaped concentrated solar collector. From the obtained result it was concluded that the efficiency of the solar collector was improved by 5-10% upon usage of nanofluid as a working fluid over simpler conventional fluid like water. It was also shown that potential of nanofluid to harness the solar energy was much higher as compared with conventional working fluid.

Chougule et al. (2012) [31], performed an experiment to evaluate the improvement in the performance of the solar water heat system involving nanofluid as a working over

conventional base fluid. Carbon nanotubes (CNT) of 10-12 nm average diameter was used for the nanofluid preparation. 0.15% volumetric concentration of fluid was taken. With the help of experiment performed on solar collector using CNT- H_2O nanofluid as a working fluid, it was found out that the greater improvement in the efficiency of the solar collector was observed, by using even a small fraction of CNT.

Chaji et al. (2013) [32], thermal efficiency of flat plate solar collector using TiO_2-H_2O nanofluid in flat plate solar collector (FPSC) was evaluated using experimental analysis. Nanofluid at three different mass flow rate of 36 liter per hour, 72 liters per hour and 108 liters per hour were used. Three different volumetric concentrations of the nanofluid (without surfactant) i.e. 0.1%, 0.2% and 0.3% were used. From the conducted experimental research it was found out that with an increment in the mass flow rate of the working fluid an improvement in the collector efficiency was seen which accounts to value of 15.7%. As, the volumetric concentration of the nanofluid was increased an enhancement in the collector efficiency was also seen but for a certain value of volumetric concentration and beyond that value of the volumetric concentration, very less or no change in the efficiency of the solar collector was witnessed.

Tiwari et al. (2013) [33], an overall comprehensive view was presented about the nanofluid's effect on the thermal performance and environmental impact of the flat plate solar collector using nanofluid as a working fluid. Nanoparticle of Al_2O_3 of an average diameter of 20-30nm was made to disperse in the water, for the formation of Al_2O_3-H_2O nanofluid. Experiment was carried on three different mass flow rate of the nanofluid of 30 LPH.60 LPH,90 LPH and 120 LPH. Four different volume concentration of the nanofluid was prepared such as 0.5%, 1%, 1.5% and 2% and used for the experimental analysis. It was found out that with an increment in the mass flow rate of the working fluid in the flat plate solar collector, an improvement in the efficiency of the solar collector was seen. Moreover at increased volume concentration of the nanofluid (dispersion of more nanoparticles) an enhancement in the efficiency of the solar collector was also seen It was found out that at an optimal volume concentration of 1.5% of Al_2O_3-H_2O nanofluid an improvement of about 31.64% in the efficiency of the solar collector was seen.

Maddah et al. (2013) [34], experimental investigation was performed to evaluate the effect on thermo-physical properties due to presence of silver and aluminium oxide nanoparticles in the base fluid of distilled water. Various thermo-physical properties such as thermal conductivity, viscosity and electrical conductivity were evaluated. Nominal diameter of 40 nm and 20 nm was taken for both Al_2O_3 nanoparticle and Ag nanoparticle respectively. Different volumetric concentrations of nanofluid from 0.25% to 5% were taken. It was found out that Increment in the viscosity and the thermal conductivity of the nanofluid was seen with an increase in the volume fraction of the nanofluid, and both electrical and thermal conductivity of the nanofluid showed an increment with an increase in the volume fraction of the nanofluid.

Akbari et al. (2011) [35], carried out computational fluid dynamics (CFD) analysis to evaluate the convection heat transfer from a horizontal tube using nanofluid (Al_2O_3-H_2O) as a working fluid. Nanofluid of volumetric concentrations less than 2% was used. Simulation was carried out for two different value of Reynolds no. (1050 and 1600). Nanofluid modelling in CFD was carried out using two different techniques: a) single phase modelling and b) two-phase modelling using three different schemes (volume of fluid, volume of mixture and eulerian). In order to solve the different governing partial differential equation, finite volume method was used. From the conducted CFD analysis, an identical behaviour of hydrodynamic field was obtained with both single phase modelling and two-phase modelling. Moreover all different schemes of two-phase modelling have shown an identical behaviour. Accurate result for the convective heat transfer was obtained with two-phase modelling as compared with single phase modelling. There was also an over-prediction of the value of enhanced convection heat transfer coefficient at certain points, when two phase model was applied.

Tarybakhsh et al. (2013) [36], computational fluid dynamics (CFD) investigation was carried to study the effect on convective heat transfer due to wall/ nanoparticle interaction (Brownian) motion in nanofluid. Al_2O_3 (alumina) nanoparticle was used for preparation of water base nanofluid. Tube of typical dimension of 0.2μm and 1μm in diameter and length respectively was subjected to constant temperature of 24^{o}C. Velocity of nanoparticle taken was 1m/s in x-direction, while in y-direction periodic motion was applied. Adiabatic wall of the nanoparticle was assumed. Transient solver was used for carrying out CFD simulation. Base fluid of Newtonian type having a

laminar flow was taken during the simulation. From the performed CFD simulation, it was seen that there will be significant improvement on the convective heat transfer coefficient of nanofluid, which was mainly due to associated Brownian motion of the nanoparticles suspended within the base fluid. Decrement in both boundary layer effect and hydrodynamic was also seen, due to motion of particle near the wall.

Yu and Xie (2011) [37], various preparation techniques for nanofluids like one step and two step method have been reviewed. They have highlighted that two step method is widely used for the preparation of the nanofluid, in which firstly the nanomaterial are made to disperse in the base fluid of water, ethylene glycol, Therminol VP-1 etc, and then they are made to mix in a base fluid with an application of magnetic forces followed by the sonication of the particles in the ultrasonicator. While in one step method, both production of nanomaterials and the dispersion of the nanomaterials in the base fluid takes place simultaneously. They remarked that the nanomaterial prepared by this method are highly stable and are easily dispersible in the base fluid. Stability issue of nanofluid, along the evaluating parameters for the stability judgment and remedial method to promote stability of the nanofluid was also highlighted. Lastly wider band of application areas of the nanofluid was highlighted such as electronic applications, industrial cooling systems. space and defense, enhancement of heat and mass transfer, solar absorption, energy storage biomedical applications, used in engine fuel, lubrication oil and as coolant.

Said et al. (2013) [38], experimental analysis of the thermophysical properties of the alumina nanoparticle based nanofluid was carried out. Two different types of base fluid such as water, water-ethylene glycol mixture (40:60 by mass) were used for the preparation of the nanofluid. Nanofluid of two different volumetric concentrations 0.5% and 1% were used. Experimental investigation was performed on flat plate solar collector using the nanofluid to study effect on pumping power due to, two main parameters of density and viscosity. Water based nanofluid was found to be more promising as compared with water-ethylene mixture base nanofluid, as lesser problem of sedimentation and aggregation were seen. Linear relationship was established between thermal conductivity and the volume concentration of the nanofluid for both two different base fluid (water and water-ethylene glycol mixture).While exponential decrement type of behaviour was obtained between viscosity of the nanofluid and temperature .

Pravin et al. (2014) [39], performance in terms of heat transfer through a direct absorption solar collector (DASC) and entropy generation due to forced convection mode of heat transfer was investigated using numerical simulation. Copper (Cu) nanoparticle was used for preparing copper oxide-water (Cu-H_2O) nanofluid. Finite element method with galerkins weighted averages was used for carrying out the numerical simulation. From the obtained numerical simulated results it was found out that increment in the value of mean nusselt no. and entropy generation was seen with an increase in the value of the both reynolds no. and volume of fraction of Cu nanoparticles. Finally it was also presented that there is increment in the forced convection heat transfer and reduction in the entropy generation was seen in direct absorption solar collector using Cu as a nanoparticle in the base fluid.

Zhongyang et al. (2014) [40], carried out numerical and experimental simulation of a nanofluid based direct absorption solar collector (DASC). Graphite nanoparticle was used to prepare the nanofluid. Close agreement was formed between both simulated and experimental results. An improvement in the outlet temperature of the fluid was seen when nanofluid was used as the working fluid as compared with conventional fluid like water, an improvement of about 30-100 K was witnessed, while efficiency of the system was improved by 2-25% when nanofluid is used as compared with water as a main working fluid. From the conducted simulation research,

Qinbo et al. (2014) [41], experiment was performed on a flat plate solar collector, employing Cu-H_2O as working fluid, in order to compare the efficiency of nanofluid based solar collector with a solar collector employing conventional fluid (water). Cu nanoparticle of 25 nm size was used. Two step method was used for the preparation of the nanofluid of two different concentrations (0.1% by wt. and 0.2% by wt.). Working fluid with a mass flow rate of 140 L/h was used. From the conducted experimental research, a great enhancement in the thermal conductivity of the nanofluid as a working fluid was seen, as compared with conventional working fluid like water. An enhancement of about 23.83% was seen when Cu-H_2O nanofluid (25 nm and 0.1% by wt.) was used as a working fluid. Moreover Cu- H_2O nanofluid (25 nm and 0.1% by wt) shows greater efficiency as compared with Cu- H_2O nanofluid (25 nm and 0.2% by wt).

Zamzamian et al. (2014) [42], experimental analysis of copper-ethylene (Cu-EG) nanofluid based flat plate solar collector was done to study the effect of dispersed (Cu) nanoparticles in a ethylene glycol base fluid on collector's efficiency. Cu nanoparticle of an average diameter of 10 nm was used. Two different fractions of nanofluid (0.2% by wt., 0.3%by wt.) were taken. Nanofluid was prepared with the help of one step method, where $NaH_2PO_2.H_2O$ was used for reducing $CuSO_4.5H_2O$ in a ethylene glycol based solvent. Two different mass flow rates (0.016kg/s and 0.050 kg/s) were taken during experimentation. It was indicated that as the wt. % concentration of nanofluid was increased, then increment in the collector efficiency was seen. At 0.3 wt% of Cu-EG nanofluid and at a mass flow rate of 1.5 liters per min. lowest removed energy parameter was achieved.

Alim et al. (2013) [43], both entropy generation and the pressure drop were calculated for nanofluid based flat plate solar collector. Different oxide nanoparticle (Al_2O_3, TiO_2, SiO_2, CuO) were made to disperse into the water, for the formation of the desired nanofluid to be used as a working fluid in flat plate solar collector. Nanofluid flow behaviour inside the fluid domain was assumed to be steady and laminar axial flow. Nanofluid of different volume fraction ranging from 1-4% was made to flow with a different mass flow rate ranging from 1-4 liters per min, with in the collector tube. From the conducted research, it was concluded that there was reduction in entropy generation and enhancement of heat transfer coefficient of 4.34% and 22.5% takes place respectively with $CuO\text{-}H_2O$ nanofluid as working fluid. Besides this, pumping power was also increased by 1.58% with same $CuO\text{-}H_2O$ nanofluid as main working fluid.

Moghadam et al. (2014) [44], an experimental analysis on the flat plate solar collector using copper oxide-water ($CuO\text{-}H_2O$) nanofluid was carried out. Copper-oxide nanoparticle (CuO) of an average size of 40 nm was used. Nanofluid of 0.4% volume of fraction at three different mass flows (1 kg/min, 2 kg/min and 3 kg/min) was made to flow inside an absorber tube. It was shown that at mass flow rate of 1kg/min, an improvement of about 21.8% in efficiency of solar collector was seen as compared with conventional fluid water. It was also concluded that there is an existence of an optimum mass flow rate for particular volume of fraction of nanofluid, at which maximum efficiency is achieved.

CHAPTER-3

GAP STUDY & OBECTIVES

3.1 Gap Study

- Performance of nanofluid based parabolic solar collector was mainly evaluated using theoretical and mathematical analysis, such theoretical analysis alone can't predict the actual performance of collector, as they are based upon certain assumptions. Therefore, experimental investigations are required to validate the results.
- CFD investigation of solar collector was carried out using simplified codes and boundary conditions, such as uniform heat flux and also there is no provision of tracking mechanism during simulation of absorber tube (HCE).

Based upon above depicted areas of concerns, it was decided to carry out both experimental and CFD analysis of a parabolic shaped concentrating solar collector employing nanofluid of different volumetric concentrations and base fluids at different volume flow rates.

3.2 Objectives

Main objective of this thesis is to conduct both experimental and computational fluid dynamics (CFD) analysis, in order to evaluate the performance of system consisting of parabolic shaped concentrating solar collector, using nanofluid as a working fluid with different volumetric concentration and different base fluid . System performance has to be evaluated at different volumetric mass flow rates. Following are the set objectives of the proposed thesis work.

1) To investigate experimentally and through computational fluid dynamics (CFD), the performance of solar collector (thermal efficiency and instantaneous efficiency) employing different working fluids :
    - H_2O (DI)
    - Al_2O_3-H_2O (DI) at three volumetric concentrations: 0.05%, 0.075%, 0.10% and 0.125%
    - H_2O-$C_2H_6O_2$ (60:40 by volume)

- Al_2O_3-$C_2H_6O_2$-H_2O(DI) at four different volumetric concentrations: 0.05%, 0.075%, 0.10% and 0.125%

2) To evaluate the effect on the performance of parabolic shaped concentrating solar collector at different mass flow rates (80 LPH, 50 LPH and 30 LPH) of working fluid using both experimental and CFD approach.
3) To compare the solar collector efficiencies for each different working fluid comprising of water, water based nanofluid, water-ethylene mixture and water-ethylene mixture based nanofluid.
4) To compare experimentally evaluated collector's performance with the CFD simulated collector's overall performance.

CHAPTER-4

EXPERIMENTAL METHODOLOGY

In this chapter the following topics are included:

a) Experimental setup and working procedure
b) Characterization of nanoparticles
c) Preparation of nanofluids
d) Theoretical modeling of thermo-physical properties of nanofluids
e) Experimentally measurement of thermophysical properties of nanofluids

4.1 Experimental Setup

Parabolic shaped concentrating solar collector is used for carrying out experimental work with nanofluid as working fluid which is depicted in figure 4.1. Main components of parabolic shaped concentrating solar collector includes: a) absorber tube with glass cover b) parabolic shaped reflector c) piping arrangement d) ball valve f) storage tank and g) temperature measuring device. Table 4.1 describes the specification of the parabolic trough concentrating solar collector. The storage tank is placed at the bottom of the receiver pipes level so that proper flow of the working fluid is regulated. Working fluids used are water, $C_2H_6O_2$-H_2O(DI) where $C_2H_6O_2$-H_2O(DI) is mixed in ratio of 40:60 by volume, Al_2O_3-H_2O (DI) nanofluid of four different concentration of 0.05%, 0.075%,0.1% and 0.125% and Al_2O_3-$C_2H_6O_2$-H_2O(DI) nanofluid of four different concentration of 0.05%, 0.075%, 0.1% and 0.125% ,where $C_2H_6O_2$-H_2O(DI) is mixed in ratio of 40:60 by volume. The test is conducted for each prepared working fluid at three different mass flow rates of 80 LPH, 50 LPH and 30 LPH. Recording of working fluid inlet and outlet temperatures, wind velocity and solar flux is done from 9.30 am to 2.30 pm with an interval of 30 min with each of working fluid at specified mass flow rates. Experiment is conducted outdoor in the month of April and May 2015.

Figure 4.1 Parabolic shaped concentrating solar collector

Table 4.1: Specifications of parabolic shaped concentrating solar collector

Parameter	**Value**
Collector length, L	1.20 m
Collector breadth, W	0.915 m
End plate thickness	2 mm
Aperture area, $A_{apper.}$	1.0188 m^3
Rim angle	90 degrees
Focal length	0.30 m
Receiver inside diameter (D_i)	0.027 m
Receiver outside diameter (D_o)	0.028m
Receiver length	1000 nm
Glass envelope inside diameter, (D_{ci})	0064 nm
Glass envelope outside diameter, (D_{co})	0.066 nm
Insulation on pipes	Aluminum foil, superlon
Concentration ratio, C_r	9.66

4.1.2 Components of parabolic shaped concentrating solar collector

Main component of parabolic shaped concentrating solar collector are as follows:

1. Absorber tube

Absorber tube is also called as the receiver tube which is depicted in the figure 4.2. It is made up of copper and is black coated from outside so as to absorb the maximum solar radiations. The working fluid (HTF) is made to flow inside the absorber tube, which on absorbing the solar energy enters the storage tank. Absorber tube is provided with glass cover in order to avoid re-radiation losses. The length of the absorber tube is 4 ft and inside and outside diameter of absorber tube are of 27 mm and 28 mm respectively. While typical dimension of glass tube is 3ft having inside and outside diameters of 64 mm and 66 mm respectively.

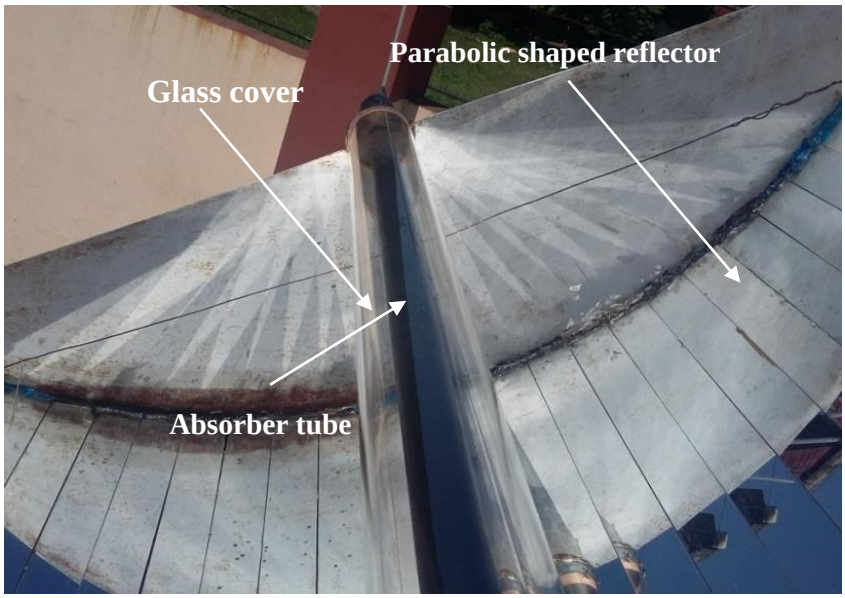

Figure 4.2 Parabolic reflector and absorber tube along with glass cover

2. Reflector

Typically parabolic shaped reflector which is made up of mirror strips is used which is shown in figure 4.2. Main purpose of the reflector is to concentrate the solar radiations over the absorber tube, which is normally place at the focal point of the parabola. Parabolic shaped reflector is made from a stainless steel having a dimension of 1.20 m × 0.90 m. The main purpose of using stainless steel is to provide the mechanical strength to the solar collector. Mirror strips having a reflectivity of 96% is place over the reflector sheet. Twenty six mirror strips of dimension 5 mm × 914.4 mm are pasted over the parabolic sheet with the help of adhesive paste. Figure 4.2, also shows the reflector concentrating the solar rays on the absorber tube.

3. Tracking Mechanism

Manual Tracking mechanism is employed in the parabolic shaped concentrating collector, which tracks the sun throughout the day i.e. from north to south. Manual tracking mechanism used is depicted in the figure 4.3. The bicycle hub is made to be inserted inside the welded cast iron structure which is provided with the handle. Clutch wire is also fitted into the hub with the help of the nut joint.

Figure 4.3 Tracking mechanism

4. Support structure

Support frame work of the parabolic shaped concentrating solar collector is made up of cast iron, as it provides the greater rigidity and has greater hardness and flexibility. The framework is coated with green paint in order prevent it from rust. Frame work used in the collector is shown in figure 4.4.

5. Piping arrangement with insulation cover

Plastic pipes of is used to circulate the fluid throughout the system starting from storage tank to the absorber tube and then finally back to the storage tank. Piping arrangement is also provided with insulation covering of superlon insulation and also with the aluminum foil, in order to the heat transfer losses from working fluid (HTF) which is depicted in figure 4.4.

6. Storage tank

Storage tank is basically a reservoir which stores the working fluid, and from it the working fluid (HTF) is made to circulate n the system with the help of pump provided in the storage tank. The plastic tank of 10 liters is used as a storage tank. Tank is well insulated from all sides with the help of insulting sheets in order avoid the heat transfer losses. Storage tank is also provided with the glass wool covering to avoid

any possibility of heat transfer. Storage tank and its associated insulation is shown in figure 4.4

Figure 4.4 Storage tank with insulation cover and insulating pipes

7. Control valve

Ball valve control is provided in the system in order to regulate the flow of the working fluid (HTF) as shown in figure 4.5. Three different flow rates of 80 LPH, 50LPH and 30 LPH are regulated by it.

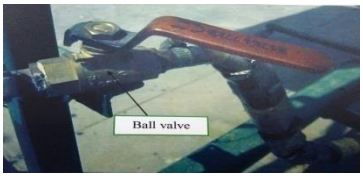

Figure 4.5: Ball valve

8. Pump

Submersible pump having a power of 18W and maximum flow rate of 1100 l/hr is used to circulate the working fluid in the solar collector system, which is depicted in the figure 4.6.

Figure 4.6 Submersible pump

4.1.3 Working procedure

The working fluid from the storage tank is circulated to the absorber tube by using submersible pump which is placed inside the storage tank. The volume flow rate is varied with the help of ball valve. In the receiver tube, working fluid absorbs heat and goes back to the storage tank. The working fluid is then re-circulated again. The readings of working fluid inlet and outlet temperatures, wind velocity and solar flux is done with the help of thermometer, anemometer and solar power meter respectively from 9.30 am to 2.30 pm with an interval of 30 min with each of working fluid at each specified mass flow rates of 80 LPH, 50 LPH and 30LPH. Collector is manually tracked from north to south throughout the experimental time.

4.1.4 Measuring instruments Used

1. Solar power meter

Solar power meter is used for the measurement of total solar flux which is incident over the collector area. Solar power meter used in experiment is shown in figure 4.7.

Figure 4.7 Solar power meter

2. Digital anemometer

The digital anemometer is used to measure the wind velocity in m/s or in km/hr. The anemometer used in the experiment is shown in figure 4.8.

Figure 4.8 Anemometer

4. Thermometer

Figure 4.9 shows the mercury-in glass thermometer used for measuring both inlet and out temperature of the working fluid flowing inside the absorber tube. The range of thermometer is from $0^{o}C$ to $100^{o}C$.

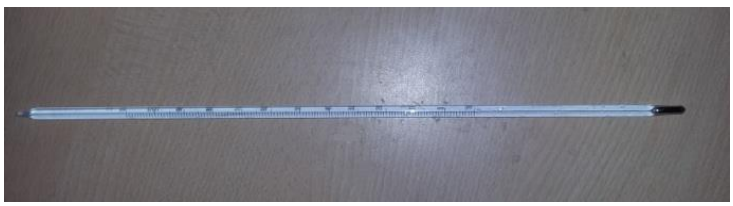

Figure 4.9 Mercury-in glass thermometer

4.2 Nanofluid Preparation

4.2.1 Properties of alumina (Al_2O_3) nanoparticle

Properties of the purchased alumina (Al_2O_3) nanoparticle are depicted in the table 4.2

Table 4.2 Physical properties of Al_2O_3 nanoparticle

Chemical name	Alumina Nanopowder
Particle size	20-30 nm
Particle shape	Spherical
Appearance	White
pH value	6.6
Density	3.97 gm/cm^3
Specific surface area	15-20 m^2/gm
Crystal form	Alpha
High purity	99%
Thermal conductivity of particle	36 W/ m-K
Special heat of particle	765 J/ kg-K

4.2.2 Nanofluid preparation techniques

There are basically two techniques which are used for preparation of nanofluid which are depicted as [36]:

1. **One step method:**. This method is very simple and is highly adaptive for the nanomaterials like copper, aluminum. Drying, storage, transportation and dispersion of the nanoparticle are avoided in this method, due to which the there is minimization in agglomeration of the nanoparticle.
2. **Two step method:** This technique makes use of both physical and chemical process for the production of the nanoparticle. Firstly nanoparticles are produced through various different methods and then they are made to disperse in an appropriate base fluid.

In the present technique two-step method is adopted for the preparation of the nanofluid.

4.2.3 Methodology adopted for preparation of nanofluid

- First of all the required amount (gm) of alumina (Al_2O_3) nanoparticle is calculated in order to make nanofluid of different volumetric concentration of 0.05%, 0.075%, 0.1% and 0.125% for each base fluid containing water and water-ethylene glycol water mixture having a ratio 60: 40 by volume respectively. Weight of nanoparticle is calculated with the help of below described formula:

$$f_v = V_{np} / V_{nf} \quad (4.1)$$

Where: $Vnp = W_{np} / \rho_{np}$ (4.2)

$V_{nf} = V_{np} + V_{bf}$ (4.3)

$V_{bf} = W_{bf} / \rho_{bf}$ (4.4)

Expression in a modified form is given as:

$$f_v = \frac{V_{np}}{V_{np}+V_{bf}} = \frac{W_{np}/\rho_{np}}{(W_{np}/\rho_{np})+ V_{nf}} \quad (4.5)$$

Where, V_{np} = quantity of nanoparticle

V_{bf} = quantity of base fluid

V_{nf} =quantity of nanofluid

W_{np}=weight of the nanoparticle

W_{bf} =weight of nanofluid

Quantity of base fluid (water or water-ethylene glycol mixture) = 7 liters

Density of alumina (Al_2O_3) nanoparticle, ρ_{np} =3.97 gm/cm^3

Calculated weight of nanoparticle for preparation of the nanofluid of different concentration is depicted in table 4.3.

Table 4.3 required amount of nanoparticle (grams)

Volumetric concentration %	Weight of nanoparticles (gms.) for 1 liter
0.05%	1.985
0.075%	2.9775
0.1%	3.970
0.125%	4.9625

- Then calculated amount (grams.) of the alumina nanoparticle is then weighted for each volumetric concentration of nanofluid using weighing machine.

- Weighted alumina nanoparticle for each volumetric concentration of 0.05%, 0.075%, 0.1% and 0.125% is mixed with water and water-ethylene glycol mixture (having a ratio of 60:40 ratio by volume respectively), for a preparation of nanofluid of desired base fluid.
- Sample prepared by above step is then made to stir for 30 minutes (for 1 liter) in a magnetic stirrer, as shown in figure 4.10

Figure 4.10 Magnetic stirrer

- Properly stirred sample is then placed in ultrasonicator bath as shown in figure 4.11. This process is called sonication of nanoparticles, where ultrasonics rays are made to traverse through the sample and a properly dispersion of nanoparticle takes place. Figure 4.12 shows the finally prepared samples which are ready for the usage as working fluid in parabolic shaped concentrating solar collector.

Figure 4.11 Ultrasonicator water bath

Figure 4.12 various prepared working fluid: (a) Distilled water, (b) 0.05% vol. conc. Al_2O_3-H_2O (DI), (c) 0.075% vol. conc. Al_2O_3-H_2O (DI), (d) 0.1% vol. conc.Al_2O_3-H_2O (DI), (e)) 0.125% vol. conc. Al_2O_3-H_2O, (f) H_2O-$C_2H_6O_2$ (60:40 by volume), (g) 0.05% vol. conc. Al_2O_3 –H_2O- $C_2H_6O_2$(60:40 by volume), (h) 0.075% vol. conc. Al_2O_3 –H_2O- $C_2H_6O_2$(60:40 by volume), (i)) 0.1% vol. conc. Al_2O_3 –H_2O- $C_2H_6O_2$(60:40 by volume) and (j) 0.125% vol. conc. Al_2O_3 –H_2O- $C_2H_6O_2$(60:40 by volume)

4.3 Theoretical Modelling for Thermophysical Properties of Nanofluid

1. Density of nanofluid [29]

$$\rho_{nf} = f_v\rho_{np} + (1 - f_v)\rho_{bf} \qquad (4.6)$$

Where ρn_p, ρ_{nf}, ρ_{bf}, are the density of nanoparticle (kg/m^3), density of nanofluid ($kg/m^{3)}$, density of base fluid (kg/m^3) respectively and f_v is the volume concentration of nanofluid.

2. Specific heat of nanofluid [26]

$$C_{nf} = \frac{f_v\,\rho_{nf} C_{np} + (1 - f_v)\rho_{bf} C_{bf}}{\rho_{nf}} \tag{4.7}$$

Where: C_{nf}, C_{np}, C_{bf} are the specific heat of the nanofluid, nanoparticle and base fluid respectively in J/kg-K.

3. Thermal conductivity of nanofluid [26]

$$K_{nf} = \left[\frac{K_{np} + 2K_{bf} + 2f_v(K_{np} - K_{bf})}{K_{np} + 2K_{bf} - F_v(K_{np} - K_{bf})}\right] K_{bf} \tag{4.8}$$

Where: K_{nf}, K_{bf}, K_{np} are the thermal conductivity of the nanofluid, base fluid and nanofluid respectively in the W/m-K.

4. Dynamic viscosity of nanofluid [29]

$$\mu_{nf} = \frac{\mu_{bf}}{(1 - f_v)^{2.5}} \tag{4.9}$$

Where: μ_{nf}, μ_{bf} are the dynamic viscosity of the nanofluid and base fluid respectively.

4.4 Experimentally Measurement of Thermophysical Properties of Nanofluid

1. Density measurement

Density of the nanofluid is measured through digital device called as density meter (DMA-35 of Anton Paar) as shown in figure 4.13. 2ml. sample is required.

Figure 4.13 Digital density meter

2. Thermal conductivity measurement

Thermal conductivity of the nanofluid of different volumetric concentration is measured through KD-2 Pro as shown in figure 4.14. KD-2 Pro is based on transient hot wire method. Sample of 15 ml is required for the measurement. Single needle sensor is used for the measurement of the thermal conductivity.

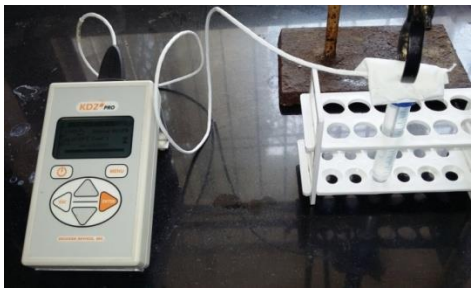

Figure 4.14 KD2 Pro

3. Dynamic viscosity measurement

Dynamic viscosity of the nanofluid is measure through Brookfield rheometer (Anton Paar) which is shown in figure 4.15. It consists of cope and cone shape like device and a spindle is dipped into the sample whose property is to be measured. Spindle is made to rotate and due to which the viscous drag is produced in the fluid against the spindle. The viscous drag is measured with the help of deflection produced within the calibrated spring.

Figure:4.15 Brokfield rheometer

4. Specific heat measurement

The specific heat of the nanofluid of various different volumetric concentrations and base fluid is measured with the help of KD-2 Pro which is shown in figure 4.14. It is based on transient hot line source method. Dual needle is used for the measurement of the specific heat.

CHAPTER 5

CFD METHODOLOGY

In order to carryout computational fluid dynamics simulation of the absorber tube following depicted methodology is adopted

5.1 Geometrical Modelling of Absorber Tube

First of all the 3 –D geometry of absorber tube (HCE), is drawn in geometry modeler of ANSYS FLUENT 14.5, which is depicted in figure 5.1. The desired model of the absorber tube consist of two concentric circle one for the heat collector element (fluid domain) in which working fluid is made to flow and other for the glass cover to evacuate the heat absorber tube. The absorber tube is split into two parts: a) upper part and b) lower part of the absorber tube facing the reflector. Upper part receives the incoming direct solar radiation, while lower half part is radiated by the concentrated heat flux from the parabolic shaped reflector.

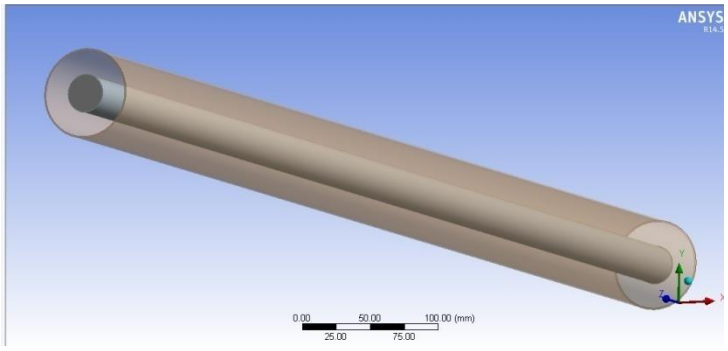

Figure 5.1 Geometry model of HCE (absorber tube)

5.2 Mesh Generation

In this section, discretization of the geometry is done over created 3-D geometry of the absorber tube which is shown in figure 5.2. Mesh of hexahedral shape of size 0.3 mm is applied over the 3-D geometry.

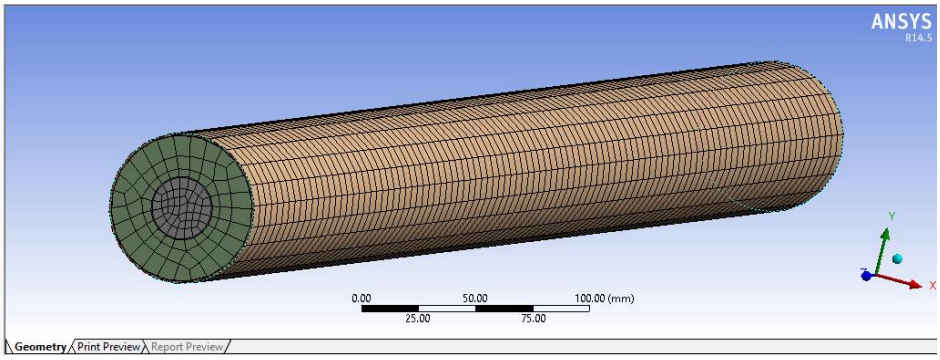

Figure 5.2 Meshed model of HCE (absorber tube)

5.3 Material Properties

Under this element of the CFD simulation, various thermo-physical properties of the material (solid and fluid) associated with CFD simulation of parabolic shaped concentrating solar collector are specified. Table depicted 5.1 below shows the various thermo-physical properties of material involved during CFD simulation.

Table 5.1 Thermophysical properties of various materials associated with HCE

Sample material	Density(kg/m^3)	Specific heat (J/kg/K)	Thermal conductivity (W/mK)	Viscosity (pa.s)
Water	1000	4187	0.667	4.06e-4
0.05% Al_2O_3-H_2O	1148.5	3595.5	0.766	4.615e-4
0.075% Al_2O_3-H_2O	1227.5	3353.7	0.819	4.933e-4
0.1% Al_2O_3-H_2O	1297	3139.556	0.876	05.283e-4
0.125% Al_2O_3-H_2O	1371.25	2948.59	0.935	5.668e-3
H_2O-$C_2H_6O_2$ (60:40 by vol.)	1057	3970	0.42	1.59e-3
0.05% % Al_2O_3-H_2O- $C_2H_6O_2$	1179.85	3103.625	0.546	1.148e-3
0.075% % Al_2O_3- H_2O-$C_2H_6O_2$	1253.75	3025.582	0.585	1.2273-3
0.1% % Al_2O_3-H_2O- $C_2H_6O_2$	1326.7	2842.75	0.625	1.314e-3
0.01% % Al_2O_3-H_2O- $C_2H_6O_2$	1400.175	2679.107	0.6696	1.4102e-3
glass	2200	910	1.75	-
Copper	8.954e3	380	386	-

5.4 Physical Modelling

Various physical models applied for carrying out CFD simulation of a parabolic shaped concentrating solar collector are as follows:

5.4.1 Flow Behavior model

Under this scheme of CFD, the behavior of the fluid under the conducted research is specified. From the calculated Reynolds no. for all different types of working fluid turbulence behavior of the fluid is seen. For turbulence modelling, standard k-ε model is used where k stand for energy associate with turbulence and ε (epsilon) stands for turbulent dissipation.

5.4.2 Energy model

Energy model is tuned on to visualize the heat transfer effects from the absorber tube. Through the energy model, temperature of the working fluid is specified and heat flux is specified for the wall boundary.

5.4.3 Radiation model

Surface to surface (S2S) radiation model is used to simulate the radiation heat transfer, which is arising in the closed set of the diffuse surfaces. In the S2S radiation model, the view-factors of the participating zone are calculated. Surface of the outer glass shield and absorber tube are taken into consideration during the calculation of shape factor.S2S radiation model assumes that the surfaces are grey and diffuse i.e. there is no dependency of the wavelength of the incoming radiation on the surface, and equality of absorptivity and the emmisivity of the surface is maintained, which is in accordance with the Kirchoff's law. In the conducted CFD simulation semi-transparent and opaque surfaces are considered for both glass cover and absorber surface respectively.

5.4.4 Solar load cell

Solar load cell is used for modelling the solar fluxes. In the solar load cell, value of latitude, longitude of the location and date & time of the experiment are specified. Values of the mesh orientation, i.e. negative z axis for the north and while for east positive x- axis is also specified in the solar calculator for the present research. On

substitution of all the required inputs in the solar collector, values for direct normal solar radiation on the ground diffuse solar radiation for both vertical and horizontal surface, ground reflected solar radiation for vertical surface and vector for sun direction are obtained. Solar ray tracing is also used.

5.5 Boundary Conditions and Governing Equations

Boundary conditions are applied, in order to solve the various governing equation so as to obtain the simulation results. Following depicted governing equation are involved with the conducted research:

a) Continuity equation

$$\frac{\partial \rho}{\partial t} + \frac{\partial (\rho u_j)}{\partial x_i} = 0 \tag{5.1}$$

b) Momentum equation:

$$\frac{\partial (\rho u_i)}{\partial t} + \frac{\partial (\rho u_i \rho u_j)}{\partial x_i} = \frac{\partial}{\partial x_j}\left[\rho \delta_{ij} + \mu\left(\frac{\partial u_i}{\partial x_j} + \frac{\partial u_j}{\partial x_i}\right)\right] + \rho g_i \tag{5.2}$$

c) Energy equation:

$$\frac{\partial (\rho C_p T)}{\partial t} + \frac{\partial (\rho u_i C_p T)}{\partial x_i} - \frac{\partial \left[\lambda \frac{\partial T}{\partial x_j}\right]}{\partial x_j} = S_T \tag{5.3}$$

d) Turbulence Kinetic energy equation:

$$\frac{\partial (\rho k)}{\partial t} + \frac{\partial (\rho k u_i)}{\partial x_i} = \frac{\partial y \left[\Gamma_k \frac{\partial k}{\partial x_j}\right]}{\partial x_j} + G_k - Y_k + S_k \tag{5.4}$$

Where, u_i is time averaged velocity vector, ρ is density of fluid, c_p is specific heat of fluid, T is temperature, δ_{ij} is kronecker delta function, G_k is generation of turbulence KE due to mean velocity gradients, Y_k represents contribution of fluctuating dilatation in compressible turbulence to overall dissipation rate. λ is bulk viscosity coefficient, x_i and x_j are spatial coordinate, k is thermal conductivity of the fluid, μ_t is eddy viscosity and $\Gamma_k = (\mu_t/\sigma_k)$ and S_k is transport of KE due to diffusion.

Various boundary condition applied to solve above depicted governing equation are given in table 5.2.

Table 5.2 various boundary conditions applied over a HCE

Zone	Boundary condition
Inlet	Mass flow rat inlet and fluid inlet temperature
Outlet	Out flow condition
Upper part of absorber tube	No slip condition and heat flux as modeled by S2S and solar load cell
Lower part of absorber tube facing the absorber tube	No slip condition and heat flux (concentrated by mirror reflector)

5.6 Numerical Methodology

Different governing equation of mass, momentum and energy are solved through the finite volume method using pressure based segregated spatially implicit solver which is available in the ANSYS FLUENT 14.5. Analysis is carried for a transient state Semi implicit pressure linked equations (SIMPLE) type of pressure correction approach is used for achieving the coupling between momentum and continuity equation, For solving the momentum and energy equation first order differencing scheme is used. Due to variation in density and presence of swirling type of flows, PRESTO! Scheme is used for interpolation of pressure. By keeping residual target as 10^{-4} for all governing equation (except for energy equation), the convergence criterion is monitored.

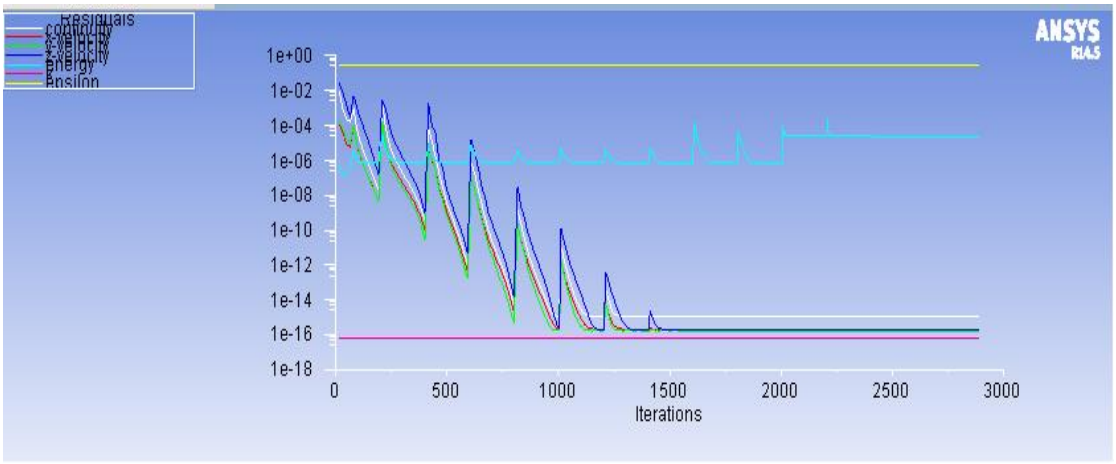

Figure 6.3 Residuals in various flow parameters with 0.125% vol. conc. Al_2O_3-H_2O(DI) nanofluid at 80 LPH

CHAPTER 6

RESULTS AND DISCUSSIONS

6.1 Computational Fluid Dynamics (CFD) Temperature Contours

Various temperature contours obtained within the absorber tube (HCE) for various working fluids (water, alumina-water based nanofluid of different volumetric concentrations, water-ethylene glycol mixture and alumina-water-ethylene glycol mixture based nanofluid) at time interval of 12-12.30 pm and at volume flow rate of 80 LPH is presented in figure 6.1-6.10. Temperature distribution for various working fluids is obtained through ANSYS fluent 14.5.

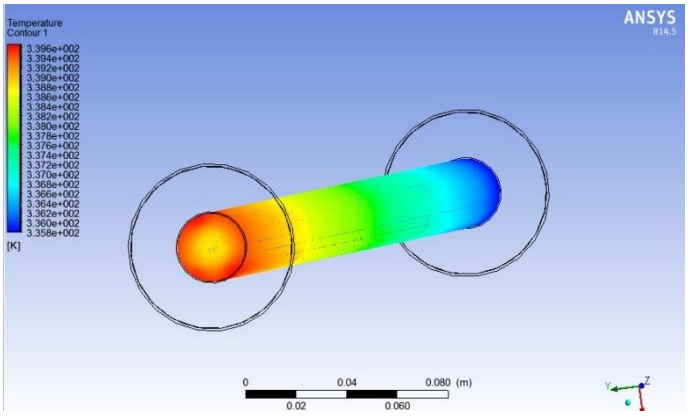

Figure 6.1 Temperature contour with water as a working fluid at 80 LPH

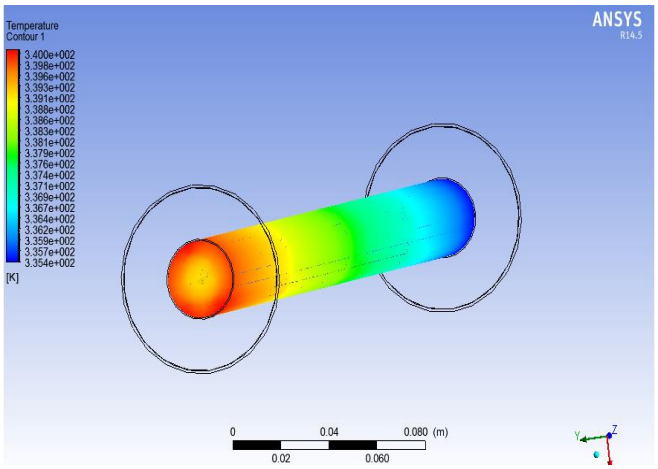

Figure 6.2 Temperature contour with 0.05% vol. conc. alumina-water nanofluid as a working fluid at 80 LPH

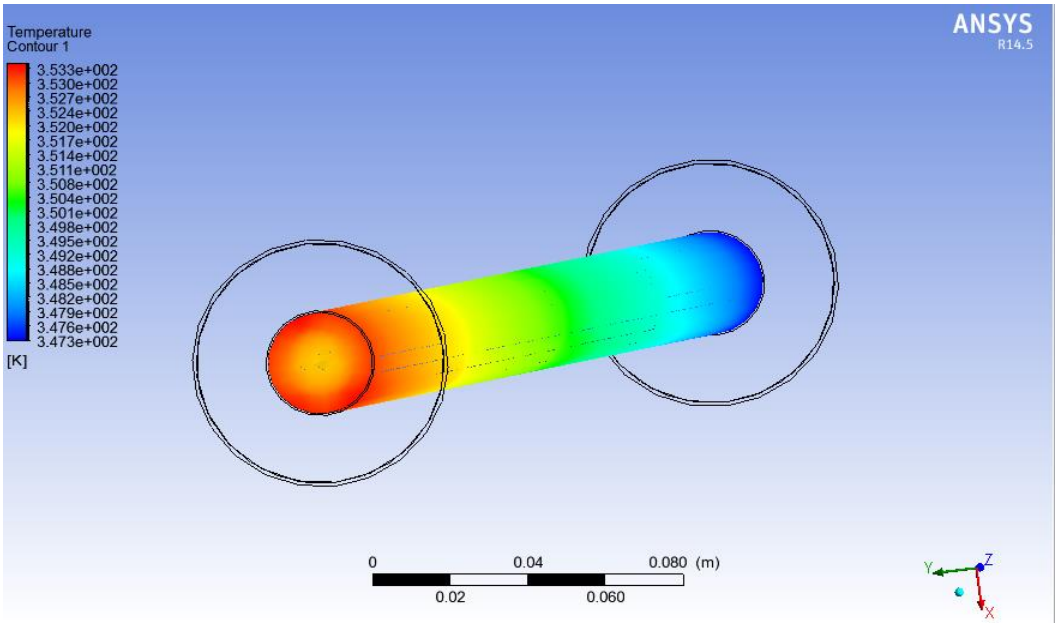

Figure 6.3 Temperature contour with 0.075% vol. conc. alumina-water nanofluid as a working fluid at 80 LPH

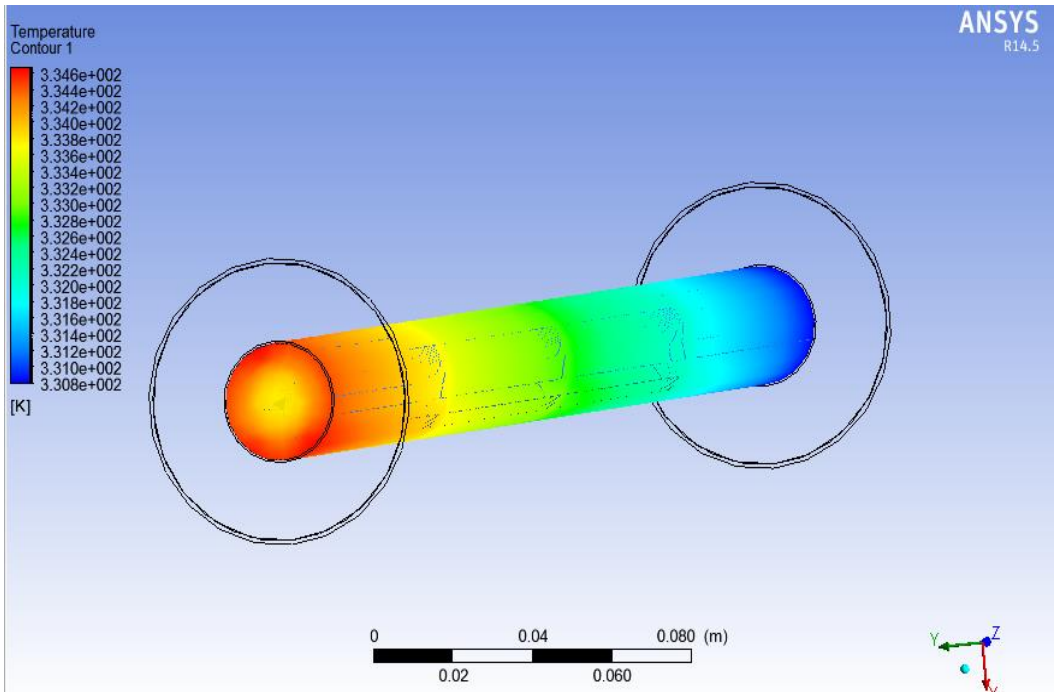

Figure 6.4 Temperature contour with 0.1% vol. conc. alumina-water nanofluid as a working fluid at 80 LPH

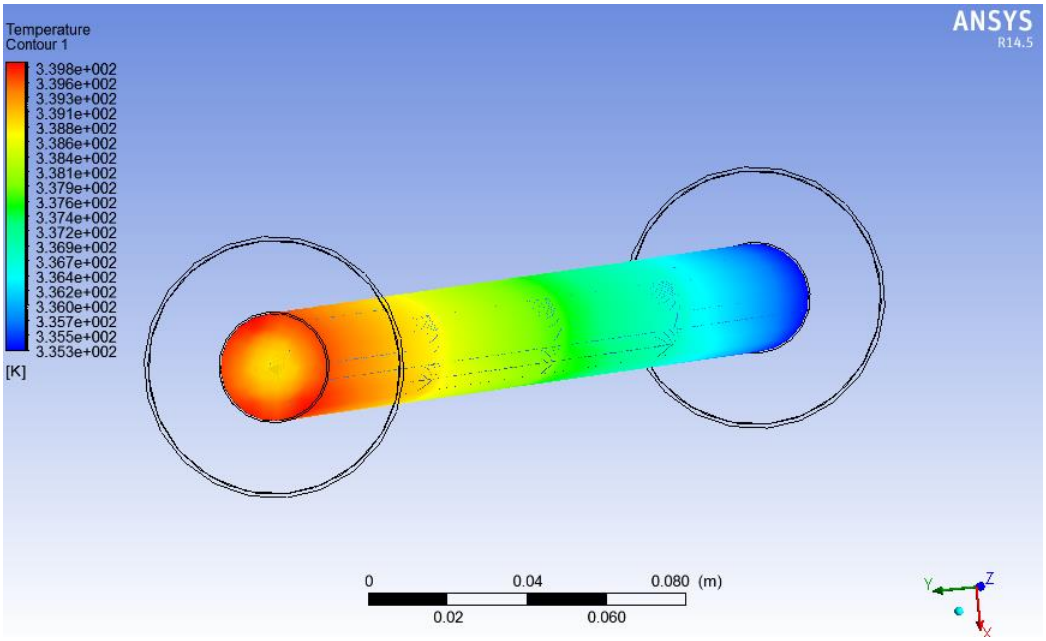

Figure 6.5 Temperature contour with 0.125% vol. conc. alumina-water nanofluid as a working fluid at 80 LPH

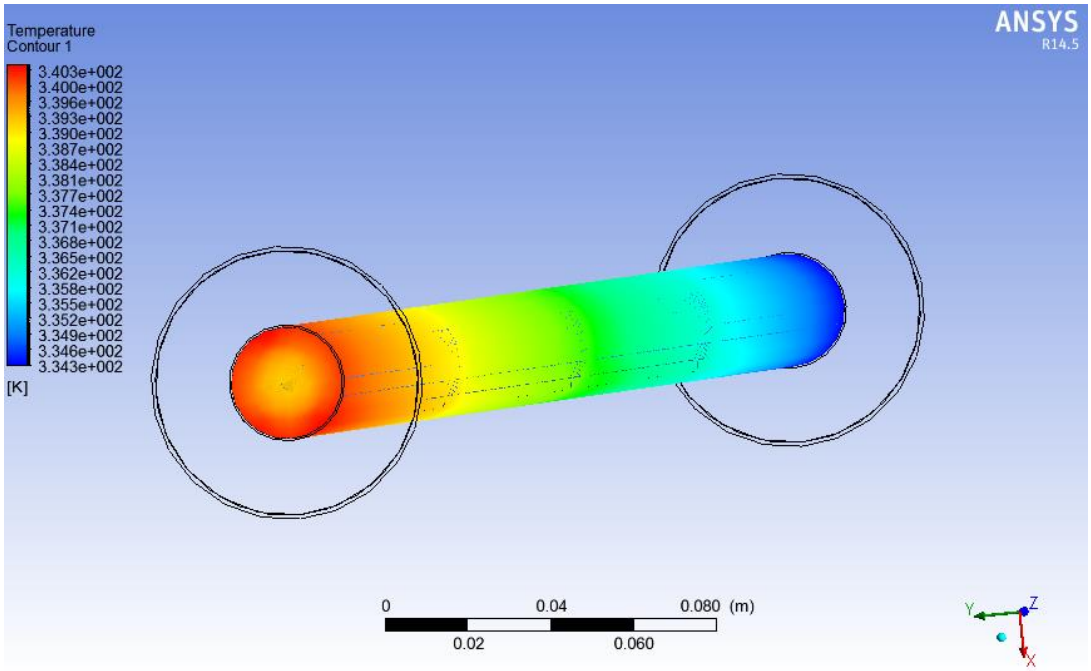

Figure 6.6 Temperature contour with water-ethylene glycol mixture (60:40 by volume) as a working fluid at 80 LPH

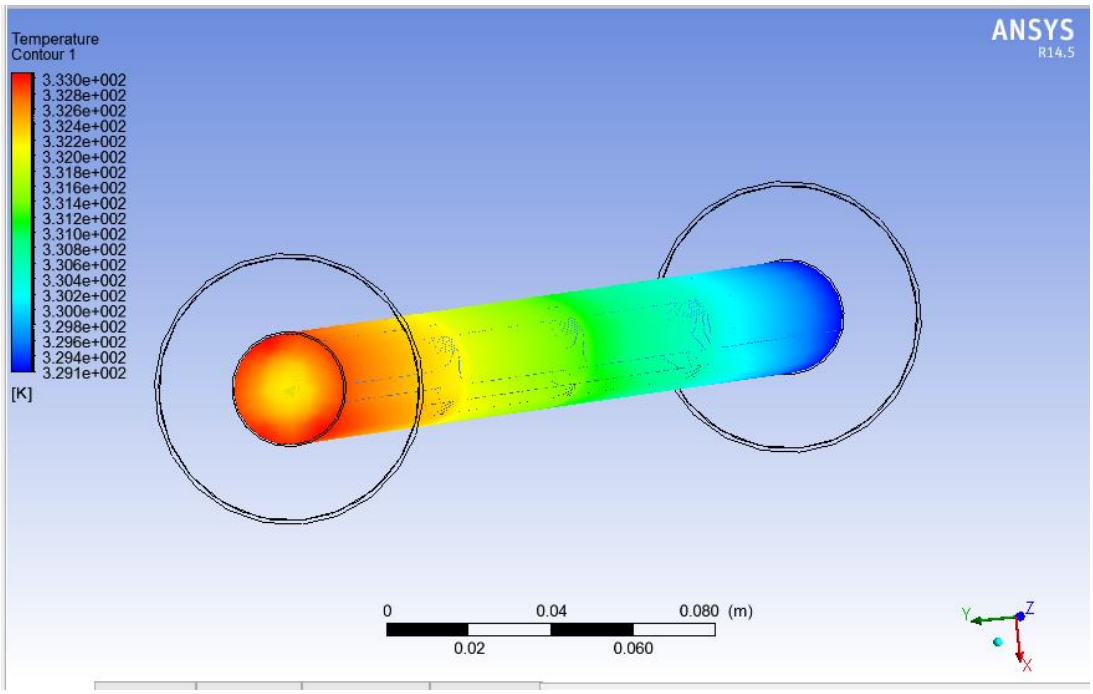

Figure 6.7 Temperature contour with 0.05% vol. conc. alumina-water-ethylene glycol mixture (60:40 by volume) nanofluid as a working fluid at 80 LPH

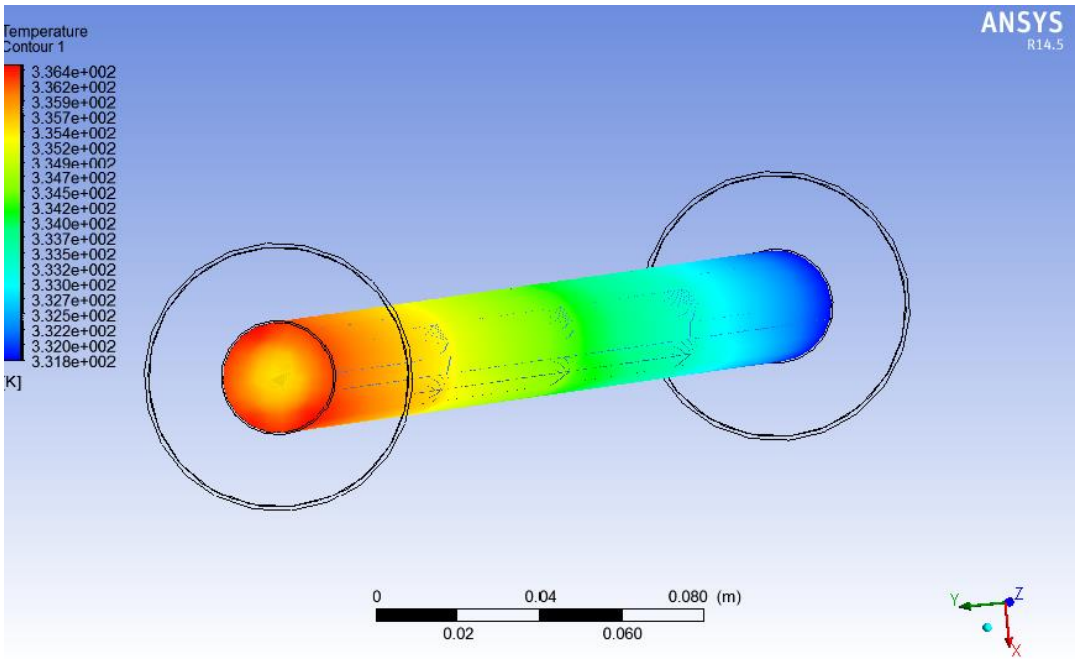

Figure 6.8 Temperature contour with 0.075% vol. conc. alumina-water-ethylene glycol mixture (60:40 by volume) nanofluid as a working fluid at 80 LPH

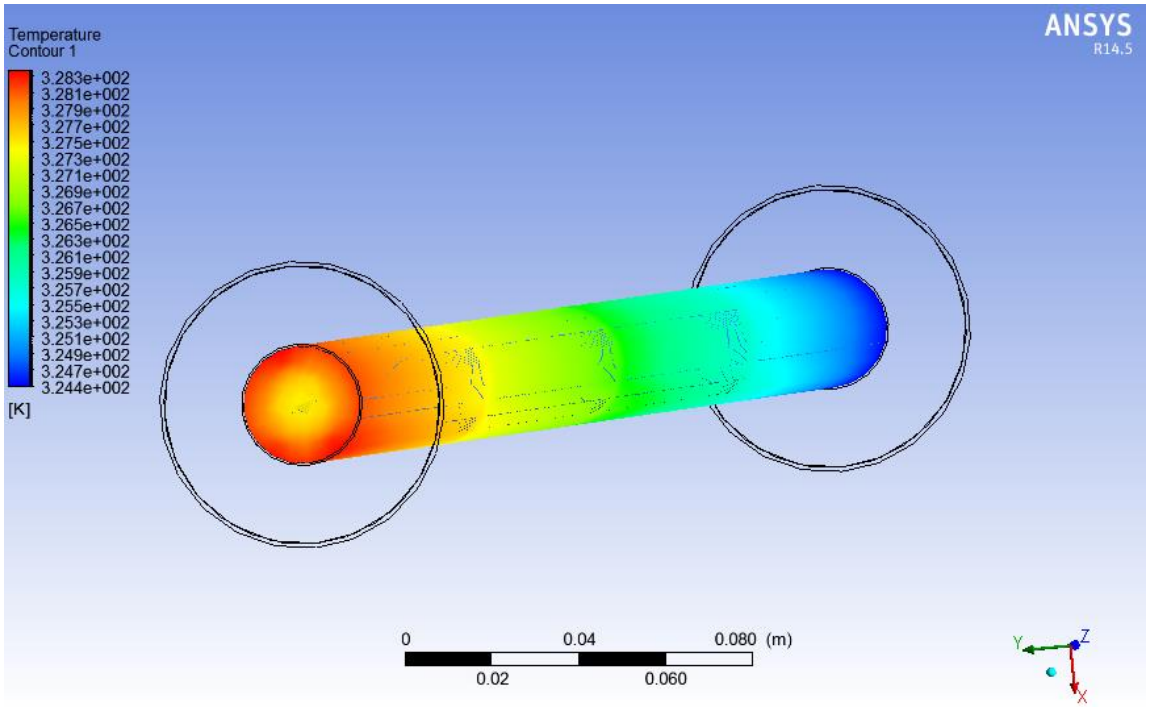

Figure 6.9 Temperature contour with 0.1% alumina-water-ethylene glycol mixture (60:40 by volume) as a working fluid at 80 LPH

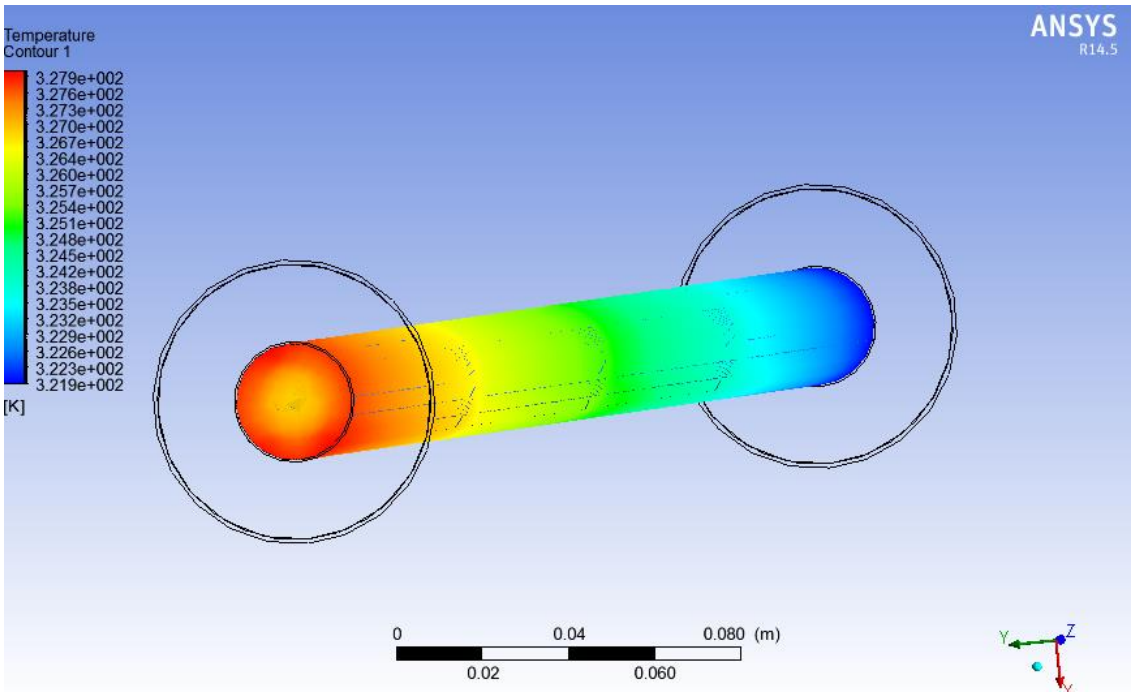

Figure 6.10Temperature contour with 0.125% alumina-water-ethylene glycol mixture (60:40 by volume) as a working fluid at 80 LPH

6.2 Governing Equation for Efficiency Calculation

Following different governing equations are used for evaluating the parabolic solar collector's efficiency with different working fluids at different mass flow rates:

1) **Absorbed Flux**

$$S = G_T R_b (\alpha\tau) \beta Y \quad (6.1)$$

2) **Convective heat transfer coefficient**

$$h_f = N_u \times \frac{k}{D_i} \quad (6.2)$$

Where: $N_u = 0.023 \times Re^{0.8} \times Pr^{0.4}$

$Pr = (\mu \times C_p) / k$

$Re = (\rho \times V \times D_i) / \mu$

$V = (4\dot{m}) / (\pi \times D_i^2 \times \rho)$

3) **Useful heat gain**

$$q_u = \dot{m}\, C_p\, (T_{out} - T_{in}) \quad (6.3)$$

4) **Instantaneous efficiency, η_i**

$$\eta_i = \frac{\dot{m} c_p (T_{out} - T_{in})}{G_t\, R_b W\, L} \quad (6.4)$$

5) **Thermal efficiency, η_t**

$$\eta_t = \frac{\dot{m} c_p (T_{out} - T_{in})}{G_t\, A_{apper}\, t} \quad (6.5)$$

6) **Overall efficiency, η_o**

$$\eta_o = \frac{\dot{m} c_p (T_{out} - T_{in})}{G_{avg.}\, A_{apper}} \quad (6.6)$$

Where: G_T is global solar intensity in W/m^2, R_b is bond resistance, α is absorptivity of the absorber tube, τ is glass cover transmissivity for solar radiation, β is specular reflectivity and γ is intercept factor, N_u is Nusselt number, K is thermal conductivity in W/m-K, D_i is inner diameter of absorber tube in m, Pr is prandtl number, μ is

dynamic viscosity in Pa-s, C_p is specific heat in J/kg-K, ρ is density in kg/m^3, Re is reynolds number, V is average velocity in m/s and ṁ is mass flow rate in kg/sec, W is width of the solar collector in m, L is the length of the absorber tube in m, A_{aper} is the aperture area of the solar collector in m^2, t is the time duration and G_{avg} is the average value of solar radiation in W/m^2.

6.3 Variation of Instantaneous Efficiency for Various Working Fluids (during day time, 9.30 am to 2.30 pm)

Variation of instantaneous efficiency both experimental instantaneous efficiency and simulated instantaneous with various working fluid and at different volume flow rates with respect to time of day is presented in following figure 6.11-6.22. It is seen that both experimental and simulated values of instantaneous efficiency is maximum at initial period of time for all working fluid and afterwards drop in the values (both simulated and experimental, which is mainly due to associated heat losses.

It is also seen that the instantaneous efficiency increases with mass flow rate. At lower mass flow rate fluid residence time is more, due to which working fluid absorbs maximum amount of incoming solar energy and at same time working fluid do suffers from excessive radiation looses as emissive radiation from fluid scales with the fourth power of temperature. Around 23%, 38% and 65% maximum instantaneous efficiency is seen with 0.125% Al_2O_3-H_2O (DI) nanofluid at 30 LPH,50 LPH and 80LPH respectively. Maximum instantaneous efficiency of about 18%, 25% and 40% is seen with water as a working fluid at 30LPH, 50 LPH and 80 LPH respectively.

It is also observed that the instantaneous efficiency is maximum for the nanofluid (of different volumetric concentration: 0.05%, 0.075%, 0.1% and 0.125%) than base fluid i.e. higher values of instantaneous efficiency is seen with water and water based nanofluid as compared to base fluid of water and water-ethylene glycol mixture based nanofluid respectively. Which is mainly due to improved thermal properties like thermal conductivity and heat transfer coefficient of the nanofluid as compared with the base fluid. Moreover as the volumetric concentration is made to increase then, correspondingly rise in the instantaneous efficiency is also seen. It is seen that with 0.125% volumetric concentration maximum value of instantaneous efficiency is seen as compared with nanofluid of remaining volumetric concentration It is also seen that both experimental and simulated values of instantaneous efficiency are in close agreement.

1) Variation of experimental instantaneous efficiency at 30 LPH with water and water based nanofluid of different volumetric concentration (0.05%, 0.075%, 0.1% and 0.125%).

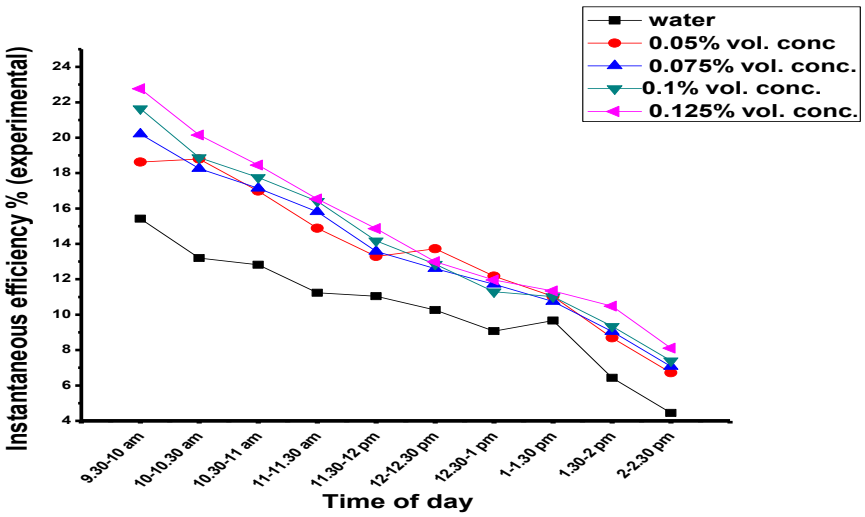

Figure 6.11 Variation of experimental instantaneous efficiency at 30 LPH with H_2O and Al_2O_3-H_2O (DI) based nanofluid of different volumetric concentration

2) Variation of simulated instantaneous efficiency at 30 LPH with water and water based nanofluid of different volumetric concentration (0.05%, 0.075%, 0.1% and 0.125%)

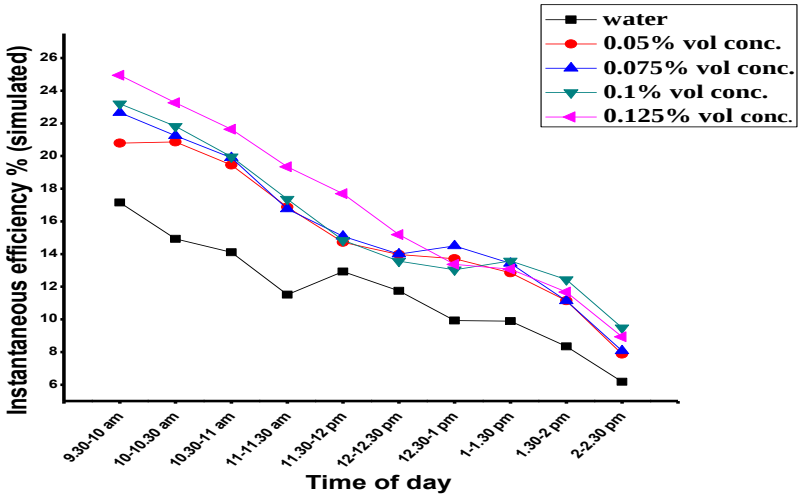

Figure 6.12 Variation of simulated instantaneous efficiency at 30 LPH with H_2O and Al_2O_3-H_2O (DI) nanofluid of different volumetric concentration

3) Variation of experimental instantaneous efficiency at 50 LPH with water and water based nanofluid of different volumetric concentration (0.05%, 0.075%, 0.1% and 0.125%).

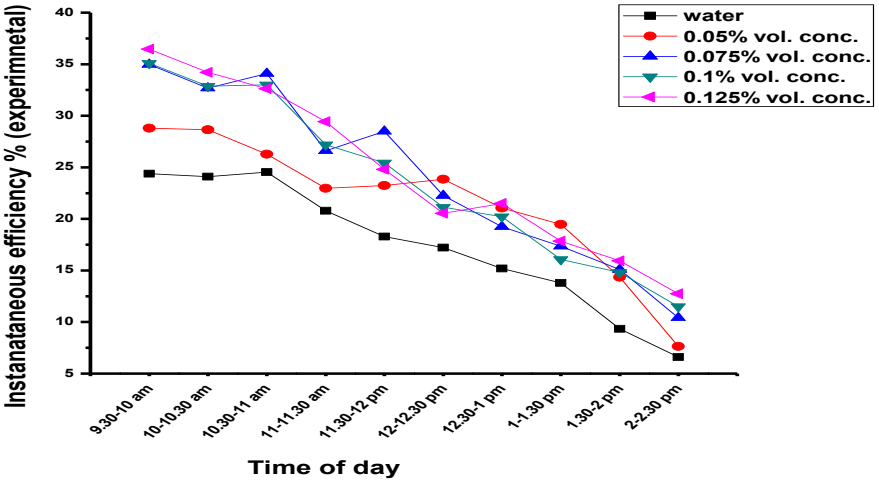

Figure 6.13 Variation of experimental instantaneous efficiency at 50 LPH with H_2O and Al_2O_3-H_2O (DI) based nanofluid of different volumetric concentration

4) Variation of simulated instantaneous efficiency at 50 LPH with water and water based nanofluid of different volumetric concentration (0.05%, 0.075%, 0.1% and 0.125%).

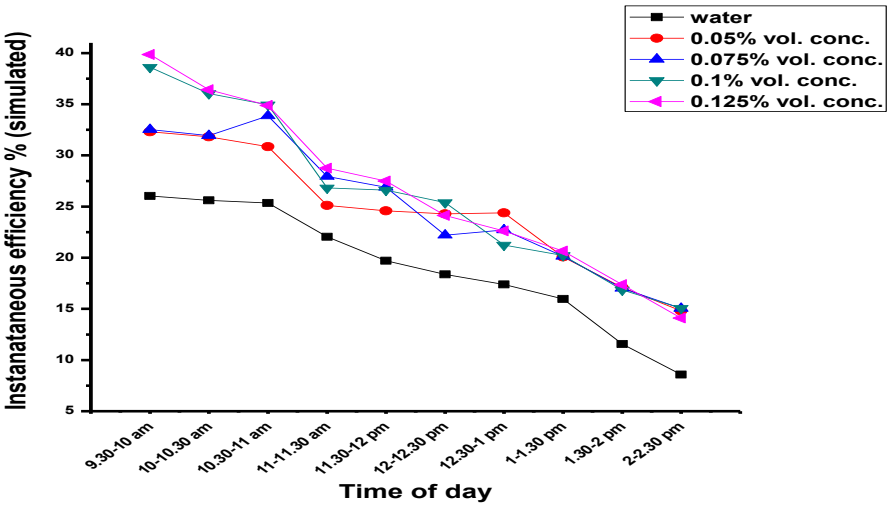

Figure 6.14 Variation of simulated instantaneous efficiency at 50 LPH with H_2O and Al_2O_3-H_2O (DI) based nanofluid of different volumetric concentration

5) Variation of experimental instantaneous efficiency at 80 LPH with water and water based nanofluid of different volumetric concentration (0.05%, 0.075%, 0.1% and 0.125%).

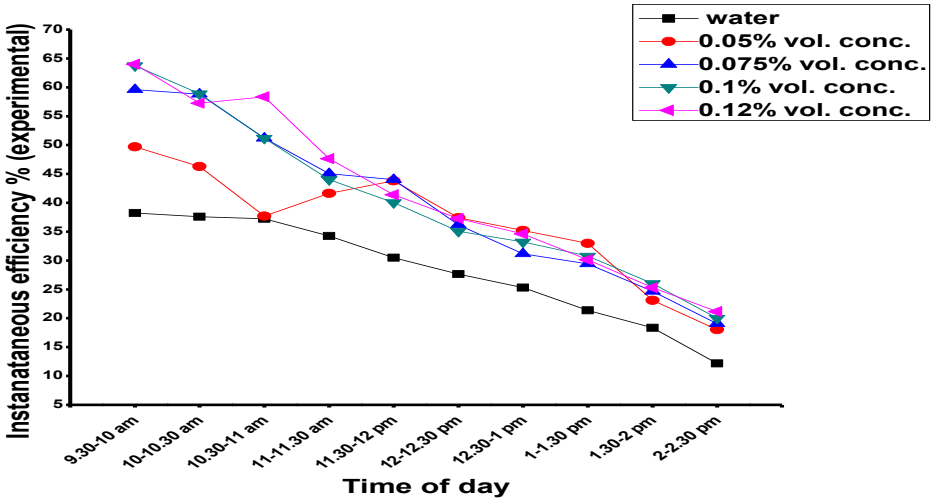

Figure 6.15 Variation of experimental instantaneous efficiency at 80 LPH with H_2O and Al_2O_3-H_2O (DI) based nanofluid of different vol. conc.

6) Variation of simulated instantaneous efficiency at 80 LPH with water and water based nanofluid of different volumetric concentration (0.05%, 0.075%, 0.1% and 0.125%).

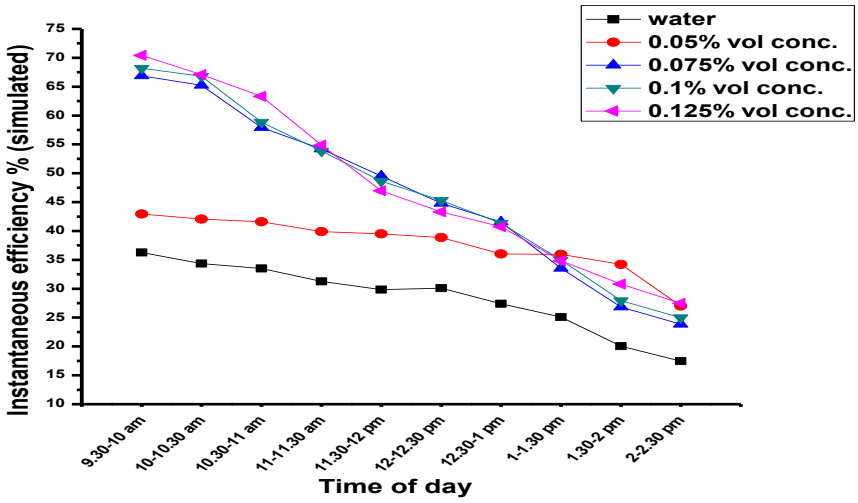

Figure 6.16 Variation of simulated instantaneous efficiency at 80 LPH with H_2O and Al_2O_3- H_2O (DI) based nanofluid of different volumetric concentration

7) Variation of experimental instantaneous efficiency at 30 LPH with water and water-ethylene based nanofluid of different volumetric concentration

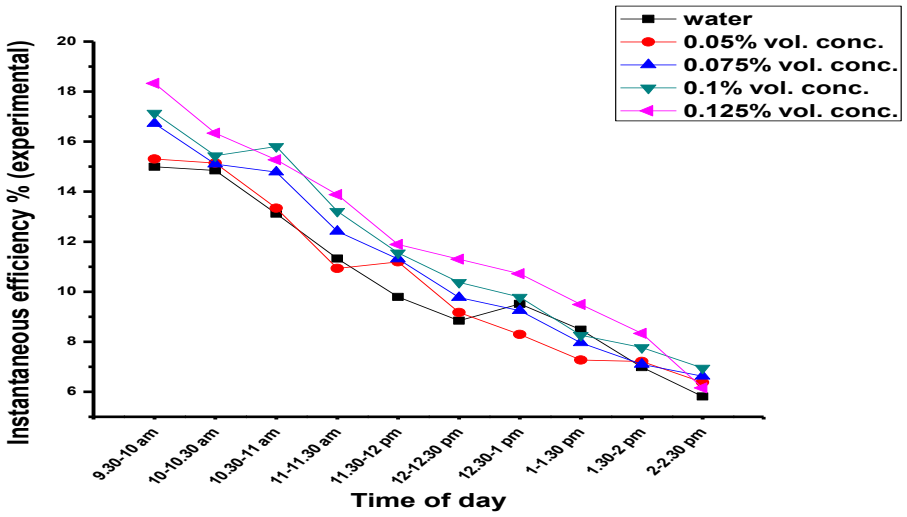

Figure 6.17 variation of experimental instantaneous efficiency at 30 LPH with H_2O-$C_2H_6O_2$ (60:40 by vol.) and Al_2O_3- H_2O-$C_2H_6O_2$ (60:40 by vol.) based nanofluid of different volumetric concentration

8) Variation of simulated instantaneous efficiency at 30 LPH with water-ethylene and water –ethylene glycol based nanofluid of different volumetric concentration

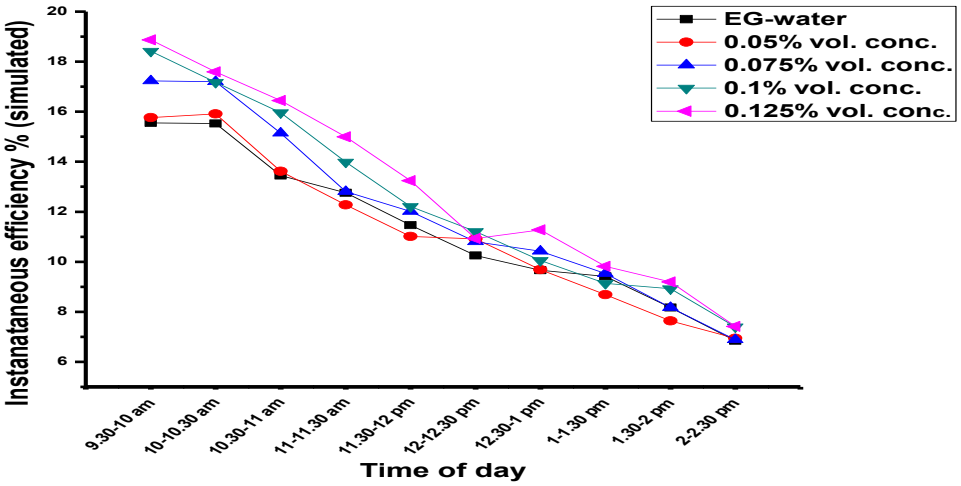

Figure 6.18 variation of simulated instantaneous efficiency at 30 LPH with H_2O-$C_2H_6O_2$ (60:40 by vol.) and Al_2O_3- H_2O-$C_2H_6O_2$ (60:40 by vol.) based nanofluid of different volumetric concentration

9) Variation of experimental instantaneous efficiency at 50 LPH with water-ethylene and water-ethylene glycol based nanofluid of different volumetric concentration.

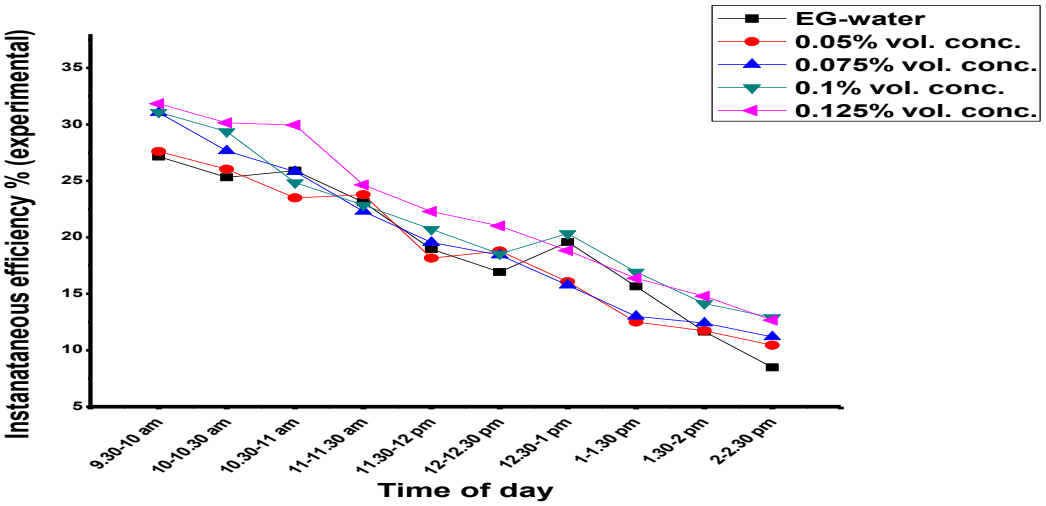

Figure 6.19 variation of experimental instantaneous efficiency at 50 LPH with H_2O-$C_2H_6O_2$ (60:40 by vol.) and Al_2O_3- H_2O-$C_2H_6O_2$ (60:40 by vol.) based nanofluid of different volumetric concentration

10) Variation of simulated instantaneous efficiency at 50 LPH with water-ethylene and water-ethylene glycol based nanofluid of different volumetric concentration

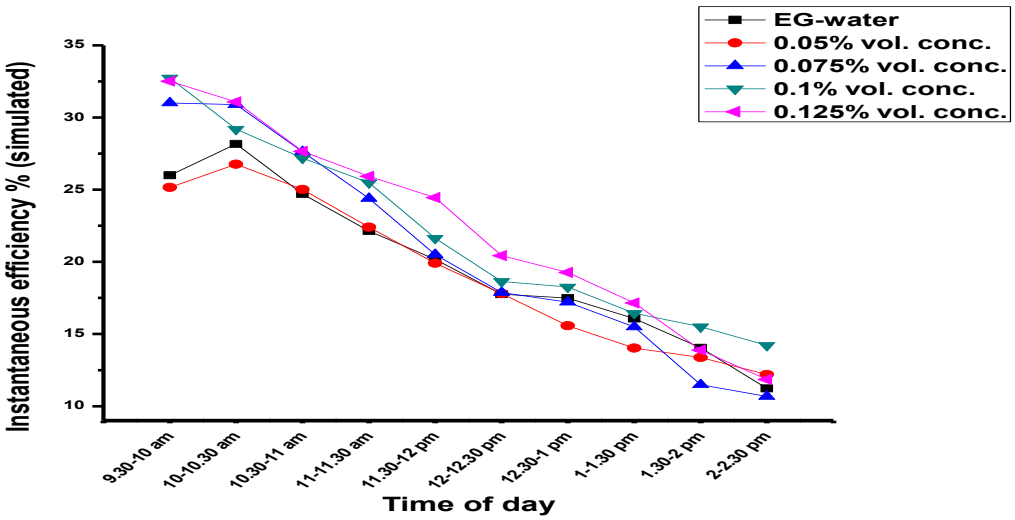

Figure 6.20 variation of simulated instantaneous efficiency at 50 LPH with H_2O-$C_2H_6O_2$ (60:40 by vol.) and Al_2O_3- H_2O-$C_2H_6O_2$ (60:40 by vol.) based nanofluid of different volumetric concentration

11) Variation of experimental instantaneous efficiency at 80 LPH with water-ethylene and water-ethylene glycol based nanofluid of different volumetric concentration.

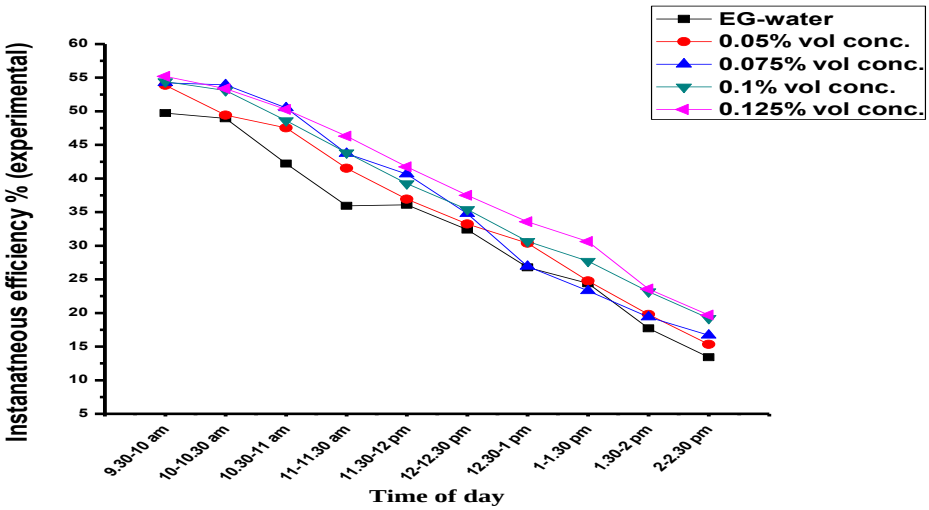

Figure 6.21 variation of experimental instantaneous efficiency at 80 LPH with H_2O-$C_2H_6O_2$ (60:40 by vol.) and Al_2O_3- H_2O-$C_2H_6O_2$ (60:40 by vol.) based nanofluid of different volumetric concentration

12) Variation of simulated instantaneous efficiency at 80 LPH with water-ethylene and water –ethylene glycol based nanofluid of different volumetric concentration.

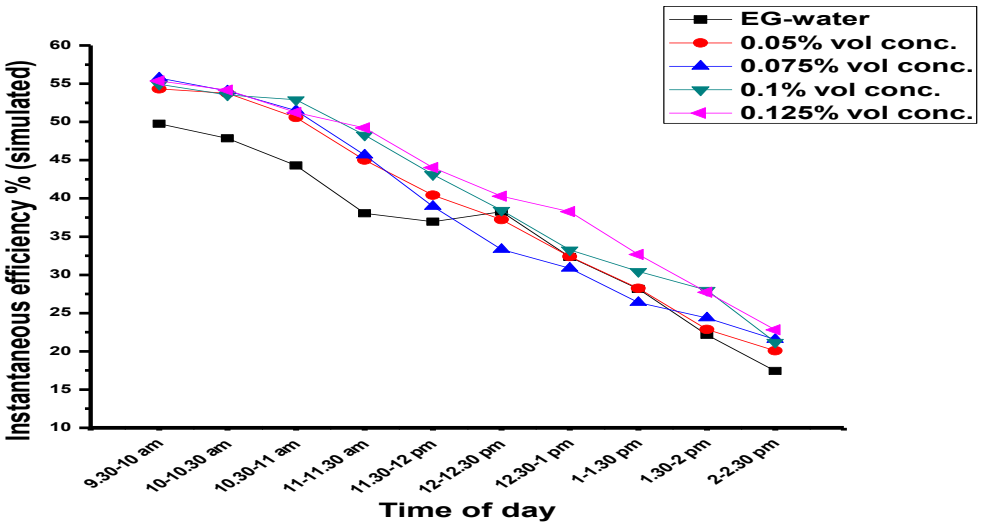

Figure 6.22 Variation of simulated instantaneous efficiency at 80 LPH with H_2O-$C_2H_6O_2$ (60:40 by vol.) and Al_2O_3- H_2O-$C_2H_6O_2$ (60:40 by vol.) based nanofluid of different volumetric concentration

6.4 Variation of Thermal Efficiency for Various Working Fluids (during day time, 9.30 am to 2.30 pm)

Variation of thermal efficiency both experimental thermal efficiency and simulated instantaneous efficiency with respect to time of day for various working fluid (water, water based nanofluid of different volumetric concentration, water-ethylene glycol mixture and water-ethylene glycol mixture based nanofluid of different volumetric concentration) is presented in the figure 6.23-6.34.

Also effect of different mass flow rate on thermal efficiency is also presented. From the depicted graphs, it is seen that at higher mass flow rate, higher value of thermal efficiency is seen with all working fluids (water, water based nanofluid of different volumetric concentration, water-ethylene glycol mixture and water-ethylene glycol mixture based nanofluid of different volumetric concentration).Though at lower mass flow rate, fluid residence time is high due to which fluid absorbs maximum amount of solar energy, but on the other hand fluid also looses energy due to radiation heat transfer as this mode of heat transfer scales with fourth power of the temperature of working fluid.

It is also inferred that both experimental and simulated values of thermal efficiency is maximum at initial period of time for all working fluid and afterwards drop in the values (both simulated and experimental) is seen, which is mainly due to associated heat losses. Around 8%, 13% and 23% thermal efficiency is seen at initial time interval with 0.125% Al_2O_3-H_2O(DI) nanofluid at 30 LPH, 50 LPH and 80 LPH respectively ,while with water as a working fluid around 6.5%,8% and 14% thermal efficiency is seen at 30 LPH,50 LPH and 80 LPH respectively at initial time interval.

Thermal efficiency is maximum for the nanofluid (of different volumetric concentration) than base fluid, which is mainly due to improved thermal properties of working fluid base fluid (comprising of water and water-ethylene glycol mixture). Also as the volumetric concentration is made to increase then rise in the thermal efficiency is also seen. Moreover there is also a close agreement between both experimental and simulated values of thermal efficiency

1) Variation of experimental thermal efficiency of various working fluid (water and alumina-water based nanofluid) at 30 LPH

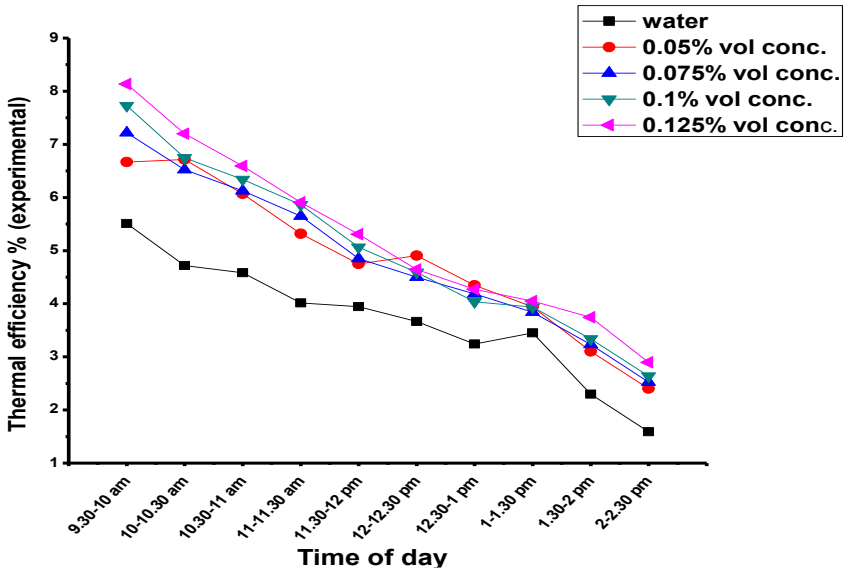

Figure 6.23 Variation of experimental thermal efficiency at 30 LPH with H_2O and Al_2O_3-H_2O (DI) based nanofluid of different vol. conc.

2) Variation of simulated thermal efficiency of various working fluid (water and alumina- water based nanofluid) at 30 LPH water

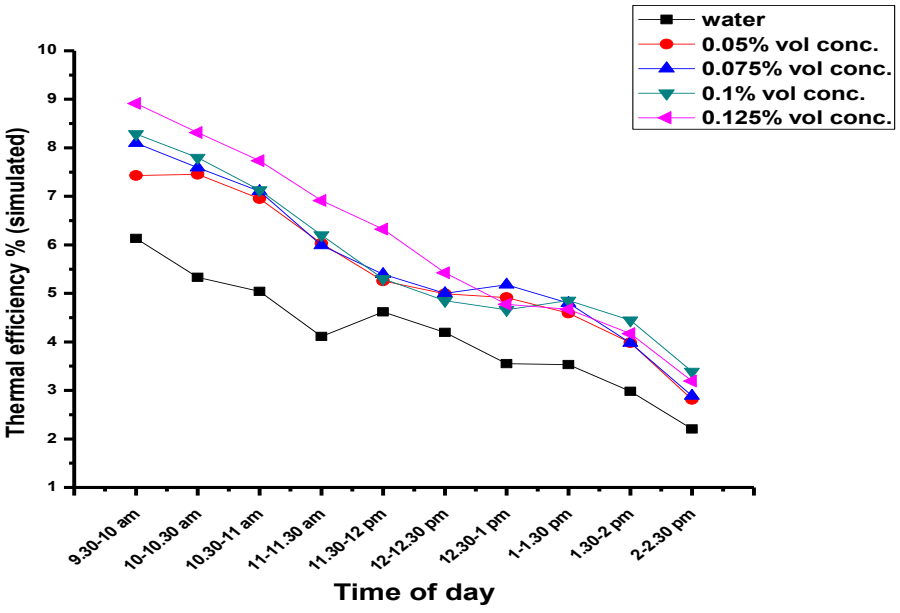

Figure 6.24 variation of simulated thermal efficiency at 30 LPH with H_2O and Al_2O_3-H_2O (DI) based nanofluid of different vol. conc.

3) Variation of experimental thermal efficiency of various working fluid (water and alumina-water based nanofluid) at 50 LPH water

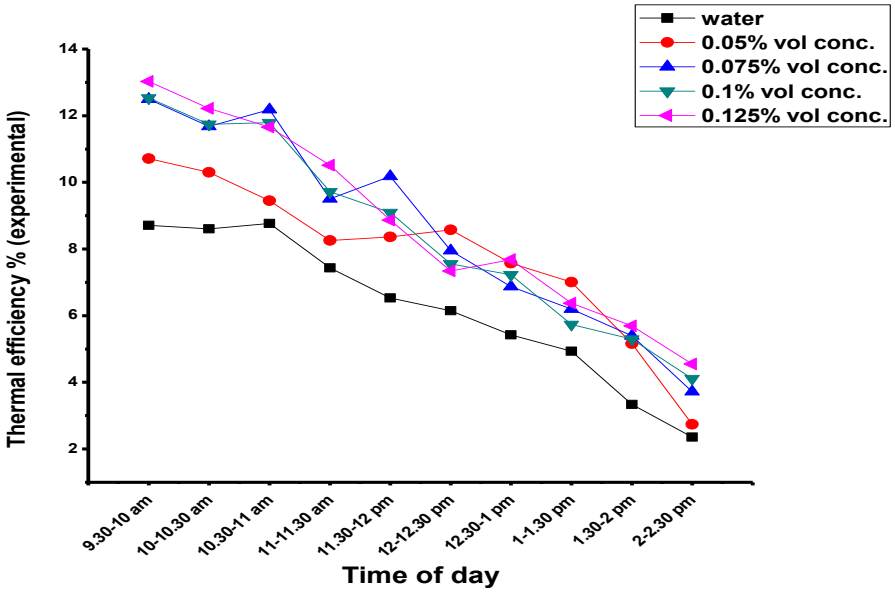

Figure 6.25 Variation of simulated thermal efficiency at 50 LPH with H_2O and Al_2O_3- H_2O (DI) based nanofluid of different volumetric concentration.

4) Variation of simulated thermal efficiency of various working fluid (water and alumina-water based nanofluid) at 50 LPH water

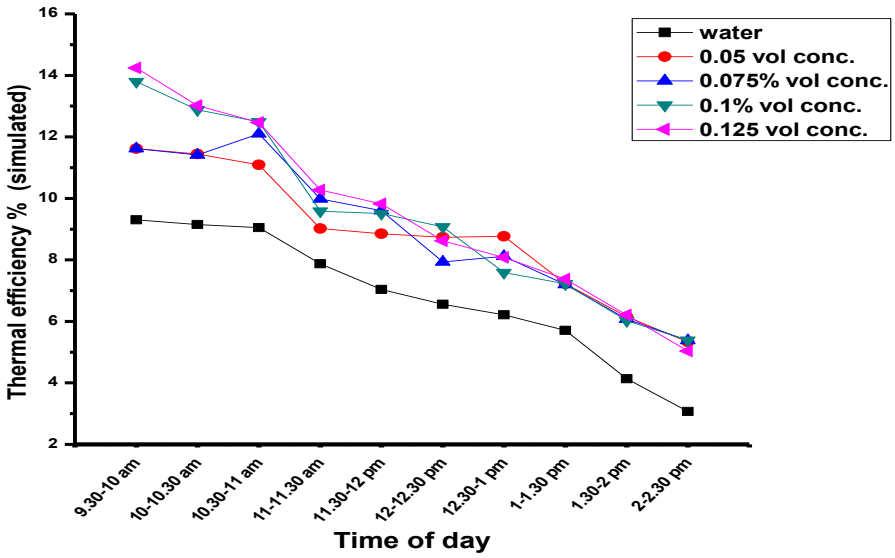

Figure 6.26 Variation of simulated thermal efficiency at 50 LPH with H_2O and Al_2O_3- H_2O (DI) nanofluid of different volumetric concentration

5) Variation of experimental thermal efficiency of various working fluid (water and alumina-water based nanofluid) at 80 LPH water

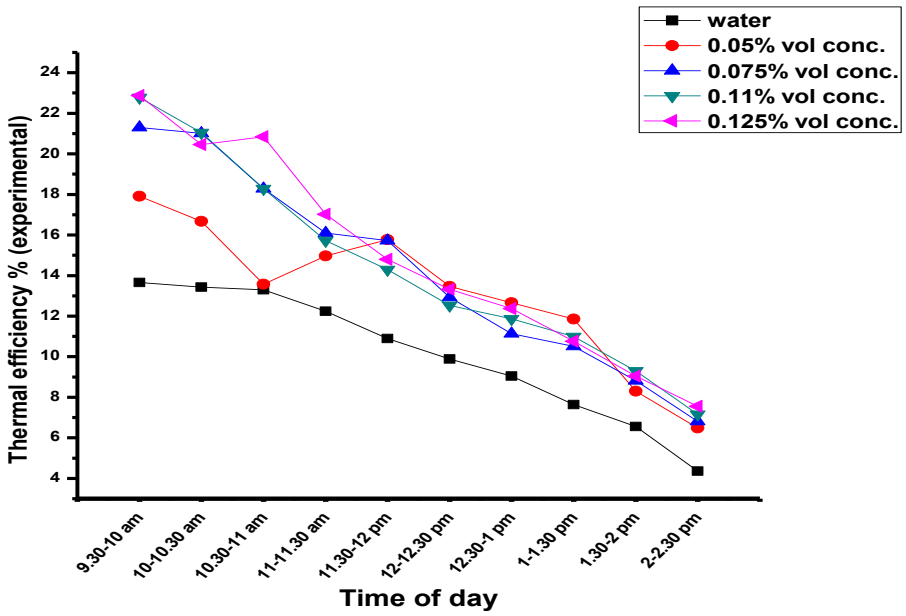

Figure 6.27 Variation of experimental thermal efficiency at 80 LPH with H_2O and Al_2O_3- H_2O (DI) based nanofluid of different volumetric concentration

6) Variation of simulated thermal efficiency of various working fluid (water and alumina-water based nanofluid) at 80 LPH water

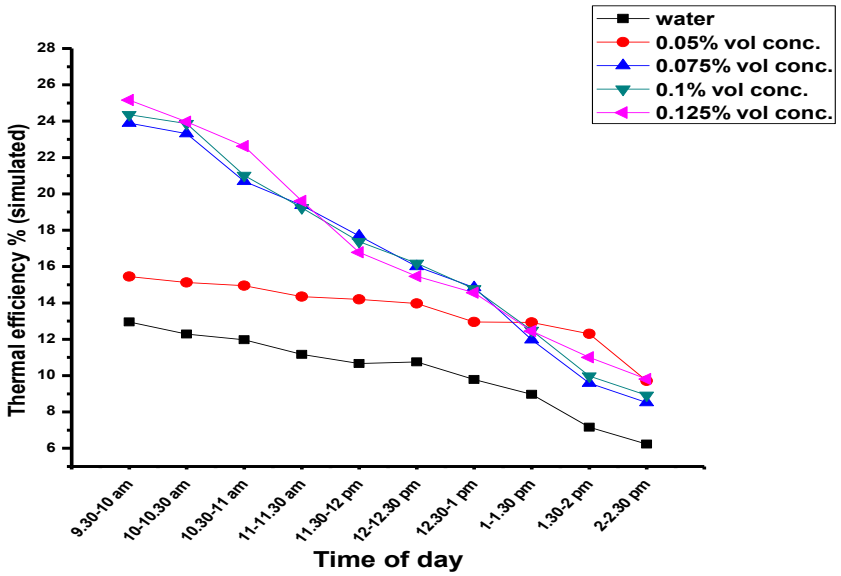

Figure 6.28 Variation of simulated thermal efficiency at 80 LPH with H_2O and Al_2O_3- H_2O (DI) based nanofluid of different volumetric concentration

7) Variation of experimental thermal efficiency of various working fluid (water-ethylene glycol and alumina- water -ethylene glycol based nanofluid) at 30 LPH

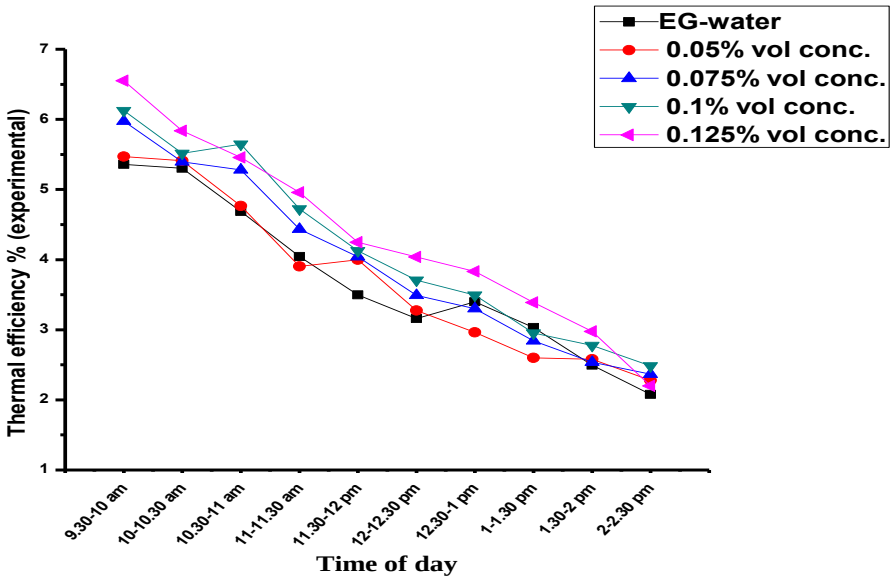

Figure 6.29 Variation of experimental thermal efficiency at 30 LPH with H_2O-$C_2H_6O_2$ (60:40 by vol.) and Al_2O_3- H_2O-$C_2H_6O_2$ (60:40 by vol.) based nanofluid of different volumetric concentration.

8) Variation of simulated thermal efficiency of various working fluid (water-ethylene glycol and alumina-water -ethylene glycol based nanofluid) at 30 LPH

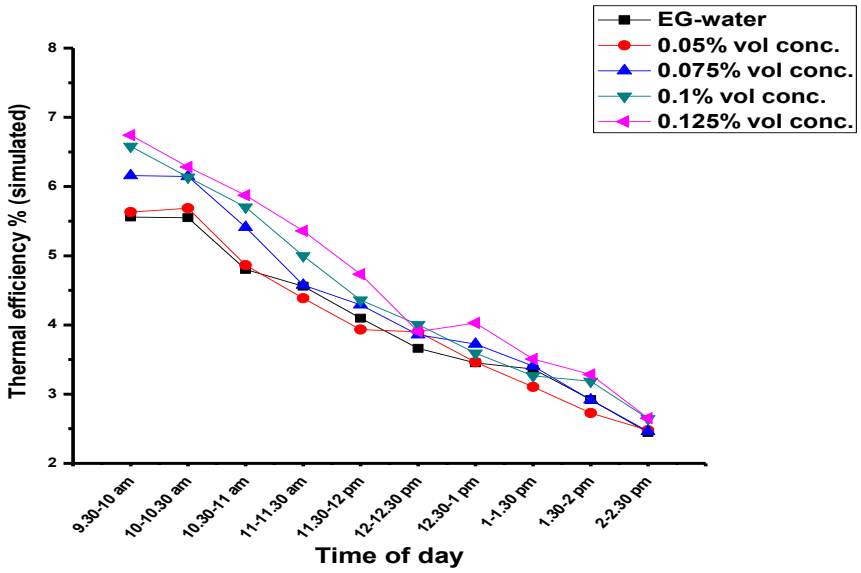

Figure 6.30 Variation of simulated thermal efficiency at 30 LPH with H_2O-$C_2H_6O_2$ (60:40 by vol.) and Al_2O_3- H_2O-$C_2H_6O_2$ (60:40 by vol.) based nanofluid of different volumetric concentration.

9) Variation of experimental thermal efficiency of various working fluid (water-ethylene glycol and alumina- water-ethylene glycol based nanofluid) at 50 LPH

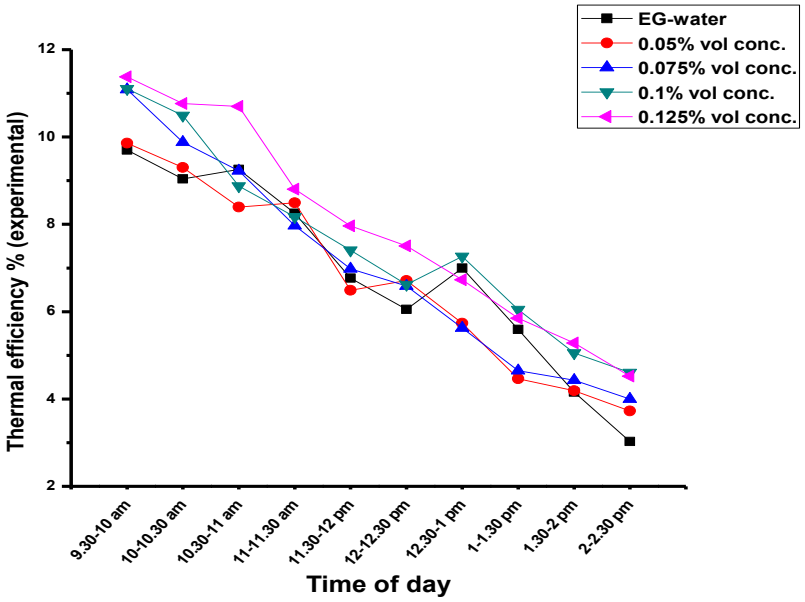

Figure 6.31 Variation of experimental thermal efficiency at 50 LPH with H_2O-$C_2H_6O_2$ (60:40 by vol.) and Al_2O_3- H_2O-$C_2H_6O_2$ (60:40 by vol.) based nanofluid of different volumetric concentration.

10) Variation of simulated thermal efficiency of various working fluid (water-ethylene glycol and alumina-water-ethylene glycol based nanofluid) at 50 LPH

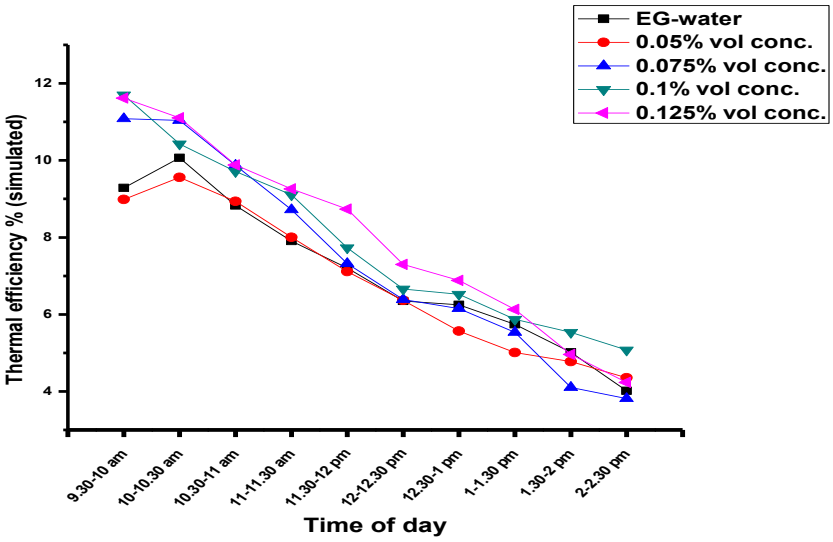

Figure 6.32 Variation of simulated thermal efficiency at 50 LPH with H_2O-$C_2H_6O_2$ (60:40 by vol.) and Al_2O_3- H_2O-$C_2H_6O_2$ (60:40 by vol.) based nanofluid of different volumetric concentration

11) Variation of experimental thermal efficiency of various working fluid (water-ethylene glycol and alumina-water - ethylene glycol based nanofluid) at 80 LPH

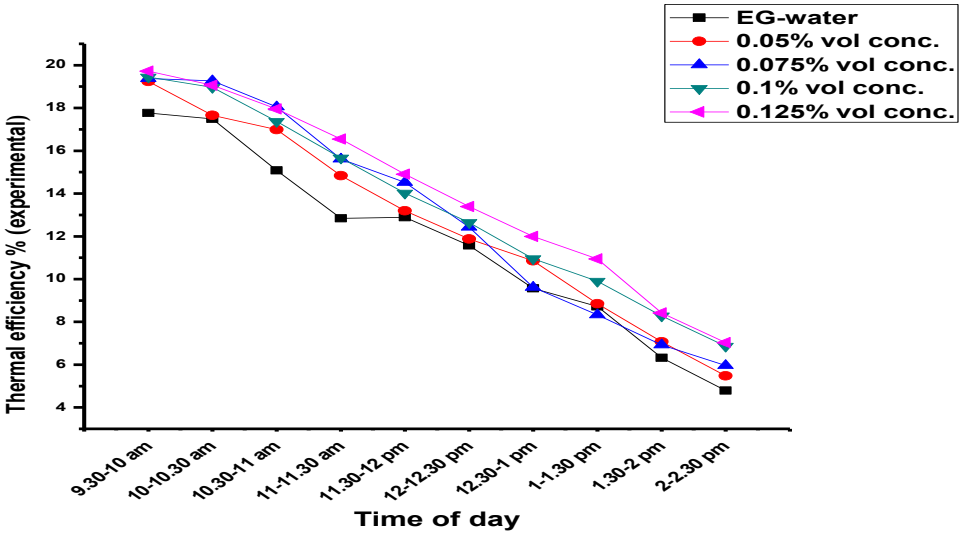

Figure 6.33 Variation of experimental thermal efficiency at 80 LPH with H_2O-$C_2H_6O_2$ (60:40 by vol.) and Al_2O_3- H_2O-$C_2H_6O_2$ (60:40 by vol.) based nanofluid of different volumetric concentration

12) Variation of simulated thermal efficiency of various working fluid (water-ethylene glycol and alumina-water –ethylene glycol based nanofluid) at 80 LPH

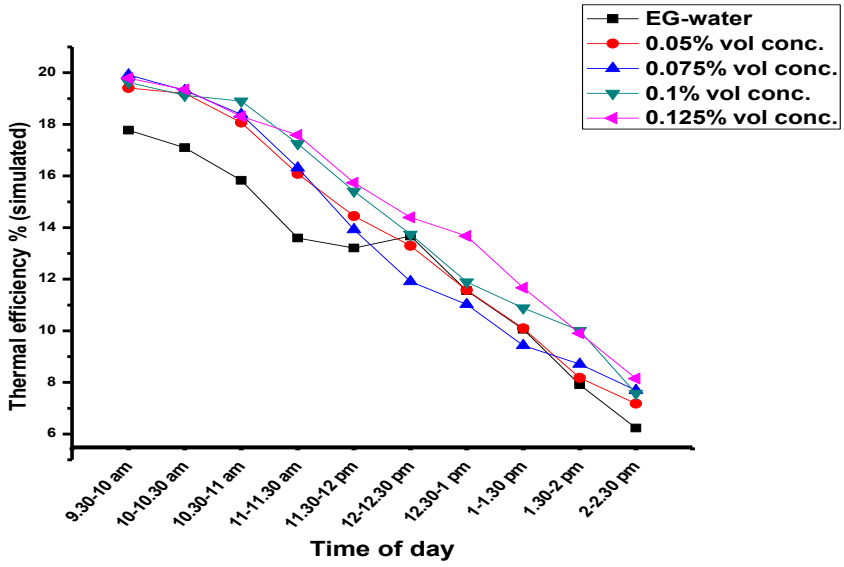

Figure 6.34 Variation of simulated thermal efficiency at 80 LPH with H_2O-$C_2H_6O_2$ (60:40 by vol.) and Al_2O_3- H_2O-$C_2H_6O_2$ (60:40 by vol.) based nanofluid of different volumetric concentration

6.5 Effect of Mass Flow Rate on Parabolic Solar Collector

Effect of different mass flow rate (30LPH,50 LPH and 80 LPH) on the solar collector's presented in graphs. Where plot of instantaneous efficiency versus reduced temperature parameter $((T_o+T_i)/2)-T_a)/G_t$ is shown for each working fluid.

1) Water as a working fluid

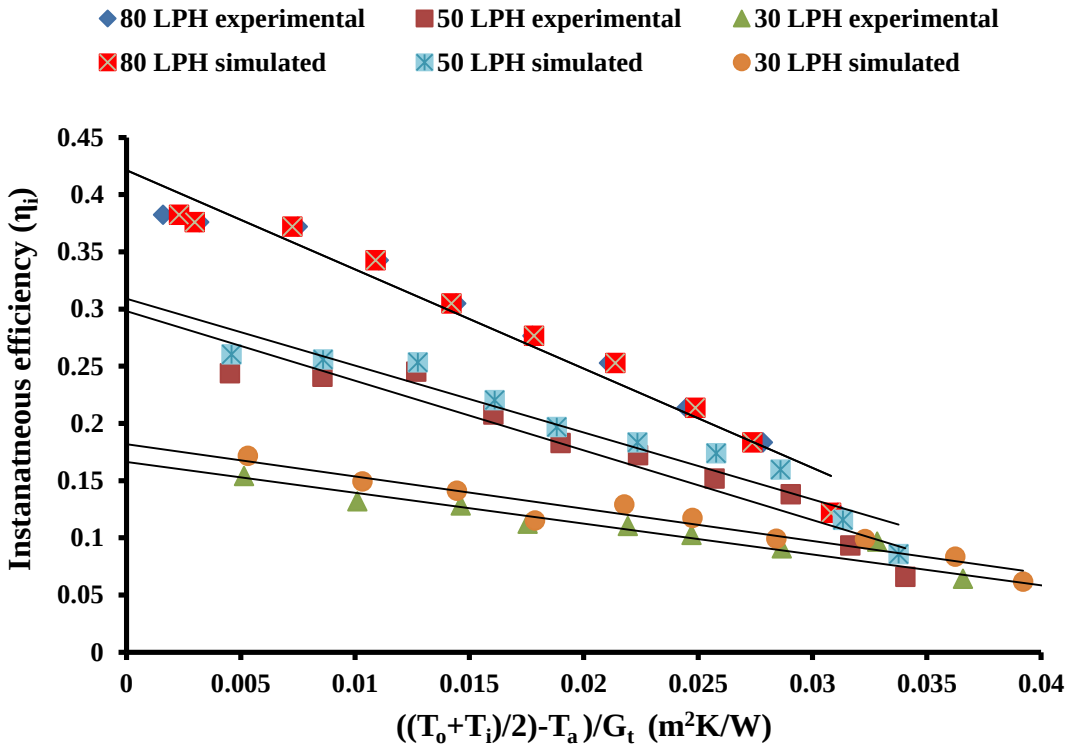

Figure 6.35 Efficiency versus $((T_o+T_i)/2)-T_a)/G_t$ curve at three flow rate for water

Figure 6.35 shows the variation of both experimental and simulated values of instantaneous efficiency versus reduced temperature parameter $((T_o+T_i)/2)-T_a)/G_t$ with water as a working fluid at different mass flow rate (30 LPH, 50 LPH and 80 LPH). It is seen that when average of T_o and T_i equals T_a then maximum collector efficiency (experimental) is 17.5%, 31% and 42.5% at 30 LPH, 50 LPH and 80 LPH respectively. While maximum collector efficiency (when average of T_o and T_i equals T_a) through simulated results is 18%, 32% and 42.5% at 30 LPH, 50 LPH and 80 LPH respectively. It is seen that collector efficiency is enhanced with increasing volume flow rate. Table 6.1 shows the calculated values of F_RU_L and $F_R(\tau\alpha)$

Table 6.1 Collector efficiency parameters at three flow rates for water as working fluid.

Flow rate	Case	F_RU_L	$F_R(\tau\alpha)$
80 LPH	Experimental	8.671	0.421
80 LPH	Simulated	8.671	0.421
50 LPH	Experimental	5.847	0.298
50 LPH	Simulated	6.079	0.309
30 LPH	Experimental	2.694	0.166
30 LPH	Simulated	2.818	0.181

2) 0.05% vol. conc. alumina-water nanofluid as a working fluid

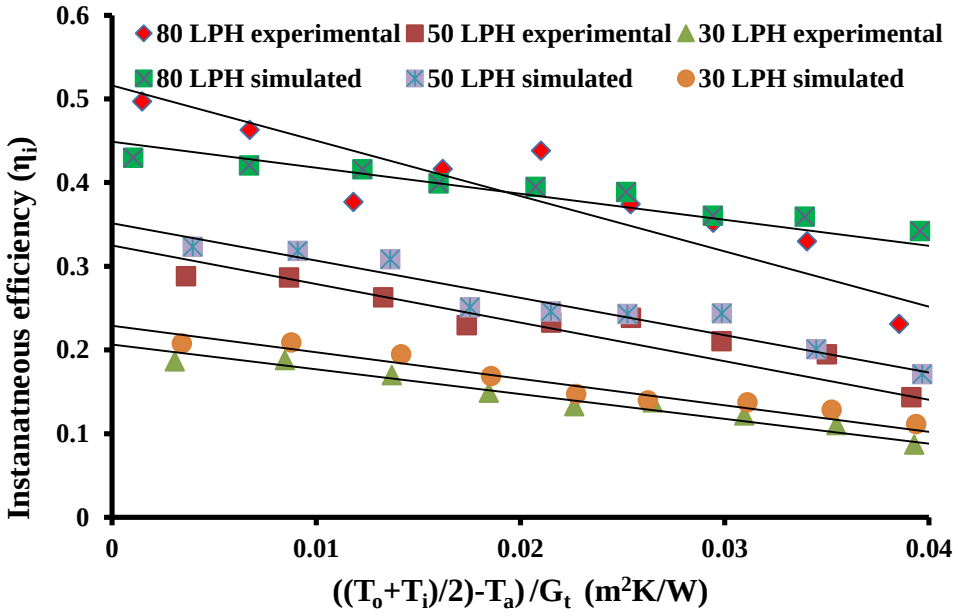

Figure 6.36 Efficiency versus $((T_o+T_i)/2)-T_a)/G_t$ curve at three flow rate for 0.05% vol. conc. alumina-water nanofluid

Figure 6.36 shows the variation of both experimental and simulated values of instantaneous efficiency versus reduced temperature parameter $((T_o+T_i)/2)-T_a)/G_t$ with 0.05% alumina-water as a working fluid at different mass flow rate (30 LPH, 50 LPH and 80 LPH). It is seen that when average of T_o and T_i equals T_a then maximum collector efficiency (experimental) is 21%, 33% and 52% at 30 LPH, 50LPH and 80 LPH respectively. While maximum collector efficiency (when average of T_o and T_i equals T_a) through simulated results is 23%,34% and 47.5% at 30 LPH, 50 LPH and

80 LPH respectively. It is seen that the collector efficiency is enhanced with increasing volume flow rate. Table 6.2 shows the calculated values of F_RU_L and $F_R(\tau\alpha)$

Table 6.2 Collector efficiency parameters at three flow rates for 0.05% vol. conc. Al_2O_3-H_2O (DI) as working fluid.

Flow rate	Case	F_RU_L	$F_R(\tau\alpha)$
80 LPH	Experimental	6.607	0.516
80 LPH	Simulated	3.11	0.448
50 LPH	Experimental	4.611	0.325
50 LPH	Simulated	4.460	0.351
30 LPH	Experimental	2.954	0.206
30 LPH	Simulated	3.169	0.229

3) 0.075% vol. conc. alumina-water nanofluid as a working fluid

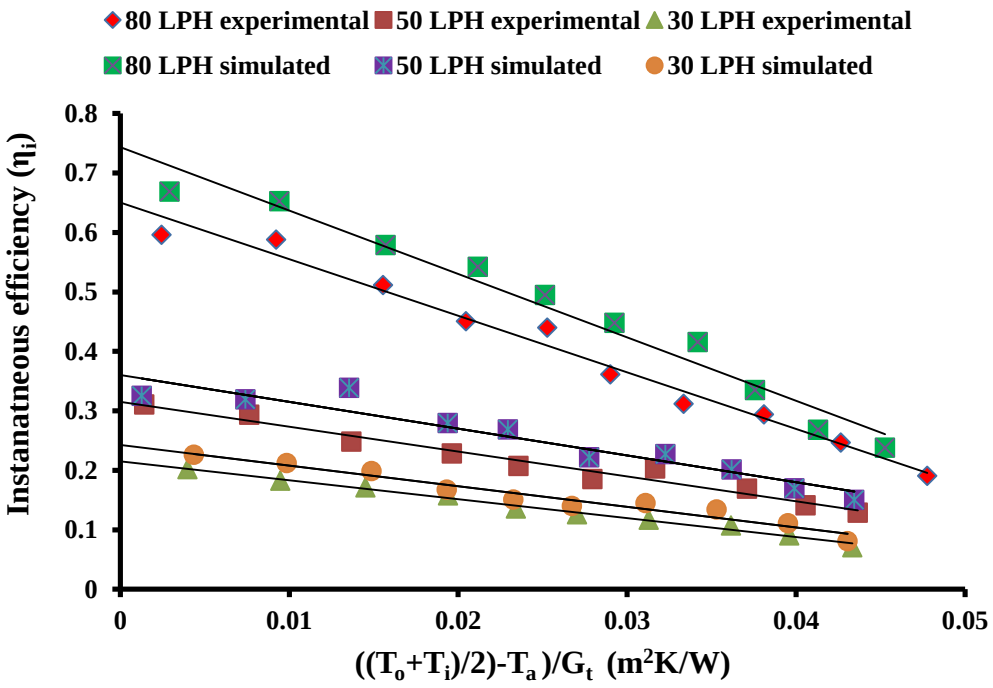

Figure 6.37 efficiency versus $((T_o+T_i)/2)-T_a)/G_t$ curve at three flow rate for 0.075% vol. conc. alumina-water nanofluid

Figure 6.37 shows the variation of both experimental and simulated values of instantaneous efficiency versus reduced temperature parameter $((T_o+T_i)/2)-T_a)/G_t$ with 0.075% alumina-water nanofluid as a working fluid at different mass flow rate (30 LPH, 50 LPH and 80 LPH). It is seen that when average of T_o and T_i equals T_a then

maximum collector efficiency (experimental) is 22%, 33% and 64% at 30 LPH, 50LPH and 80 LPH respectively. While maximum collector efficiency (when average of T_o and T_i equals T_a) through simulated results is 25%, 37% and 72% at 30 LPH, 50 LPH and 80 LPH respectively. It is seen that the collector efficiency is enhanced with increasing volume flow rate. Table 6.3 shows the calculated values of F_RU_L and $F_R(\tau\alpha)$

Table 6.3 Collector efficiency parameters at three flow rates for 0.075% vol. conc. Al_2O_3-H_2O (DI) as working fluid.

Flow rate	Case	F_RU_L	$F_R(\tau\alpha)$
80 LPH	Experimental	9.50	0.65
80 LPH	Simulated	10.66	0.743
50 LPH	Experimental	4.18	0.314
50 LPH	Simulated	4.503	0.360
30 LPH	Experimental	3.190	0.215
30 LPH	Simulated	3.473	0.242

4) 0.1% vol. conc. alumina-water nanofluid as a working fluid

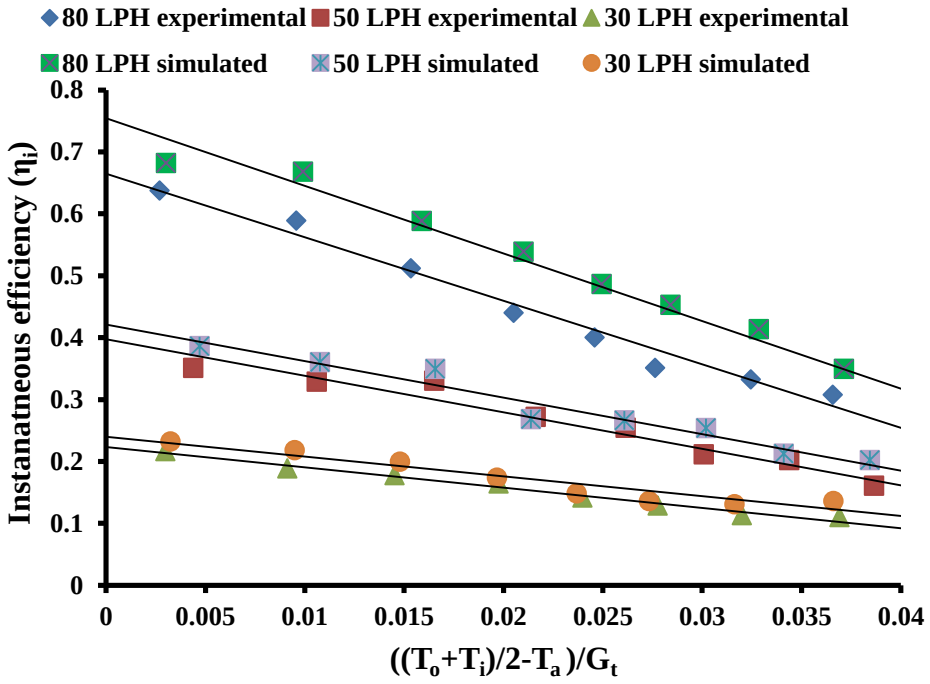

Figure 6.38 efficiency versus $((T_o+T_i)/2)-T_a)/G_t$ curve at three flow rate for 0.1% vol. conc. alumina-water nanofluid

Figure 6.38 shows the variation of both experimental and simulated values of instantaneous efficiency versus reduced temperature parameter $((T_o+T_i)/2)-T_a)/G_t$ with 0.1% alumina-water nanofluid as a working fluid at different mass flow rate (30 LPH, 50 LPH and 80 LPH). It is seen that when average of T_o and T_i equals T_a then maximum collector efficiency (experimental) is 22%, 40% and 68% at 30 LPH, 50LPH and 80 LPH respectively. While maximum collector efficiency (when average of T_o and T_i equals T_a) through simulated results is 25%, 42% and 77% at 30 LPH, 50 LPH and 80 LPH respectively. It is seen that the collector efficiency is enhanced with increasing volume flow rate. Table 6.4 shows the calculated values of F_RU_L and $F_R(\tau\alpha)$.

Table 6.4 Collector efficiency parameters at three flow rates for 0.1% vol. conc. Al_2O_3-H_2O (DI) as working fluid.

Flow rate	Case	F_RU_L	$F_R(\tau\alpha)$
80 LPH	Experimental	10.26	0.664
80 LPH	Simulated	10.39	0.754
50 LPH	Experimental	5.903	0.397
50 LPH	Simulated	5.898	0.421
30 LPH	Experimental	3.283	0.223
30 LPH	Simulated	3.196	0.239

5) 0.125% vol. conc. alumina-water nanofluid as a working fluid

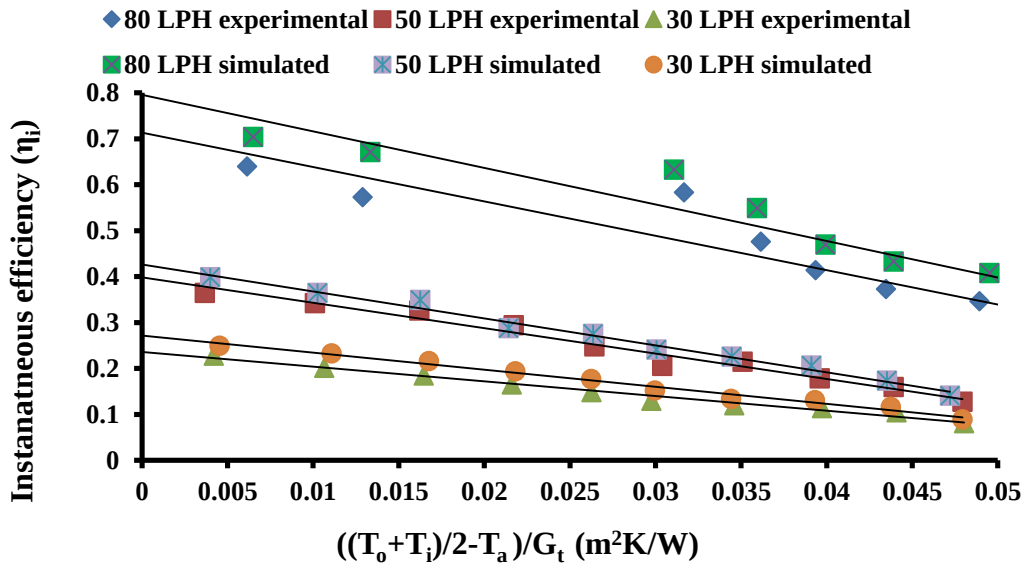

Figure 6.39 efficiency versus $((T_o+T_i)/2)-T_a)/G_t$ curve at three flow rate for 0.125% vol. conc. alumina-water nanofluid

Figure 6.39 shows the variation of both experimental and simulated values of instantaneous efficiency versus reduced temperature parameter $((T_o+T_i)/2)-T_a)/G_t$ with 0.125% alumina-water nanofluid as a working fluid at different mass flow rate (30 LPH, 50 LPH and 80 LPH). It is seen that when average of T_o and T_i equals T_a then maximum collector efficiency (experimental) is 26%, 40% and 71.5% at 30 LPH, 50LPH and 80 LPH respectively. While maximum collector efficiency (when average of T_o and T_i equals T_a) through simulated results is 28%, 44% and 80% at 30 LPH, 50 LPH and 80 LPH respectively. It is seen that the collector efficiency is enhanced with increasing volume flow rate. Table shows the calculated values of F_RU_L and $F_R(\tau\alpha)$.

Table 6.5 Collector efficiency parameters at three flow rates for 0.125% vol. conc. Al_2O_3-H_2O (DI) as working fluid.

Flow rate	Case	F_RU_L	$F_R(\tau\alpha)$
80 LPH	Experimental	7.954	0.795
80 LPH	Simulated	7.480	0.713
50 LPH	Experimental	5.538	0.398
50 LPH	Simulated	5.874	0.426
30 LPH	Experimental	3.190	0.235
30 LPH	Simulated	3.715	0.271

6) Ethylene glycol-water mixture(40:60 by volume) as a working fluid

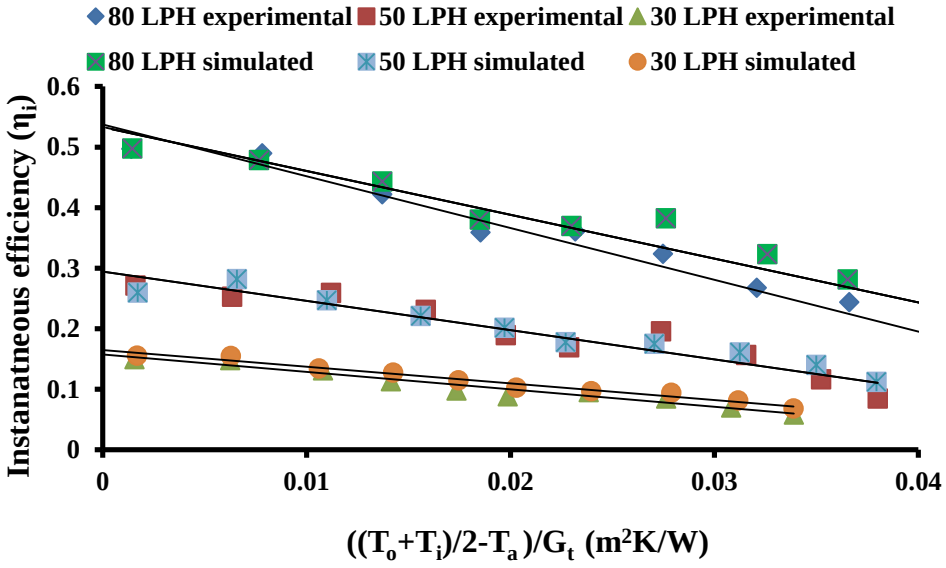

Figure 6.40 efficiency versus $((T_o+T_i)/2)-T_a)/G_t$ curve at three flow rate for ethylene glycol-water mixture (40:60 by volume)

Figure 6.40 shows the variation of both experimental and simulated values of instantaneous efficiency versus reduced temperature parameter $((T_o+T_i)/2)-T_a)/G_t$ with Ethylene glycol-water (40:60 by volume) as a working fluid at different mass flow rate (30 LPH, 50 LPH and 80 LPH). It is seen that when average of T_o and T_i equals T_a then maximum collector efficiency (experimental) is 15%, 30% and 55% at 30 LPH, 50LPH and 80 LPH respectively. While maximum collector efficiency (when average of T_o and T_i equals T_a) through simulated results is 16%, 30% and 55% at 30 LPH, 50 LPH and 80 LPH respectively. It is seen that the collector efficiency is enhanced with increasing volume flow rate. Table shows the calculated values of F_RU_L and $F_R(\tau\alpha)$.

Table 6.6 Collector efficiency parameters at three flow rates for $C_2H_6O_2$-H_2O (DI) mixture (40:60 by vol.) as working fluid.

Flow rate	Case	F_RU_L	$F_R(\tau\alpha)$
80 LPH	Experimental	7.241	0.532
80 LPH	Simulated	8.543	0.537
50 LPH	Experimental	4.833	0.294
50 LPH	Simulated	4.833	0.294
30 LPH	Experimental	2.746	0.164
30 LPH	Simulated	2.879	0.157

7) 0.05% vol. conc. alumina-ethylene glycol-water mixture(40:60 by volume) as a working fluid

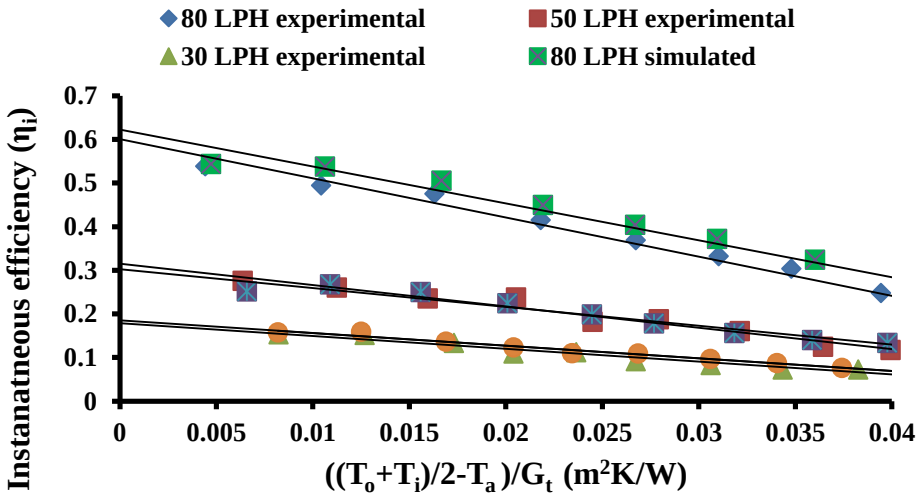

Figure 6.41 efficiency versus $((T_o+T_i)/2)-T_a)/G_t$ curve at three flow rate for 0.05% vol. conc. Al_2O_3- $C_2H_6O_2$-H_2O (DI) mixture (40:60 by vol.)

Figure 6.41 shows the variation of both experimental and simulated values of instantaneous efficiency versus reduced temperature parameter $((T_o+T_i)/2)-T_a)/G_t$ with 0.05% alumina-ethylene glycol-water (40:60 by volume) as a working fluid at different mass flow rate (30 LPH, 50 LPH and 80 LPH). It is seen that when average of T_o and T_i equals T_a then maximum collector efficiency (experimental) is 18%, 31% and 60% at 30 LPH, 50LPH and 80 LPH respectively. While maximum collector efficiency (when average of T_o and T_i equals T_a) through simulated results is 18.5%, 32% and 62% at 30 LPH, 50 LPH and 80 LPH respectively. It is seen that the collector efficiency is enhanced with increasing volume flow rate. Table 6.6 shows the calculated values of F_RU_L and $F_R(\tau\alpha)$.

Table 6.7 Collector efficiency parameters at three flow rates for 0.05% Al_2O_3-$C_2H_6O_2$-H_2O (DI) mixture (40:60 by vol.) nanofluid as working fluid.

Flow rate	Case	F_RU_L	$F_R(\tau\alpha)$
80 LPH	Experimental	8.543	0.600
80 LPH	Simulated	8.970	0.622
50 LPH	Experimental	4.902	0.315
50 LPH	Simulated	4.316	0.302
30 LPH	Experimental	2.897	0.185
30 LPH	Simulated	2.942	0.178

8) 0.075% vol. conc. alumina-ethylene glycol-water (40:60 by volume) as a working fluid

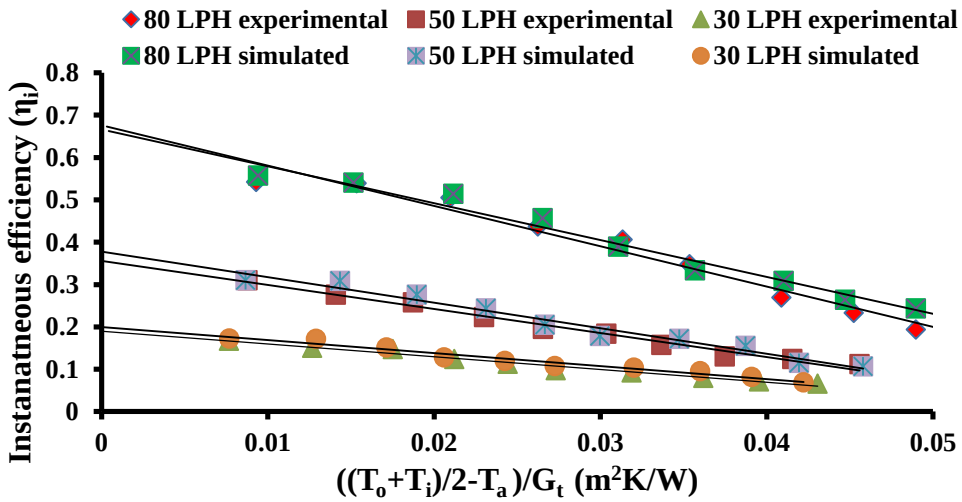

Figure 6.42 efficiency versus $((T_o+T_i)/2)-T_a)/G_t$ curve at three flow rate for 0.075% vol. conc. Al_2O_3- $C_2H_6O_2$-H_2O (DI) mixture (40:60 by vol.)

Figure 6.42 shows the variation of both experimental and simulated values of instantaneous efficiency versus reduced temperature parameter $((T_o+T_i)/2)-T_a)/G_t$ with 0.05% alumina-ethylene glycol-water (40:60 by volume) as a working fluid at different mass flow rate (30 LPH, 50 LPH and 80 LPH). It is seen that when average of T_o and T_i equals T_a then maximum collector efficiency (experimental) is 20%, 37% and 70% at 30 LPH, 50LPH and 80 LPH respectively. While maximum collector efficiency (when average of T_o and T_i equals T_a) through simulated results is 20.5%, 38% and 70% at 30 LPH, 50 LPH and 80 LPH respectively. It is seen that the collector efficiency is enhanced with increasing volume flow rate. Table shows the calculated values of F_RU_L and $F_R(\tau\alpha)$.

Table 6.8 Collector efficiency parameters at three flow rates for 0.075% vol. conc. Al_2O_3- $C_2H_6O_2$-H_2O (DI) (40:60 by vol.) nanofluid as working fluid.

Flow rate	Case	F_RU_L	$F_R(\tau\alpha)$
80 LPH	Experimental	8.543	0.600
80 LPH	Simulated	8.970	0.622
50 LPH	Experimental	4.902	0.315
50 LPH	Simulated	4.316	0.302
30 LPH	Experimental	2.897	0.185
30 LPH	Simulated	2.942	0.178

9) 0.1% vol. conc. alumina-ethylene glycol-water mixture (40:60 by volume) as a working fluid

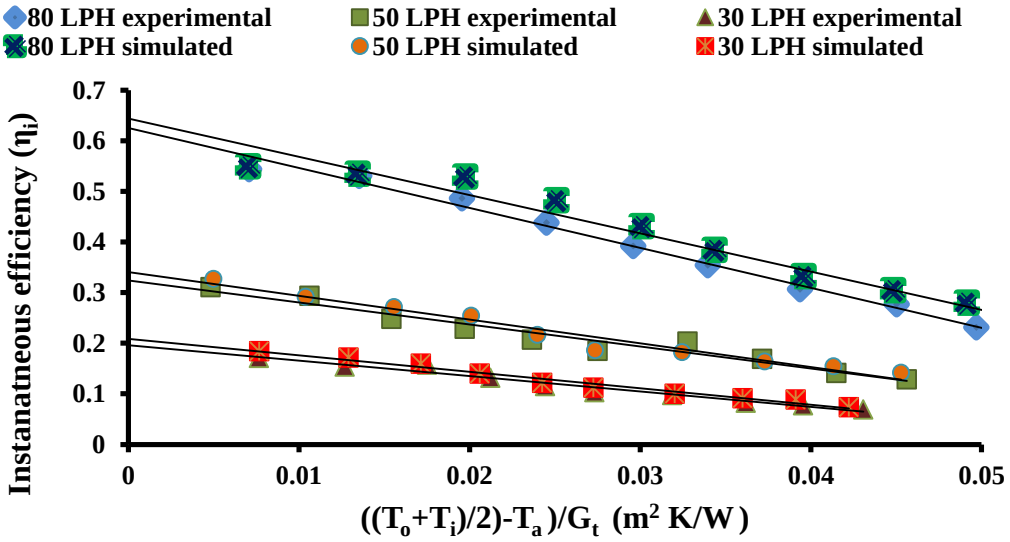

Figure 6.43 efficiency versus $((T_o+T_i)/2)-T_a)/G_t$ curve at three flow rate for 0.1% vol. conc. Al_2O_3- $C_2H_6O_2$-H_2O (DI) mixture (40:60 by vol.)

Figure 6.43 shows the variation of both experimental and simulated values of instantaneous efficiency versus reduced temperature parameter $((T_o+T_i)/2)-T_a)/G_t$ with 0.1% alumina-ethylene glycol-water (40:60 by volume) as a working fluid at different mass flow rate (30 LPH, 50 LPH and 80 LPH). It is seen that when average of T_o and T_i equals T_a then maximum collector efficiency (experimental) is 21.5%, 33.5% and 64.5% at 30 LPH, 50LPH and 80 LPH respectively. While maximum collector efficiency (when average of T_o and T_i equals T_a) through simulated results is 22.5%, 35% and 66% at 30 LPH, 50 LPH and 80 LPH respectively. It is seen that the collector efficiency is enhanced with increasing volume flow rate. Table shows the calculated values of F_RU_L and $F_R(\tau\alpha)$.

Table 6.9 Collector efficiency parameters at three flow rates for 0.1% vol. conc. Al_2O_3- $C_2H_6O_2$-H_2O (DI) mixture (60:40 by vol.) nanofluid as working fluid.

Flow rate	Case	F_RU_L	$F_R(\tau\alpha)$
80 LPH	Experimental	7.566	0.644
80 LPH	Simulated	7.902	0.625
50 LPH	Experimental	4.349	0.324
50 LPH	Simulated	4.678	0.340
30 LPH	Experimental	3.047	0.196
30 LPH	Simulated	3.253	0.208

10) 0.125% vol. conc. alumina-ethylene glycol-water mixture(40:60 by volume) as a working fluid

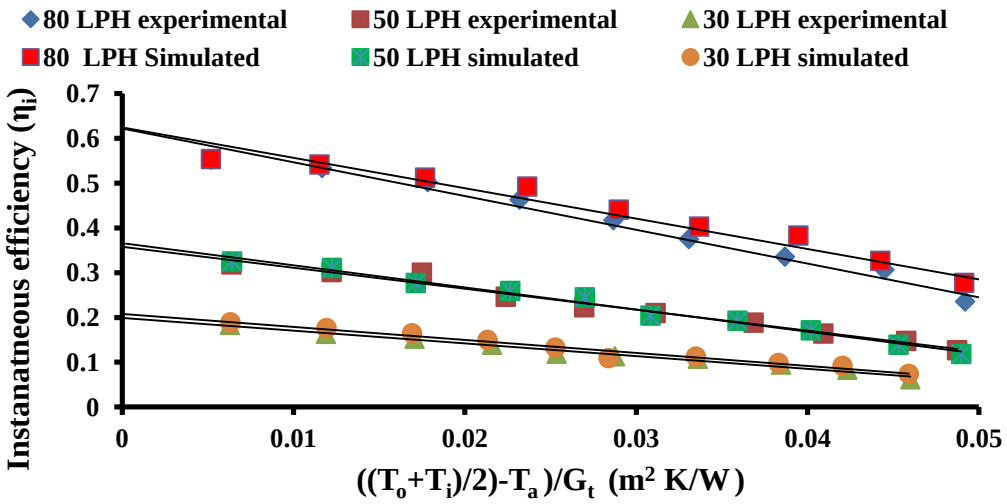

Figure 6.44 efficiency versus $((T_o+T_i)/2)-T_a)/G_t$ curve at three flow rate for 0.125% vol. conc. Al_2O_3- $C_2H_6O_2$-H_2O (DI) mixture (40:60 by vol.)

Figure 6.44 shows the variation of both experimental and simulated values of instantaneous efficiency versus reduced temperature parameter $((T_o+T_i)/2)-T_a)/G_t$ with 0.125% alumina-ethylene glycol-water (40:60 by volume) as a working fluid at different mass flow rate (30 LPH, 50 LPH and 80 LPH). It is seen that when average of T_o and T_i equals T_a then maximum collector efficiency (experimental) is 22%, 38% and 62% at 30 LPH, 50LPH and 80 LPH respectively. While maximum collector efficiency (when average of T_o and T_i equals T_a) through simulated results is 22.5%, 39% and 63.5% at 30 LPH, 50 LPH and 80 LPH respectively. It is seen that the collector efficiency is enhanced with increasing volume flow rate. Table shows the calculated values of F_RU_L and $F_R(\tau\alpha)$.

Table 6.10 Collector efficiency parameters at three flow rates for 0.125% vol. conc. Al_2O_3- $C_2H_6O_2$-H_2O (DI) mixture (60:40 by vol.) nanofluid as working fluid.

Flow rate	Case	F_RU_L	$F_R(\tau\alpha)$
80 LPH	Experimental	6.78	0.624
80 LPH	Simulated	7.549	0.622
50 LPH	Experimental	4.685	0.357
50 LPH	Simulated	4.936	0.365
30 LPH	Experimental	2.850	0.199
30 LPH	Simulated	2.906	0.208

6.6 Effect of Different Working Fluids on Solar Collector's Overall Efficiency

Effect of different working fluids on the collector's overall efficiency (both experimental and simulated value) is depicted in figure

1) Effect of water and alumina-water based nanofluid of various vol. conc. as a working fluid on collector's overall efficiency at 30 LPH

Figure 6.45 shows the comparison of water and water based nanofluid of different volumetric concentration at volume flow rate of 30 LPH on collector overall efficiency through both experimental and simulated results respectively. From experimental results it is seen that an improvement of about 7.87%, 8.12%, 9.29% and 9.71% is seen with usage of Al_2O_3-H_2O nanofluid of 0.05%, 0.075%, 0.1% and 0.125% respectively as compared with water, while from CFD simulated results an

improvement of about 8.06%, 8.29%, 8.83% and 10.66% is seen with usage of Al_2O_3-H_2O nanofluid of 0.05%, 0.075%, 0.1% and 0.125% respectively as compared with water. Moreover there is also a close agreement between both experimental and simulated results.

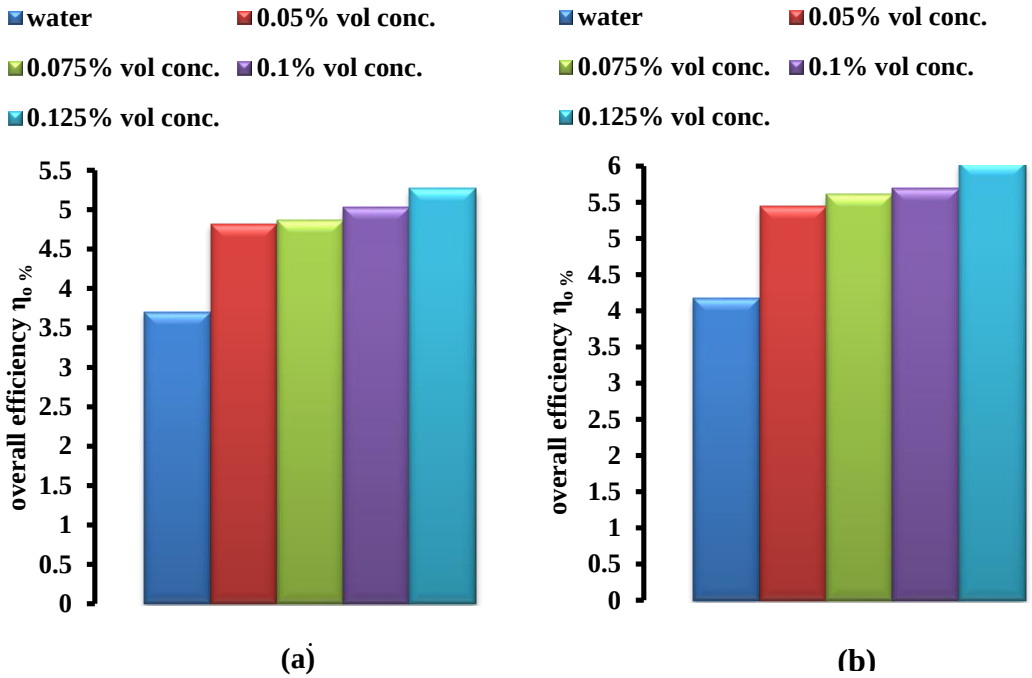

Figure 6.45 Effect of water and alumina-water based nanofluid of various vol. conc. as a working fluid on collector's overall efficiency at 30 LPH (a) Experiential value (b) Simulated value.

2) Effect of water and alumina-water based nanofluid of various vol. conc. as a working fluid on collector's overall efficiency at 50 LPH

Figure 6.46 shows the comparison of water and water based nanofluid of different volumetric concentration at volume flow rate of 50 LPH on collector overall efficiency through both experimental and simulated results respectively. From experimental results it is seen that an improvement of about 7.96%, 8.11%, 8.84% and 11.87% is seen with usage of Al_2O_3-H_2O nanofluid of 0.05%, 0.075%, 0.1% and 0.125% respectively as compared with water, while from CFD simulated results an improvement of about 8.08%, 8.32%, 9.47% and 12.43% is seen with usage of Al_2O_3-H_2O nanofluid of 0.05%, 0.075%, 0.1% and 0.125% respectively as compared with water. Moreover there is also a close agreement between both experimental and simulated results.

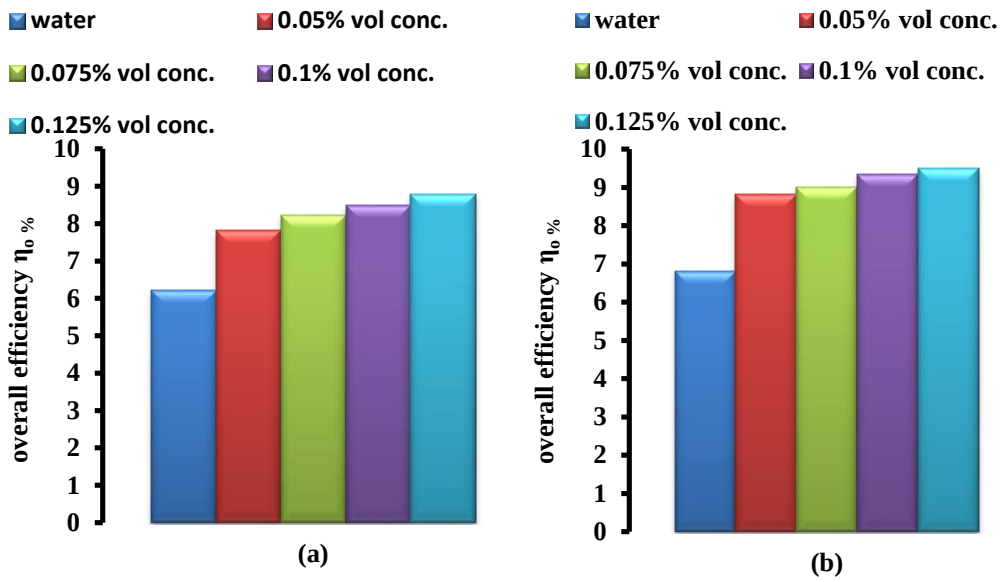

Figure 6.46 Effect of water and alumina-water based nanofluid of various vol. conc. as a working fluid on collector's overall efficiency at 50 LPH (a) Experiential value (b) Simulated value

3) Effect of water and alumina-water based nanofluid of various vol. conc. as a working fluid on collector's overall efficiency at 80 LPH

Figure 6.47 shows the comparison of water and water based nanofluid of different volumetric concentration at volume flow rate of 30 LPH on collector overall efficiency through both experimental and simulated results respectively. From experimental results it is seen that an improvement of about 7.98%, 8.31%, 9.40% and 13.98% is seen with usage of Al_2O_3-H_2O nanofluid of 0.05%, 0.075%, 0.1% and 0.125% respectively as compared with water, while from CFD simulated results an improvement of about 8.23%, 8.87%, 11.19% and 16.84% is seen with usage of Al_2O_3-H_2O nanofluid of 0.05%, 0.075%, 0.1% and 0.125% respectively as compared with water. Moreover there is also a close agreement between both experimental and simulated results.

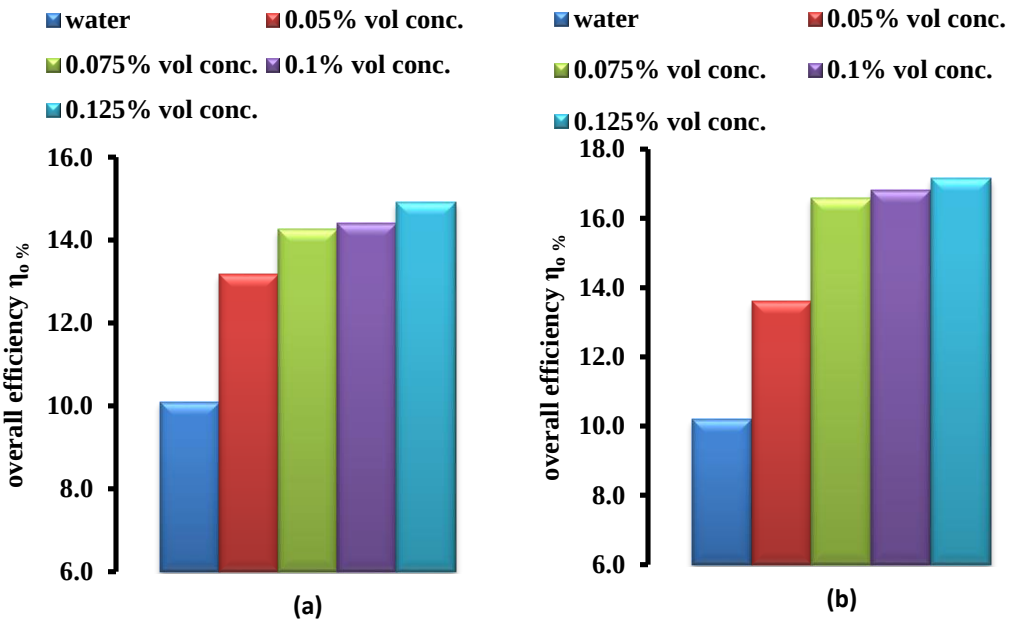

Figure 6.47 Effect of water and alumina -water based nanofluid of various vol. conc. as a working fluid on collector's overall efficiency at 80 LPH (a) Experiential value (b) Simulated value

4) Effect of water-ethylene glycol (60: 40 by vol.) and alumina water-ethylene glycol (60:40 by vol.) based nanofluid of various vol. conc. as a working fluid on collector's overall efficiency at 30 LPH

Figure 6.48 shows the comparison of water-ethylene glycol (60:40 by vol.) and alumina water-ethylene glycol (60:40 by vol.) based nanofluid of different volumetric concentration at volume flow rate of 30 LPH on collector overall efficiency through both experimental and simulated results respectively. From experimental results it is seen that an improvement of about 4%, 7%%, 12.1% and 14.9% is seen with usage of Al_2O_3-$C_2H_6O_2$-H_2O nanofluid of 0.05%, 0.075%, 0.1% and 0.125% respectively as compared with water, while from CFD simulated results an improvement of about 5.7%, 6.9%, 9.09 % and 14.06% is seen with usage of Al_2O_3-$C_2H_6O_2$-H_2O nanofluid of 0.05%, 0.075%, 0.1% and 0.125% respectively as compared with water. Moreover there is also a close agreement between both experimental and simulated results.

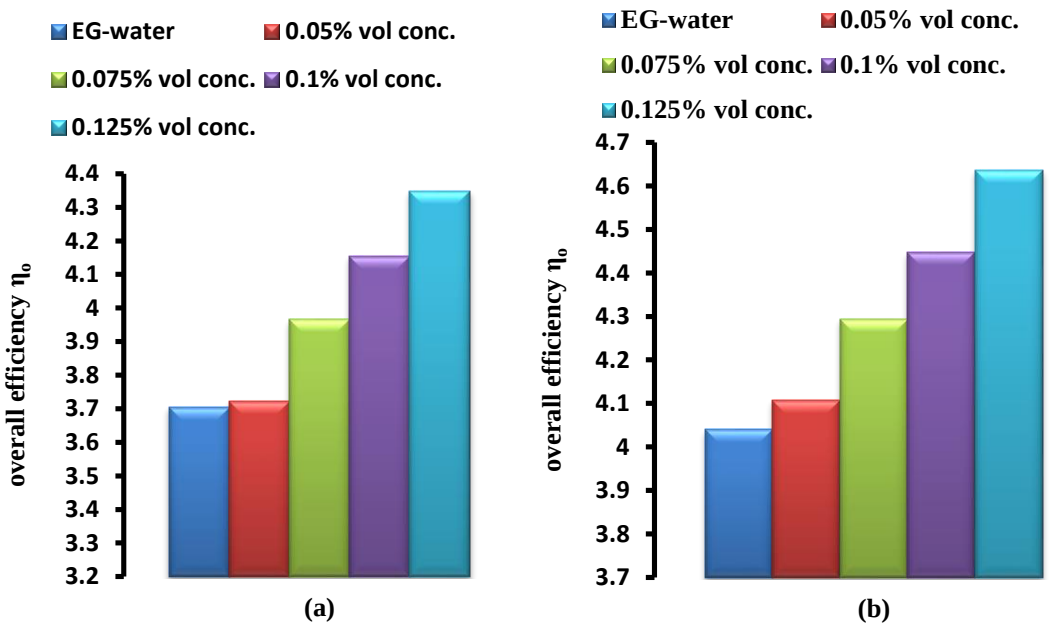

Figure 6.48 Effect of water- ethylene glycol mixture (60:40 by vol.) and alumina-water-ethylene glycol mixture (60:40 by vol.) based nanofluid as a working fluid on collector's overall efficiency at 30 LPH (a) Experiential value (b) Simulated value

5) Effect of water-ethylene glycol (60:40 by vol.) and alumina water-ethylene glycol (60:40 by vol.) based nanofluid of various vol. conc. as a working fluid on collector's overall efficiency at 50 LPH

Figure 6.49 shows the comparison of water-ethylene glycol mixture (60: 40 by vol.) and alumina water-ethylene glycol mixture (60:40 by vol.) based nanofluid of different volumetric concentration at volume flow rate of 50 LPH on collector overall efficiency through both experimental and simulated results respectively. From experimental results it is seen that an improvement of about 2.8%, 5.8%, 9.8% and 15.8% is seen with usage of n Al_2O_3-$C_2H_6O_2$-H_2O nanofluid of 0.05%, 0.075%, 0.1% and 0.125% respectively as compared with water, while from CFD simulated results an improvement of about 3.2%, 5.8%, 10.82% and 13.3% is seen with usage of Al_2O_3-$C_2H_6O_2$-H_2O nanofluid of 0.05%, 0.075%, 0.1% and 0.125% respectively as compared with water. Moreover there is also a close agreement between both experimental and simulated results.

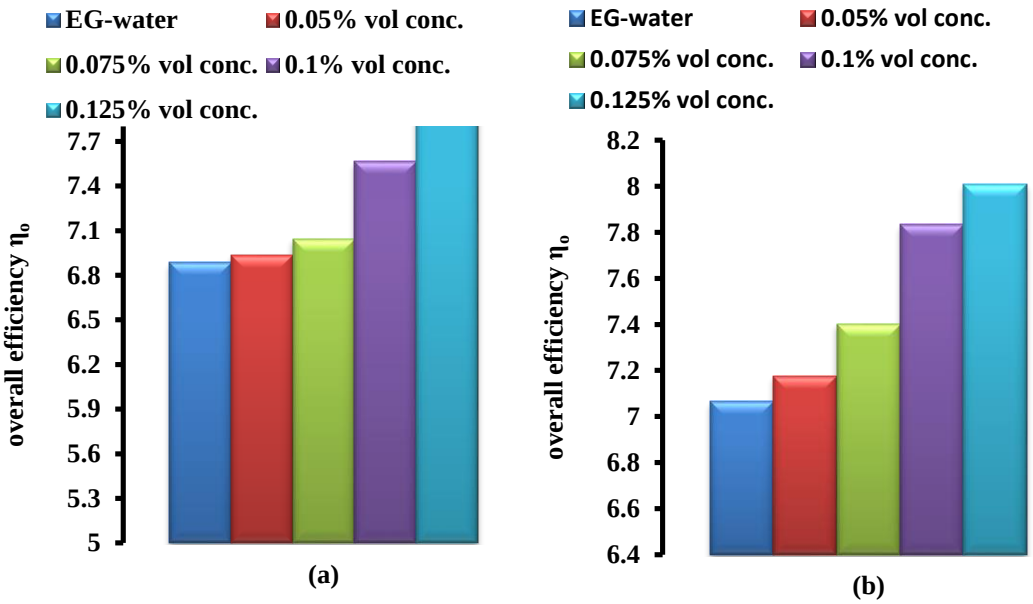

Figure 6.49 Effect of water- ethylene glycol mixture (60:40 by vol.) and alumina-water-ethylene glycol mixture (60:40 by vol.) based nanofluid as a working fluid on collector's overall efficiency at 50 LPH (a) Experiential value (b) Simulated value

6) Effect of water-ethylene glycol (60: 40 by vol.) and alumina water-ethylene glycol (60:40 by vol.) based nanofluid of various vol. conc. as a working fluid on collector's overall efficiency at80 LPH.

Figure 6.50 shows the comparison of water-ethylene glycol (60: 40 by vol.) and alumina water-ethylene glycol (60:40 by vol.) based nanofluid of different volumetric concentration at volume flow rate of 80 LPH on collector overall efficiency through both experimental and simulated results respectively. From experimental results it is seen that an improvement of about 7.7%, 11.3%, 15.6% and 16.7% is seen with usage of Al_2O_3-$C_2H_6O_2$-H_2O nanofluid of 0.05%, 0.075%, 0.1% and 0.125% respectively as compared with water, while from CFD simulated results an improvement of about 8.35%, 10.99%, 13.4% and 17.09% is seen with usage of Al_2O_3-$C_2H_6O_2$-H_2O nanofluid of 0.05%, 0.075%, 0.1% and 0.125% respectively as compared with water. Moreover there is also a close agreement between both experimental and simulated results.

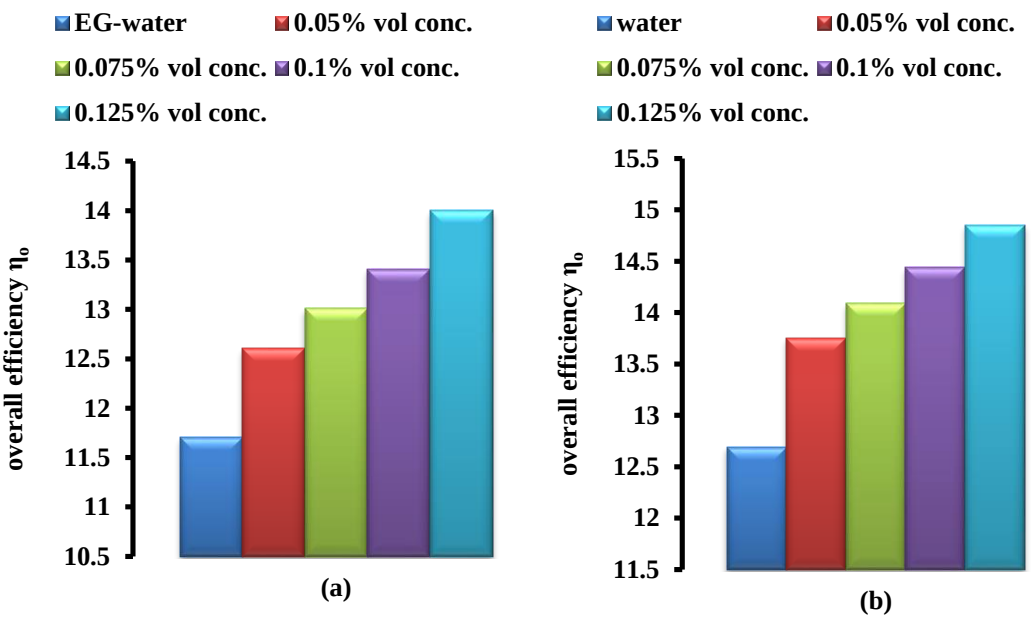

Figure 6.50 Effect of water- ethylene glycol mixture (60:40 by vol.) and alumina-water-ethylene glycol mixture (60:40 by vol.) based nanofluid as a working fluid on collector's overall efficiency at 80 LPH (a) Experiential value (b) Simulated value

CHAPTER 6

CONCLUSIONS AND FUTURE SCOPE

6.1 Conclusions

- From both experimental and CFD simulated results, it is reported that there is an improvement in the overall efficiency of the solar collector when H_2O and H_2O-$C_2H_6O_2$ mixture (60:40 by volume) is replaced by Al_2O_3-H_2O(DI) nanofluid of different volumetric concentrations (0.05%, 0.075%, 0.1% and 0.125%) and Al_2O_3-H_2O(DI)-$C_2H_6O_2$ nanofluid of different volumetric concentration(0.05%, 0.075% ,0.1% and 0.125%) respectively.
- Improvement in both thermal and instantaneous efficiency is reported through both experimental and CFD simulated results, when volumetric concentration of the nanofluid is made to increase. With 0.125% vol. conc. Al_2O_3-H_2O (DI) nanofluid at 80 LPH max. thermal and instantaneous efficiency of 24.3 % and 68.5% is seen respectively.
- With the increment in the volume flow rate of the working fluid, corresponding enhancement in the collector's efficiency is witnessed. Improvement of about 18% is seen as the volume flow rate of 0.125% vol. conc. Al_2O_3-H_2O (DI) nanofluid is increased from 30 LPH to 80 LPH.
- Al_2O_3-H_2O (DI) based nanofluid has shown better collector efficiency as compared to Al_2O_3-$C_2H_6O_2$- H_2O (DI) (60:40 by vol.) nanofluid of same volumetric concentration at same mass flow rate. Overall efficiency of 16.8 % and 13.2% is seen with 0.125% vol. conc. Al_2O_3-H_2O (DI) and 0.125% vol. conc. Al_2O_3-H_2O-$C_2H_6O_2$ (mixture of 60:40 by vol.) nanofluids respectively.
- Both experimental value of collector efficiency and simulated value of collector efficiency are in close agreement, with a difference of 11%.

6.2 Future Scope

The various investigations that can be carried out on nanofluid based parabolic shaped concentrating solar collector are as follows:

a) Both experimental and CFD analysis can be carried out with different nanoparticle (material) and of different volumetric concentration.
b) Investigation can be carried out with different base fluid like therminol VP-1 and other heat transfer fluid.
c) Effect of nanoparticle sized on collector performance can be evaluated.
d) Exergy analysis of nanofluid based parabolic solar collector can be carried out.

REFERENCES

[1] Lakalos L., Hevessy G. and Kovacs J., (2011), Advantages and disadvantages of solar energy, "*The Journal of General Revolution*", vol. 67, pp. 395-408.

[2] Barlev D., Vidu R., Stroeve P.,(2011), Innovation in concentrated solar power, "*Solar Energy Materials & Solar Cells*", vol. 95 (10), pp. 2703-2725.

[3] Reddy K.S., Kumar K.R., (2011), Solar collector field design and viability analysis of standalone parabolic trough power plants for Indian conditions, "*Energy for Sustainable Development*", vol. 16 (4), pp. 456-470.

[4] Thirugnanasambandam M., Iniyan S., Goic R., (2010), A review of solar thermal technologies, "*Renewable Sustainable Energy Reviews*", vol. 14(1), pp. 312-322.

[5] Yadav A., Kumar M., Balram, (2013), Experimental study and analysis of parabolic trough collector with various reflectors, "*International Journal of Physical Nuclear Science and Engineering*", vol. 7(12), pp. 281-285.

[6] Chow T.T., (2009), A review on photovoltaic/ thermal hybrid solar technology, "*Applied Energy*", vol. 87 (2), pp.365-379.

[7] Sozen A., Menlik T., Unvar S., (2008), Determination of efficiency of flat plate solar collectors using neural network approach, "*Energy Systems and Approach*" vol. 35, pp. 1533-1539.

[8] Zhai H., Dai V.J., Wu J.Y., Wang R.Z., Zhang L.Y., (2010), Experimental investigation and analysis of a concentrating solar collector using linear Fresnel lens, " *Energy Conversion and Management*", vol. 51, pp. 48-55.

[9] Tian Y., Zhao C.Y., (2013), A review of solar collectors and thermal storage in solar thermal applications, "*Applied Energy*", vol. 104, pp. 538-553.

[10] Philip John, Shima P.D., (2012), Thermal properties of nanofluids, "*Advances in Colloidal and Interface Surface*", vol.10 (4), pp. 30-45.

[11] Lee S., Choi S., Li S., Eastman J.A., (1999), Measuring thermal conductivity of fluids containing oxide nanoparticles, "*Journal of Heat Transfer*", vol. 121 (2), pp.280-289.

[12] Wong K.V., De Leon O., (2010), Applications of nanofluids: current and future, "*Advances in Mechanical Engineering*", vol. (10), article ID 519659, pp. 1-11 doi: 10.1155/2015/519659.

[13] Mahian O., Kianifar A., Kalogirou S.A., Pop I., Wongwises S., (2013), A review of the applications of nanofluids in solar energy, "*International Journal of Heat and Mass transfer*" vol. 57 (2), pp. 582-594.

[14] Yousefi T., Veisy F., Shojaeizadeh E., Zinadini S.,(2012c), An experimental investigation on the effect of pH variation of MWCNT-H_2O nanofluid on the efficiency of a flat plate solar collector, " *Solar Energy*", vol. 86 (2), pp. 771-779.

[15] Zhang X., Gu H., Fuji M., (2007), Effective thermal conductivity and thermal diffusivity of nanofluids containing spherical and cylindrical nanoparticles, "*Experimental Thermal and Fluid Science*", vol. 31(6), pp. 593-599.

[16] Tyagi H., Phelan P., Prasher R., (2009), Predicted efficiency of a low temperature nanofluid-based direct absorption solar collector, "*Journal of Solar Engineering*", vol. (31), pp. 041004-1 to 7.

[17] Natarajan E. & Satish R., (2009), Role of nanofluids in solar water heater, "*International Journal of Advanced Manufacturing Technology",* special issue, doi 10.1007/s00170-008-1876-8.

[18] Khullar V., Tyagi H., (2010), Applications of nanofluids as the working fluid in concentrating parabolic solar collectors, "*37th National & 4th International Conferences on Fluid Mechanics & Fluid Power*", IIT madras, Chennai, India, Dec. 16-18, paper No. FMFP 2010-179.

[19] Otanicar T.P., Phelan P.E., Prasher R.S., Rosengarten G., and taylor R.A., (2010), Nanofluid based direct absorption solar collector, "*Journal of Renewable and Sustainable Energy*", vol. 2 (3), pp. 033102-1 to 13.

[20] Saini E., Barison S., Pagura C., Mercatelli L., Sansoni P., Fontani D., Jafranceso D., and Francini F., (2010), Carbon nanohorns based nanofluids as direct sunlight absorbers, "*Journal Optic Express*", vol. 18 (5), pp. 1-9.

[21] Taylor R.A., Phelan P.E., Otanicar T.P., Walker C.A., Nguyen M., Trimble S. and Prasher R.,(2011a), Applicability of nanofluids in high flux solar collectors, " *Journal of Renewable and Sustainable Energy*", vol. 3 (2), pp. 023104-1 to 15.

[22] Taylor R.A., Phelan P.E., Otanicar T.P., Adrian R., Prasher R.P., (2011b), Nanofluid optical property characterization towards efficient direct absorption solar collectors, "*Nanoscale Research Letters*", vol. 6 (1), pp. 225.

[23] Marcetelli L., Saini E., Fontani D., Zaccanti., Martelli F., Di Ninni P., (2011), Scattering and absorption properties of carbon nanohorns-based nanofluids for solar energy applications, "*Journal of the European Optical Society- Rapid Publications*", vol. 6, pp. 11025-1 to 5.

[24] Han D., Meng Z., Wu D., Zhang C., Zhu H., (2011), Thermal properties of carbon black aqueous nanaofluids for solar absorption, " *Nanoscale Research Letters*", vol. 6, pp. 1-7.

[25] Saini E., Mercatelli L., Barison S., Pagura C., Agresti F., Colla L., Sansoni P., (2011), Potential of carbon nanohorns-based suspensios for solar thermal collectors, "*Solar Energy Materials & Solar Cells",* vol. 95 (11), pp. 2994-3000.

[26] Yousefi T., Veisy F., Shojaeizadeh E., Zinadini S., (2012a), An experimental investigation on the effect of Al_2O_3-H_2O nanofluid on the efficiency of flat plate solar collectors, " *Renewable Energy*", vol. 39, pp. 293-298.

[27] Yousefi T., Veisy F., Shojaeizadeh E., Zinadini S.,(2012b), An experimental investigation on the effect of MWCNT-H_2O nanofluid on the efficiency of flat plate solar collectors, " *Experimental Thermal and Fluid Science*", vol. 39, pp. 207-212.

[28] Saidur R., Leong K.Y., Mohammad H.A., (2011), A review on applications and challenges of nanofluids, " *Renewable and Sustainable Energy Reviews*", vol. 15 (3), pp. 1646-1668.

[29] Khullar V., Tyagi H., (2012a), A study on environmental impact of nanofluid based concentrating solar water heating system, "*International Journal of Environmental Studies*", vol. 69 (2), pp. 220-232.

[30] Khullar V., Tyagi H., Phelan P.E., Otanicar T.P., Singh H., Taylor R.A., (2012b), Solar energy harvesting using nanofluids-based concentrating solar collector, "J*ournal of Nanotechnology in Engineering and Medicine*", vol. 3, pp. 031003-1 to 9.

[31] Chougule S., Pise T., Madane K., Pravin A., (2012), Performance of nanofluid charged solar water heater by solar tracking system, In: Proceedings of "IE*EE-International Conference On Advances In Engineering Science And Management (ICAESM-2012)"* March 30-31, 2012, pp. 247-253.

[32] Chaji H., Ajabshirchi Y., Esmaeilzadeh E., Heris Saeid Z., Hedyatizadeh M., Kahani M., (2013), Experimental study on thermal efficiency of flat plate solar collector using TiO_2/ water nanofluid, "*Modern Applied Science*" published by Canadian Centre of science and Education, vol. 7 (10), pp.60-69.

[33] Tiwari A.K., Ghosh P., Sarkar J., Purthi A., (2013), Solar water heating using nanofluids- a comprehensive overview and environmental impact analysis, "*International Journal of Emerging Technology and Advanced Engineering*", vol. 3 (3): ICERTSD 2013, pp. 221-224.

[34] Maddah H., Rezazadeh M., Maghsoudi M, Nasirkohdan S., (2013), The effect of silver and aluminium oxide nanoparticles on thermophysical properties of nanofluids, "*Journal of Nanostructure in Chemistry*", vol. 3, pp.1-6.

[35] Akbari M., Galanis N. and Behzadmehr A., (2011), Comparative analysis of a single & two phase models for CFD studies of nanofluid heat transfer, "*International journal of thermal sciences*", vol. 50, pp. 1343-1354.

[36] Tarybaksh M.R., Neyestanak A. L., Mohammad A., Tarybaksh H., (2013), CFD study on wall/ nanoparticle interaction in nanofluids convective heat transfer, "*Advances in Materials Science & Engineering*" vol. 2, article ID 651365, pp. 1-8, doi: 10.1155.

[37] Yu W., Xie H., (2012), A review on nanofluids: preparation, stability mechanisms & applications, "*Journal of nanomaterials*"vol. 1, article ID 435873, pp. 1-17, doi:10.1155/2012/435873.

[38] Said Z., Sajid M.H., Alim M.A., Saidur R., Rahim N.A., (2012), Experimental investigation of the thermophysical properties of Al_2O_3 nanofluid & its effect on a flat plate solar collector, "*International communications in Heat and Mass Transfer*", vol. 48, pp. 94-107.

[39] Pravin S., Nasrin R., Alim M.A., (2014), Heat transfer & entropy generation through nanofluid filled direct absorption solar collector, "*International Journal of Heat and Mass Transfer*", vol. 71, pp. 386-395.

[40] Zhoangyang L., Wang C., Wei W., Xiao G., Ni M., (2014), Performance improvement of a nanofluid solar collector based on direct absorption collection (DAC) concepts, "*International Journal of Heat and Mass Transfer"*, vol. 75, pp. 262-271.

[41] Qinbo H., Zeng S., Wang S., (2014), Experimental investigation on the efficiency of flat plate collectors with nanofluids, " *Applied Thermal Engineering*", vol. 61, pp. 1-7.

[42] Zamzamiam A., Rad M.A., Neyestani M.K., (2014), An experimental study on the effect of flat plate solar collectors, "*Renewable Energy*", vol. 71, pp. 658-664.

[43] Alim M.A., Abdin Z., Saidur R., Hepbasli A., Khairul., Rahim N.A., (2013), Analyses of entropy generation & pressure drop for a conventional flat plate solar collector using different types of metal oxide nanofluid, "*Energy Building*s", vol. 66, pp. 289-296.

[44] Moghadam A.J., Gord M.F., Sajadi M., Zadeh M.H., (2014), Effect of CuO/water nanofluid on the efficiency of a flat plate solar collector, "*Experimental Thermal Science*", vol. 58, pp. 9-14

APPENDIX A

Table A.1 Experimental and simulated data for water as a working fluid at 30 LPH (8/4/2015)

Time	T_{in} (^oC)	T_{out}) (^oC). (Exp.)	T_{out} (^oc) (Sim.)	Exp. G_t (W/m^2)	Sim. G_t (W/m^2)
9.30-10am	36.2	40.1	40.7	808	838
10-10.30 am	40.8	44.3	44.78	847	852
10.30-11 am	45	48.5	48.97	872	899
11-11.30 am	48.8	52.1	52.118	938	921
11.30-12 pm	52.7	55.9	56.532	926	947
12-12.30 pm	56.3	59.4	59.876	965	973
12.30- 1 pm	59.9	62.6	62.897	951	964
1-1.30 pm	63	65.8	65.918	926	943
1.30-2 pm	65.8	67.6	68.176	894	910
2-2.30 pm	68	69.2	69.718	862	889

Time	η_i (Exp.)	η_i (Sim.)	η_t (Exp.)	η_t (Sim.)
9.30-10am	15.42241	17.15804	5.510167	6.130276
10-10.30 am	13.20334	14.92597	4.717329	5.332796
10.30-11 am	12.8248	14.11009	4.582084	5.041298
11-11.30 am	11.24114	11.51107	4.016267	4.112712
11.30-12 pm	11.04175	12.92929	3.945032	4.619416
12-12.30 pm	10.2644	11.74313	3.667295	4.19562
12.30- 1 pm	9.071567	9.933648	3.241117	3.549124
1-1.30 pm	9.661535	9.887185	3.451903	3.532524
1.30-2 pm	6.433304	8.342652	2.298511	2.980688
2-2.30 pm	4.448085	6.174766	1.589225	2.206139

Table A.2 Experimental and simulated data for water as a working fluid at 50 LPH (9/4/2015)

Time	T_{in} (^oC)	T_{out}) (^oC). (Exp.)	T_{out} (^oc) (Sim)	Exp. G_t (W/m^2)	Sim. G_t (W/m^2)
9.30-10am	34.8	38.5	38.902	808	839
10-10.30 am	38.3	42.1	42.416	840	856
10.30-11 am	42	46	46.135	868	869
11-11.30 am	46	49.6	49.832	922	926
11.30-12 pm	49.6	52.9	53.218	961	978
12-12.30 pm	52.9	56	56.227	959	965
12.30- 1 pm	56	58.7	59.108	947	952
1-1.30 pm	58.7	61.1	61.543	926	948
1.30-2 pm	61.1	62.7	63.118	913	929
2-2.30 pm	62.7	63.8	64.153	888	901

Time	η_i (Exp.)	η_i (Sim.)	η_t (Exp.)	η_t (Sim.)
9.30-10am	24.38587	26.03644	8.71266	9.30238
10-10.30 am	24.09085	25.60645	8.60725	9.14875
10.30-11 am	24.54076	25.33982	8.76800	9.05349
11-11.30 am	20.79311	22.03750	7.42903	7.87363
11.30-12 pm	18.28683	19.70051	6.53357	7.03866
12-12.30 pm	17.21436	18.36003	6.15040	6.55973
12.30- 1 pm	15.18314	17.38569	5.42468	6.21161
1-1.30 pm	13.80219	15.97042	4.93129	5.70596
1.30-2 pm	9.33248	11.56787	3.33434	4.13300
2-2.30 pm	6.59671	8.58793	2.35689	3.06832

Table A.3 Experimental and simulated data for water as a working fluid at 80 LPH (10/4/2015)

Time	T_{in} (^oC)	T_{out}) (^oC). (Exp.)	T_{out} (^oc) (Sim)	Exp. G_t (W/m^2)	Sim. G_t (W/m^2)
9.30-10am	34.5	38	37.828	780	782
10-10.30 am	37.8	41.4	41.14	816	828
10.30-11 am	41.5	45.2	44.85	847	852
11-11.30 am	45.3	49	48.66	920	916
11.30-12 pm	49	52.4	52.374	950	963
12-12.30 pm	52.4	55.5	55.786	955	959
12.30- 1 pm	55.5	58.3	58.51	943	936
1-1.30 pm	58.3	60.6	60.98	917	910
1.30-2 pm	60.6	62.5	62.72	882	901
2-2.30 pm	62.5	63.7	64.252	839	856

Time	η_i (Exp.)	η_i (Sim.)	η_t (Exp.)	η_t (Sim.)
9.30-10am	36.26	38.23	13.66	12.96
10-10.30 am	34.37	37.59	13.43	12.28
10.30-11 am	33.50	37.22	13.30	11.97
11-11.30 am	31.25	34.27	12.24	11.17
11.30-12 pm	29.85	30.49	10.90	10.67
12-12.30 pm	30.08	27.66	9.88	10.75
12.30- 1 pm	27.40	25.30	9.04	9.79
1-1.30 pm	25.09	21.37	7.64	8.97
1.30-2 pm	20.05	18.35	6.56	7.16
2-2.30 pm	17.44	12.19	4.35	6.23

APPENDIX B

Table A.4 Experimental and simulated data for 0.05% alumina-water nanofluid as a working fluid at 30 LPH (18/4/2015)

Time	T_{in} (^oC)	T_{out}) (^oC). (Exp.)	T_{out} (^oc) (Sim)	Exp. G_t (W/m^2)	Sim. G_t (W/m^2)
9.30-10am	29.1	33.9	34.367	812	798
10-10.30 am	33.6	38.6	38.893	838	825
10.30-11 am	38.6	43.3	43.963	872	868
11-11.30 am	43.3	47.5	48.12	889	900
11.30-12 pm	47.5	51.3	51.736	901	907
12-12.30 pm	51.3	55.3	55.414	918	928
12.30- 1 pm	55.3	58.8	59.263	906	909
1-1.30 pm	58.8	61.9	62.343	884	896
1.30-2 pm	61.9	64.3	64.918	868	874
2-2.30 pm	64.3	66.1	66.442	842	855

Time	η_i (Exp.)	η_i (Sim.)	η_t (Exp.)	η_t (Sim.)
9.30-10am	18.625	20.79	6.665	7.429
10-10.30 am	18.799	20.869	6.715	7.4561
10.30-11 am	16.982	19.456	6.06738	6.9512
11-11.30 am	14.885	16.874	5.318	6.02879
11.30-12 pm	13.288	14.715	4.7475	5.2574
12-12.30 pm	13.728	13.968	4.90477	4.9905
12.30- 1 pm	12.172	13.7165	4.3488	4.9139
1-1.30 pm	11.032	12.849	3.9415	4.59073
1.30-2 pm	8.69	11.149	3.1014	3.9833
2-2.30 pm	6.72	7.88	2.4009	2.8153

Table A.5 Experimental and simulated data for 0.05% alumina-water nanofluid as a working fluid at 50 LPH (19/4/2015)

Time	T_{in} (^oC)	T_{out}) (^oC). (Exp.)	T_{out} (^oc) (Sim.)	Exp. G_t (W/m^2)	Sim. G_t (W/m^2)
9.30-10am	28.7	33.1	33.58	800	793
10-10.30 am	32.9	37.4	37.803	825	809
10.30-11 am	37.1	41.3	42.071	843	850
11-11.30 am	41.2	45	45.369	869	872
11.30-12 pm	45	48.9	49.158	881	888
12-12.30 pm	48.9	53	53.118	903	912
12.30- 1 pm	53	56.6	57.216	898	908
1-1.30 pm	56.6	59.8	59.961	863	878
1.30-2 pm	59.8	62.1	62.522	842	836
2-2.30 pm	62.1	63.3	64.417	826	821

Time	η_i (Exp.)	η_i (Sim.)	η_t (Exp.)	η_t (Sim.)
9.30-10am	28.8000	32.3100	10.7100	11.6200
10-10.30 am	28.6400	31.8200	10.3000	11.4400
10.30-11 am	26.2840	30.8500	9.4500	11.0900
11-11.30 am	22.9600	25.1100	8.2580	9.0200
11.30-12 pm	23.2400	24.5900	8.3600	8.8540
12-12.30 pm	23.8400	24.2800	8.5760	8.7360
12.30- 1 pm	21.0540	24.3800	7.5720	8.7700
1-1.30 pm	19.4700	20.0900	7.0040	7.2200
1.30-2 pm	14.3400	17.1000	5.1590	6.1500
2-2.30 pm	7.6290	14.8200	2.7400	5.3300

Table A.6 Experimental and simulated data for 0.05% alumina-water nanofluid as a working fluid at 80 LPH (20/4/015)

Time	T_{in} (^oC)	T_{out}) (^oC). (Exp.)	T_{out} (^oc) (Sim.)	Exp. G_t (W/m^2)	Sim. G_t (W/m^2)
9.30-10am	26.8	31.6	30.83	810.57	788.053
10-10.30 am	31.4	36.1	35.44	852	807.336
10.30-11 am	36.1	39.9	40.2	846	828.421
11-11.30 am	39.9	44.2	44.053	868	874.06
11.30-12 pm	44.2	48.8	48.344	881	880.82
12-12.30 pm	48.8	52.8	53.012	898	910.15
12.30- 1 pm	52.8	56.6	57.01	907	914.36
1-1.30 pm	56.6	60.1	60.45	892	900.06
1.30-2 pm	60.45	62.85	63.95	873	864.56
2-2.30 pm	62.85	64.65	65.55	838	840.28

Time	η_i (Exp.)	η_i (Sim.)	η_t (Exp.)	η_t (Sim.)
9.30-10am	49.7	42.96	17.908	15.45
10-10.30 am	46.3	42.04	16.67	15.12
10.30-11 am	37.7	41.58	13.57	14.95
11-11.30 am	41.62	39.89	14.97	14.34
11.30-12 pm	43.8	39.49	15.77	14.2
12-12.30 pm	37.42	38.86	13.46	13.97
12.30- 1 pm	35.2	36.02	12.66	12.95
1-1.30 pm	32.968	35.94	11.85	12.92
1.30-2 pm	23.09	34.2	8.3	12.3
2-2.30 pm	18.04	26.99	6.49	9.71

APPENDIX C

Table A.7 Experimental and simulated data for 0.075% alumina-water nanofluid as a working fluid at 30 LPH (21/4/2015)

Time	T_{in} (^oC)	T_{out}) (^oC). (Exp.)	T_{out} (^{o}c) (Sim.)	Exp. G_t (W/m^2)	Sim. G_t (W/m^2)
9.30-10am	33.6	38.7	39.516	790	817
10-10.30 am	38.4	43.2	44.083	823	837
10.30-11 am	43.1	47.8	48.591	858	864
11-11.30 am	47.7	52.1	52.429	871	883
11.30-12 pm	52.1	56	56.518	899	916
12-12.30 pm	56	59.7	60.1999	919	939
12.30- 1 pm	59.7	63.1	63.9996	908	928
1-1.30 pm	63.1	66.1	66.9982	874	908
1.30-2 pm	66	68.5	69.1088	865	874
2-2.30 pm	68.5	70.4	70.6933	841	850

Time	η_i (Exp.)	η_i (Sim.)	η_t (Exp.)	η_t (Sim.)
9.30-10am	20.20239	22.66031	7.217972	8.096144
10-10.30 am	18.25161	21.2477	6.52099	7.591443
10.30-11 am	17.14235	19.88829	6.12467	7.105748
11-11.30 am	15.80863	16.75978	5.648155	5.987985
11.30-12 pm	13.57577	15.0935	4.850394	5.392651
12-12.30 pm	12.59928	13.99694	4.501511	5.000869
12.30- 1 pm	11.71798	14.49906	4.186636	5.180268
1-1.30 pm	10.74161	13.43501	3.837796	4.800101
1.30-2 pm	9.044479	11.13118	3.231439	3.976981
2-2.30 pm	7.069965	8.07493	2.525979	2.885036

Table A.8 Experimental and simulated data for 0.075% alumina-water nanofluid as a working fluid at 50 LPH (22/4/2015)

Time	T_{in} (^oC)	T_{out}) (^oC). (Exp.)	T_{out} (^{o}c) (Sim.)	Exp. G_t (W/m^2)	Sim. G_t (W/m^2)
9.30-10am	33.5	38.7	38.551	772	810
10-10.30 am	38.6	43.6	43.67	798	828
10.30-11 am	43.6	49	49.021	826	835
11-11.30 am	49.4	53.7	54.018	843	862
11.30-12 pm	53.7	58.6	58.43	897	918
12-12.30 pm	58.6	62.5	62.52	914	921
12.30- 1 pm	62.5	65.9	66.482	922	914
1-1.30 pm	65.9	68.8	69.383	872	902
1.30-2 pm	68.8	71.3	71.679	864	883
2-2.30 pm	71.3	73	73.793	851	864

Time	η_i (Exp.)	η_i (Sim.)	η_t (Exp.)	η_t (Sim.)
9.30-10am	34.97131	32.52376	12.49466	11.62019
10-10.30 am	32.67951	31.93641	11.67584	11.41034
10.30-11 am	34.09747	33.86113	12.18245	12.09801
11-11.30 am	26.60415	27.94185	9.505212	9.983149
11.30-12 pm	28.49129	26.87367	10.17946	9.601506
12-12.30 pm	22.25496	22.19908	7.951322	7.931354
12.30- 1 pm	19.23342	22.72289	6.871775	8.118503
1-1.30 pm	17.34563	20.13981	6.197299	7.195614
1.30-2 pm	15.09158	17.0055	5.391966	6.075778
2-2.30 pm	10.41904	15.04932	3.722548	5.376869

Table A.9 Experimental and simulated data for 0.075% alumina-water nanofluid as a working fluid at 80 LPH (23/4/2015)

Time	T_{in} (^oC)	T_{out}) (^oC). (Exp.)	T_{out} (^oc) (Sim.)	Exp. G_t (W/m^2)	Sim. G_t (W/m^2)
9.30-10am	33.1	38.8	39.758	798	831
10-10.30 am	38.7	44.5	45.377	823	854
10.30-11 am	44.6	49.8	50.61	848	866
11-11.30 am	49.8	54.6	55.53	889	882
11.30-12 pm	54.6	59.4	60.11	910	929
12-12.30 pm	59.4	63.5	64.533	946	956
12.30- 1 pm	63.5	67	68.138	937	931
1-1.30 pm	67	70.2	70.728	908	928
1.30-2 pm	70.2	72.8	73.133	879	912
2-2.30 pm	72.8	74.7	75.328	832	885

Time	η_i (Exp.)	η_i (Sim.)	η_t (Exp.)	η_t (Sim.)
9.30-10am	59.60742	66.86073	21.29672	23.88821
10-10.30 am	58.81072	65.2457	21.01208	23.31118
10.30-11 am	51.17241	57.91419	18.28304	20.69176
11-11.30 am	45.05758	54.21437	16.09831	19.36988
11.30-12 pm	44.01779	49.49533	15.72681	17.68385
12-12.30 pm	36.16772	44.80657	12.92211	16.00863
12.30- 1 pm	31.17144	41.57282	11.13703	14.85326
1-1.30 pm	29.40983	33.52404	10.50763	11.97757
1.30-2 pm	24.68385	26.83772	8.819121	9.588663
2-2.30 pm	19.05718	23.83758	6.808808	8.516764

APPENDIX D

Table A.10 Experimental and simulated data for 0.1% alumina-water nanofluid as a working fluid at 30 LPH (28/4/2015)

Time	T_{in} (^oC)	T_{out}) (^oC). (Exp.)	T_{out} (^{o}c) (Sim.)	Exp. G_t (W/m^2)	Sim. G_t (W/m^2)
9.30-10am	33.6	39.1	39.698	790	817
10-10.30 am	39	44	44.878	823	837
10.30-11 am	44	48.9	49.547	858	864
11-11.30 am	48.9	53.5	53.833	871	883
11.30-12 pm	53.5	57.6	57.875	899	916
12-12.30 pm	57.6	61.4	61.69989	919	939
12.30- 1 pm	61.4	64.7	65.295	908	928
1-1.30 pm	64.7	67.8	68.598	874	892
1.30-2 pm	67.8	70.4	71.298	865	874
2-2.30 pm	70.4	72.4	72.993	841	850

Time	η_i (Exp.)	η_i (Sim.)	η_t (Exp.)	η_t (Sim.)
9.30-10am	21.63416	23.19369	7.729518	8.286711
10-10.30 am	18.87881	21.8227	6.745079	7.796882
10.30-11 am	17.74652	19.95027	6.340531	7.127895
11-11.30 am	16.41134	17.3602	5.863494	6.202507
11.30-12 pm	14.17192	14.84181	5.063386	5.302729
12-12.30 pm	12.84909	13.56785	4.590764	4.847563
12.30- 1 pm	11.2936	13.04259	4.035013	4.659897
1-1.30 pm	11.02185	13.57942	3.937922	4.851699
1.30-2 pm	9.340317	12.43692	3.337137	4.4435
2-2.30 pm	7.389897	9.479556	2.640285	3.386885

Table A.11 Experimental and simulated data for 0.1% alumina-water nanofluid as a working fluid at 50 LPH (29/4/2015)

Time	T_{in} (^oC)	T_{out}) (^oC). (Exp.	T_{out} (^{o}c) (Sim.)	Exp. G_t (W/m^2)	Sim. G_t (W/m^2)
9.30-10am	36.8	42.3	42.937	812	823
10-10.30 am	42.2	47.5	48.123	835	851
10.30-11 am	47.5	53	53.385	863	872
11-11.30 am	53	57.7	57.688	895	905
11.30-12 pm	57.7	62.2	62.443	916	923
12-12.30 pm	62.1	65.9	66.713	931	941
12.30- 1 pm	65.9	69.5	69.725	922	933
1-1.30 pm	69.5	72.3	73.082	903	918
1.30-2 pm	72.3	74.8	75.183	874	886
2-2.30 pm	74.2	76.1	76.726	856	868

Time	η_i (Exp.)	η_i (Sim.)	η_t (Exp.)	η_t (Sim.)
9.30-10am	35.08002	38.61975	12.5335	13.79818
10-10.30 am	32.87325	36.04669	11.74505	12.87887
10.30-11 am	33.00693	34.9529	11.79282	12.48808
11-11.30 am	27.19744	26.82824	9.717185	9.585277
11.30-12 pm	25.44311	26.61366	9.090394	9.508611
12-12.30 pm	21.13913	25.38908	7.552654	9.07109
12.30- 1 pm	20.22203	21.23259	7.22499	7.586045
1-1.30 pm	16.05918	20.20859	5.737675	7.220189
1.30-2 pm	14.81432	16.85249	5.292907	6.02111
2-2.30 pm	11.49564	15.07186	4.107197	5.38492

Table A.12 Experimental and simulated data for 0.1% alumina-water nanofluid as a working fluid at 80 LPH (30/4/2015)

Time	T_{in} (^oC)	T_{out}) (^oC). (Exp.)	T_{out} (^oc) (Sim.)	Exp. G_t (W/m^2)	Sim. G_t (W/m^2)
9.30-10am	36.1	42.1	42.83	780	818
10-10.30 am	41.9	47.7	48.614	816	833
10.30-11 am	47.5	52.8	53.542	858	851
11-11.30 am	52.8	57.5	58.583	885	890
11.30-12 pm	57.2	61.6	62.586	911	918
12-12.30 pm	61.1	65.1	66.23	945	939
12.30- 1 pm	65.1	68.8	69.72	923	926
1-1.30 pm	68.8	72.2	72.63	916	908
1.30-2 pm	72.2	75	75.18	892	884
2-2.30 pm	75	77.1	77.63	869	873

Time	η_i (Exp.)	η_i (Sim.)	η_t (Exp.)	η_t (Sim.)
9.30-10am	63.7426	68.17652	22.77415	24.35832
10-10.30 am	58.89941	66.78969	21.04376	23.86283
10.30-11 am	51.18724	58.83344	18.28833	21.02019
11-11.30 am	44.0076	53.84387	15.72317	19.2375
11.30-12 pm	40.02279	48.61796	14.29947	17.37038
12-12.30 pm	35.07529	45.2715	12.53181	16.17474
12.30- 1 pm	33.21797	41.3432	11.86822	14.77123
1-1.30 pm	30.75789	34.95313	10.98927	12.48816
1.30-2 pm	26.01155	27.93425	9.293488	9.980437
2-2.30 pm	20.025	24.96402	7.154595	8.919223

APPENDIX E

Table A.13 Experimental and simulated data for 0.125% alumina-water nanofluid as a working fluid at 30 LPH (1/5/2015)

Time	T_{in} (^oC)	T_{out}) (^oC). (Exp.)	T_{out} (^{o}c) (Sim.)	Exp. G_t (W/m^2)	Sim. G_t (W/m^2)
9.30-10am	37.4	43.2	43.956	786	811
10-10.30 am	43.1	48.5	49.388	827	834
10.30-11 am	48.5	53.6	54.5877	853	868
11-11.30 am	53.6	58.3	59.173	877	889
11.30-12 pm	58.3	62.6	63.525	893	911
12-12.30 pm	62.6	66.5	67.181	926	931
12.30- 1 pm	66.5	70	70.465	903	915
1-1.30 pm	70	73.2	73.758	871	887
1.30-2 pm	73.2	76.1	76.472	854	865
2-2.30 pm	76.1	78.3	78.534	837	841

Time	η_i (Exp.)	η_i (Sim.)	η_t (Exp.)	η_t (Sim.)
9.30-10am	22.7684	24.9428	8.134766	8.911641
10-10.30 am	20.14723	23.26342	7.198265	8.311628
10.30-11 am	18.44796	21.64017	6.591143	7.731666
11-11.30 am	16.53581	19.34258	5.907964	6.910777
11.30-12 pm	14.85745	17.69681	5.308314	6.322772
12-12.30 pm	12.99513	15.18231	4.642942	5.424381
12.30- 1 pm	11.95935	13.37055	4.272872	4.777071
1-1.30 pm	11.33598	13.07255	4.050153	4.670601
1.30-2 pm	10.47773	11.67144	3.743516	4.170007
2-2.30 pm	8.110066	8.930005	2.897589	3.19054

Table A.14 Experimental and simulated data for 0.125% alumina-water nanofluid as a working fluid at 50 LPH (2/5/2015)

Time	T_{in} (^oC)	T_{out}) (^oC). (Exp.)	T_{out} (^{o}c) (Sim.)	Exp. G_t (W/m^2)	Sim. G_t (W/m^2)
9.30-10am	36.1	41.9	42.527	818	829
10-10.30 am	41.7	47.3	47.714	842	849
10.30-11 am	47.3	52.8	53.256	867	878
11-11.30 am	52.8	57.9	57.8435	891	902
11.30-12 pm	57.9	62.3	62.846	912	925
12-12.30 pm	62.3	66	66.753	926	949
12.30- 1 pm	66	69.8	70.089	909	930
1-1.30 pm	69.8	72.9	73.458	893	911
1.30-2 pm	72.9	75.6	75.878	871	882
2-2.30 pm	75.6	77.7	77.969	848	864

Time	η_i (Exp.)	η_i (Sim.)	η_t (Exp.)	η_t (Sim.)
9.30-10am	36.46285	39.86848	13.02756	14.24433
10-10.30 am	34.20202	36.42769	12.2198	13.015
10.30-11 am	32.62267	34.88478	11.65553	12.46374
11-11.30 am	29.43529	28.7542	10.51673	10.27339
11.30-12 pm	24.8104	27.49719	8.864335	9.824279
12-12.30 pm	20.54786	24.13028	7.341403	8.621341
12.30- 1 pm	21.49788	22.61049	7.680828	8.078347
1-1.30 pm	17.85197	20.6491	6.378206	7.377575
1.30-2 pm	15.94122	17.36329	5.695527	6.203609
2-2.30 pm	12.73501	14.10026	4.550004	5.037785

Table A.15Experimental and simulated data for 0.125% alumina-water nanofluid as a working fluid at 80 LPH (3/5/2015)

Time	T_{in} (^oC)	T_{out}) (^oC). (Exp.)	T_{out} (^{o}c) (Sim.)	Exp. G_t (W/m^2)	Sim. G_t (W/m^2)
9.30-10am	36.8	43	43.732	797	810
10-10.30 am	42.7	48.4	49.484	819	832
10.30-11 am	58.4	64.3	65.01	832	859
11-11.30 am	64.3	69.4	70.297	881	899
11.30-12 pm	69.4	74.1	74.696	934	928
12-12.30 pm	74.1	78.4	79.083	949	947
12.30- 1 pm	78.4	82.3	82.972	927	923
1-1.30 pm	82.3	85.6	86.153	901	910
1.30-2 pm	85.6	88.3	88.901	878	882
2-2.30 pm	88.3	90.5	91.173	856	861

Time	η_i (Exp.)	η_i (Sim.)	η_t (Exp.)	η_t (Sim.)
9.30-10am	64.00726	70.41569	22.86871	25.15833
10-10.30 am	57.26468	67.09009	20.4597	23.97015
10.30-11 am	58.34781	63.31464	20.84669	22.62125
11-11.30 am	47.63105	54.88709	17.01777	19.61023
11.30-12 pm	41.40443	46.95652	14.7931	16.77677
12-12.30 pm	37.28191	43.2949	13.32019	15.46854
12.30- 1 pm	34.61631	40.75683	12.36782	14.56173
1-1.30 pm	30.13596	34.83802	10.76707	12.44704
1.30-2 pm	25.3026	30.79448	9.04019	11.00235
2-2.30 pm	21.14681	27.45544	7.555396	9.809363

APPENDIX F

Table A.16 Experimental and simulated data for water –ethylene glycol mixture (60:40% by vol.) as a working fluid at 30 LPH (4/5/2015)

Time	T_{in} (^oC)	T_{out}) (^oC). (Exp.)	T_{out} (^{o}c) (Sim.)	Exp. G_t (W/m^2)	Sim. G_t (W/m^2)
9.30-10am	39.2	43.3	43.612	804	834
10-10.30 am	43.1	47.3	47.589	832	850
10.30-11 am	47.3	51.1	51.314	852	878
11-11.30 am	51.1	54.6	55.087	909	919
11.30-12 pm	54.6	57.7	58.273	931	942
12-12.30 pm	57.7	60.6	61.029	964	955
12.30- 1 pm	60.6	63.6	63.634	927	923
1-1.30 pm	63.6	66.2	66.476	901	898
1.30-2 pm	66.2	68.3	68.646	884	880
2-2.30 pm	68.3	70	70.313	860	865

Time	η_i (Exp.)	η_i (Sim.)	η_t (Exp.)	η_t (Sim.)
9.30-10am	14.99454	15.55517	5.357294	5.557598
10-10.30 am	14.84333	15.52873	5.303269	5.548153
10.30-11 am	13.11443	13.44275	4.685562	4.802867
11-11.30 am	11.32164	12.75663	4.045031	4.557728
11.30-12 pm	9.790779	11.46503	3.49808	4.096262
12-12.30 pm	8.845578	10.24981	3.160375	3.662083
12.30- 1 pm	9.515832	9.665385	3.399846	3.453278
1-1.30 pm	8.485038	9.417114	3.031561	3.364575
1.30-2 pm	6.985094	8.172286	2.495656	2.919819
2-2.30 pm	5.812403	6.842786	2.076673	2.444812

Table A.17 Experimental and simulated data for water –ethylene glycol mixture (60:40% by vol.) as a working fluid at 50 LPH (5/5/2015)

Time	T_{in} (^oC)	T_{out}) (^oC). (Exp.)	T_{out} (^{o}c) (Sim.)	Exp. G_t (W/m^2)	Sim. G_t (W/m^2)
9.30-10am	39.2	43.4	43.698	812	848
10-10.30 am	43.2	47.6	48.173	852	865
10.30-11 am	47.6	52.3	52.128	889	898
11-11.30 am	52.3	56.6	56.468	912	923
11.30-12 pm	56.6	60.2	60.473	931	941
12-12.30 pm	60.2	63.5	63.706	955	967
12.30- 1 pm	63.5	67.2	66.819	926	930
1-1.30 pm	67.2	70.1	70.214	908	919
1.30-2 pm	70.1	72.2	72.669	884	897
2-2.30 pm	72.2	73.7	74.206	867	875

Time	η_i (Exp.)	η_i (Sim.)	η_t (Exp.)	η_t (Sim.)
9.30-10am	27.15879	25.99427	9.703378	9.287312
10-10.30 am	25.30854	28.17451	9.042313	10.06628
10.30-11 am	25.90897	24.71065	9.256836	8.828696
11-11.30 am	23.10615	22.12993	8.255437	7.906649
11.30-12 pm	18.9499	20.17028	6.770477	7.206499
12-12.30 pm	16.9342	17.76804	6.050302	6.348219
12.30- 1 pm	19.58145	17.48954	6.996119	6.248716
1-1.30 pm	15.65187	16.07244	5.592147	5.74241
1.30-2 pm	11.64182	14.03543	4.159427	5.014621
2-2.30 pm	8.47864	11.2351	3.029274	4.014111

Table A.18 Experimental and simulated data for water –ethylene glycol mixture (60:40% by vol.) as a working fluid at 80 LPH (6/5/2015)

Time	T_{in} (^oC)	T_{out}) (^oC). (Exp.)	T_{out} (^{o}c) (Sim.)	Exp. G_t (W/m^2)	Sim. G_t (W/m^2)
9.30-10am	38.3	44	44.143	822	842
10-10.30 am	43.8	49.7	49.659	864	878
10.30-11 am	49.5	54.7	55.03	883	895
11-11.30 am	54.7	59.3	59.623	918	928
11.30-12 pm	59.3	64	64.176	934	946
12-12.30 pm	64	68.3	69.134	952	962
12.30- 1 pm	68.3	71.8	72.509	937	933
1-1.30 pm	71.8	74.9	75.412	911	920
1.30-2 pm	74.9	77.1	77.676	891	899
2-2.30 pm	77.1	78.7	79.21	856	868

Time	η_i (Exp.)	η_i (Sim.)	η_t (Exp.)	η_t (Sim.)
9.30-10am	49.7172	49.75393	17.76311	17.77624
10-10.30 am	48.96005	47.84456	17.4926	17.09405
10.30-11 am	42.22273	44.3002	15.08547	15.82771
11-11.30 am	35.92682	38.03518	12.83604	13.58933
11.30-12 pm	36.07901	36.95525	12.89042	13.20349
12-12.30 pm	32.38435	38.26348	11.57038	13.67089
12.30- 1 pm	26.78133	32.34453	9.568515	11.55615
1-1.30 pm	24.39759	28.14904	8.716846	10.05717
1.30-2 pm	17.70307	22.13927	6.325008	7.909988
2-2.30 pm	13.40139	17.42875	4.78809	6.226999

APPENDIX G

Table A.19 Experimental and simulated data for 0.05% alumina- water – ethylene glycol mixture (60:40% by vol.) nanofluid as a working fluid at 30 LPH (7/5/2015)

Time	T_{in} (^oC)	T_{out}) (^oC). (Exp.)	T_{out} (^oc) (Sim.)	Exp. G_t (W/m^2)	Sim. G_t (W/m^2)
9.30-10am	42.3	46.6	46.818	785	801
10-10.30 am	46.1	50.5	50.878	812	839
10.30-11 am	50.5	54.5	54.715	838	865
11-11.30 am	54.5	58	58.484	895	907
11.30-12 pm	58	61.7	61.672	924	932
12-12.30 pm	61.7	64.8	65.419	945	952
12.30- 1 pm	64.5	67.2	67.682	910	918
1-1.30 pm	67.2	69.5	69.995	884	899
1.30-2 pm	69.5	71.7	71.888	852	874
2-2.30 pm	71.6	73.5	73.716	833	852

Time	η_i (Exp.)	η_i (Sim.)	η_t (Exp.)	η_t (Sim.)
9.30-10am	15.30703	15.7618	5.468943	5.631425
10-10.30 am	15.14219	15.91389	5.41005	5.685763
10.30-11 am	13.33853	13.61514	4.765633	4.864459
11-11.30 am	10.92791	12.27451	3.904358	4.385475
11.30-12 pm	11.18979	11.01069	3.997922	3.933932
12-12.30 pm	9.16689	10.91645	3.275175	3.900262
12.30- 1 pm	8.291145	9.684594	2.962286	3.460141
1-1.30 pm	7.270558	8.687889	2.597647	3.104036
1.30-2 pm	7.215646	7.633827	2.578028	2.727437
2-2.30 pm	6.373834	6.938828	2.277263	2.479126

Table A.20 Experimental and simulated data for 0.05% alumina- H_2O-$C_2H_6O_2$ mixture (60:40% by vol.) nanofluid as a working fluid at 50 LPH (8/5/2015)

Time	T_{in} (^oC)	T_{out}) (^oC). (Exp.)	T_{out} (^oc) (Sim.)	Exp. G_t (W/m^2)	Sim. G_t (W/m^2)
9.30-10am	40	44.3	44.941	810	832
10-10.30 am	44.1	48.8	49.186	841	885
10.30-11 am	48.7	53.1	53.573	872	907
11-11.30 am	53.2	57.8	57.612	901	917
11.30-12 pm	57.8	61.4	61.783	923	932
12-12.30 pm	61.4	65.2	65.021	942	947
12.30- 1 pm	65.2	68.4	68.328	928	935
1-1.30 pm	68.4	70.8	71.152	895	914
1.30-2 pm	70.8	73	73.332	874	882
2-2.30 pm	73	74.9	75.286	848	873

Time	η_i (Exp.)	η_i (Sim.)	η_t (Exp.)	η_t (Sim.)
9.30-10am	27.59924	25.15348	9.860741	8.986914
10-10.30 am	26.02812	26.76218	9.299406	9.561674
10.30-11 am	23.5005	25.01944	8.396331	8.939022
11-11.30 am	23.77792	22.4055	8.49545	8.005105
11.30-12 pm	18.16526	19.90136	6.490141	7.11042
12-12.30 pm	18.7877	17.80602	6.712527	6.361791
12.30- 1 pm	16.0599	15.57914	5.737931	5.566164
1-1.30 pm	12.48904	14.02138	4.462123	5.0096
1.30-2 pm	11.72336	13.36853	4.188558	4.776348
2-2.30 pm	10.43515	12.19412	3.728302	4.356752

Table A.21 Experimental and simulated data for 0.05% alumina- water – ethylene glycol mixture (60:40% by vol.) nanofluid as a working fluid at 80 LPH (9/5/2015)

Time	T_{in} (^oC)	T_{out}) (^oC). (Exp.)	T_{out} (^{o}c) (Sim.)	Exp. G_t (W/m^2)	Sim. G_t (W/m^2)
9.30-10am	39.9	45.3	46.062	816	845
10-10.30 am	45.1	50.8	51.378	859	870
10.30-11 am	50.7	56.4	56.687	893	882
11-11.30 am	56.4	61.5	61.963	915	921
11.30-12 pm	61.5	66.1	66.591	928	938
12-12.30 pm	66.1	70.3	70.861	941	953
12.30- 1 pm	70.3	74.2	74.323	956	925
1-1.30 pm	74.2	77.3	77.655	932	911
1.30-2 pm	77.3	79.7	80.042	904	893
2-2.30 pm	79.7	81.5	82.042	875	869

Time	η_i (Exp.)	η_i (Sim.)	η_t (Exp.)	η_t (Sim.)
9.30-10am	53.86113	54.32236	19.24367	19.40846
10-10.30 am	49.43054	53.75461	17.66069	19.20561
10.30-11 am	47.54852	50.5655	16.98828	18.0662
11-11.30 am	41.52051	44.99488	14.83458	16.07591
11.30-12 pm	36.92525	40.43094	13.19277	14.44529
12-12.30 pm	33.24859	37.21508	11.87916	13.29632
12.30- 1 pm	30.38927	32.39828	10.85757	11.57536
1-1.30 pm	24.77761	28.25162	8.852621	10.09382
1.30-2 pm	19.77682	22.87334	7.065923	8.172258
2-2.30 pm	15.32421	20.07616	5.475081	7.172874

APPENDIX H

Table A.22 Experimental and simulated data for 0.075% Al_2O_3- H_2O –$C_2H_6O_2$ (60:40% by vol.) nanofluid as a working fluid at 30 LPH (10/5/2015)

Time	T_{in} (^oC)	T_{out}) (^oC). (Exp.)	T_{out} (^oc) (Sim.)	Exp. G_t (W/m^2)	Sim. G_t (W/m^2)
9.30-10am	33.6	38.7	39.516	790	817
10-10.30 am	38.4	43.2	44.083	823	837
10.30-11 am	43.1	47.8	48.591	858	864
11-11.30 am	47.7	52.1	52.429	871	883
11.30-12 pm	52.1	56	56.518	899	916
12-12.30 pm	56	59.7	60.1999	919	939
12.30- 1 pm	59.7	63.1	63.9996	908	928
1-1.30 pm	63.1	66.1	66.9982	874	908
1.30-2 pm	66	68.5	69.1088	865	874
2-2.30 pm	68.5	70.4	70.6933	841	850

Time	η_i (Exp.)	η_i (Sim.)	η_t (Exp.)	η_t (Sim.)
9.30-10am	20.20239	22.66031	7.217972	8.096144
10-10.30 am	18.25161	21.2477	6.52099	7.591443
10.30-11 am	17.14235	19.88829	6.12467	7.105748
11-11.30 am	15.80863	16.75978	5.648155	5.987985
11.30-12 pm	13.57577	15.0935	4.850394	5.392651
12-12.30 pm	12.59928	13.99694	4.501511	5.000869
12.30- 1 pm	11.71798	14.49906	4.186636	5.180268
1-1.30 pm	10.74161	13.43501	3.837796	4.800101
1.30-2 pm	9.044479	11.13118	3.231439	3.976981
2-2.30 pm	7.069965	8.07493	2.525979	2.885036

Table A.23 Experimental and simulated data for 0.075%Al_2O_3- H_2O –$C_2H_6O_2$ mixture (60:40% by vol.) nanofluid as a working fluid at 50 LPH (11/5/2015)

Time	T_{in} (^oC)	T_{out}) (^oC). (Exp.)	T_{out} (^oc) (Sim.)	Exp. G_t (W/m^2)	Sim. G_t (W/m^2)
9.30-10am	33.5	38.7	38.551	772	810
10-10.30 am	38.6	43.6	43.67	798	828
10.30-11 am	43.6	49	49.021	826	835
11-11.30 am	49.4	53.7	54.018	843	862
11.30-12 pm	53.7	58.6	58.43	897	918
12-12.30 pm	58.6	62.5	62.52	914	921
12.30- 1 pm	62.5	65.9	66.482	922	914
1-1.30 pm	65.9	68.8	69.383	872	902
1.30-2 pm	68.8	71.3	71.679	864	883
2-2.30 pm	71.3	73	73.793	851	864

Time	η_i (Exp.)	η_i (Sim.)	η_t (Exp.)	η_t (Sim.)
9.30-10am	34.97131	32.52376	12.49466	11.62019
10-10.30 am	32.67951	31.93641	11.67584	11.41034
10.30-11 am	34.09747	33.86113	12.18245	12.09801
11-11.30 am	26.60415	27.94185	9.505212	9.983149
11.30-12 pm	28.49129	26.87367	10.17946	9.601506
12-12.30 pm	22.25496	22.19908	7.951322	7.931354
12.30- 1 pm	19.23342	22.72289	6.871775	8.118503
1-1.30 pm	17.34563	20.13981	6.197299	7.195614
1.30-2 pm	15.09158	17.0055	5.391966	6.075778
2-2.30 pm	10.41904	15.04932	3.722548	5.376869

Table A.24 Experimental and simulated data for 0.075% alumina- water – ethylene glycol mixture (60:40% by vol.) nanofluid as a working fluid at 80 LPH

(12/5/2015)

Time	T_{in} (^oC)	T_{out}) (^oC). (Exp.)	T_{out} (^{o}c) (Sim.)	Exp. G_t (W/m^2)	Sim. G_t (W/m^2)
9.30-10am	33.1	38.8	39.758	798	831
10-10.30 am	38.7	44.5	45.377	823	854
10.30-11 am	44.6	49.8	50.61	848	866
11-11.30 am	49.8	54.6	55.53	889	882
11.30-12 pm	54.6	59.4	60.11	910	929
12-12.30 pm	59.4	63.5	64.533	946	956
12.30- 1 pm	63.5	67	68.138	937	931
1-1.30 pm	67	70.2	70.728	908	928
1.30-2 pm	70.2	72.8	73.133	879	912
2-2.30 pm	72.8	74.7	75.328	832	885

Time	η_i (Exp.)	η_i (Sim.)	η_t (Exp.)	η_t (Sim.)
9.30-10am	34.97131	32.52376	12.49466	11.62019
10-10.30 am	32.67951	31.93641	11.67584	11.41034
10.30-11 am	34.09747	33.86113	12.18245	12.09801
11-11.30 am	26.60415	27.94185	9.505212	9.983149
11.30-12 pm	28.49129	26.87367	10.17946	9.601506
12-12.30 pm	22.25496	22.19908	7.951322	7.931354
12.30- 1 pm	19.23342	22.72289	6.871775	8.118503
1-1.30 pm	17.34563	20.13981	6.197299	7.195614
1.30-2 pm	15.09158	17.0055	5.391966	6.075778
2-2.30 pm	10.41904	15.04932	3.722548	5.376869

APPENDIX I

Table A.25 Experimental and simulated data for 0.1% Al_2O_3- H_2O –$C_2H_6O_2$ mixture (60:40% by vol.) nanofluid as a working fluid at 30 LPH (13/5/2015)

Time	T_{in} (^oC)	T_{out}) (^oC). (Exp.)	T_{out} (^{o}c) (Sim.)	Exp. G_t (W/m^2)	Sim. G_t (W/m^2)
9.30-10am	42.7	47.5	47.934	806	818
10-10.30 am	47.2	51.7	52.218	839	841
10.30-11 am	51.7	56.4	56.535	856	872
11-11.30 am	56.4	60.5	60.779	893	901
11.30-12 pm	60.5	64.2	64.478	922	938
12-12.30 pm	64.2	67.6	67.908	943	952
12.30- 1 pm	67.6	70.7	70.829	912	924
1-1.30 pm	70.7	73.2	73.534	871	893
1.30-2 pm	73.2	75.5	75.878	852	864
2-2.30 pm	75.5	77.5	77.679	828	847

Time	η_i (Exp.)	η_i (Sim.)	η_t (Exp.)	η_t (Sim.)
9.30-10am	17.14016	18.41573	6.123889	6.57963
10-10.30 am	15.43687	17.17288	5.515332	6.135581
10.30-11 am	15.80275	15.95837	5.646056	5.701656
11-11.30 am	13.21421	13.9881	4.721212	4.997712
11.30-12 pm	11.54993	12.20592	4.126595	4.360969
12-12.30 pm	10.3771	11.21015	3.707561	4.005196
12.30- 1 pm	9.783078	10.05784	3.495328	3.593496
1-1.30 pm	8.26096	9.133915	2.951501	3.263393
1.30-2 pm	7.769568	8.920833	2.775935	3.187263
2-2.30 pm	6.951977	7.404273	2.483824	2.645421

Table A.26 Experimental and simulated data for 0.1% Al_2O_3- H_2O –$C_2H_6O_2$ (60:40% by vol.) nanofluid as a working fluid at 50 LPH (14/5/2015)

Time	T_{in} (^oC)	T_{out}) (^oC). (Exp.)	T_{out} (^{o}c) (Sim.)	Exp. G_t (W/m^2)	Sim. G_t (W/m^2)
9.30-10am	42.3	47.6	47.918	818	823
10-10.30 am	47.3	52.4	52.509	833	856
10.30-11 am	52.4	57	57.467	888	894
11-11.30 am	57	61.4	61.872	923	917
11.30-12 pm	61.4	65.5	65.636	949	939
12-12.30 pm	65.5	69.2	69.245	958	964
12.30- 1 pm	69.2	73.1	72.713	920	923
1-1.30 pm	73.1	76.3	76.192	907	902
1.30-2 pm	76.3	78.9	79.172	882	889
2-2.30 pm	78.9	81.2	81.462	856	865

Time	η_i (Exp.)	η_i (Sim.)	η_t (Exp.)	η_t (Sim.)
9.30-10am	31.07992	32.74457	11.10433	11.69908
10-10.30 am	29.36855	29.19026	10.49289	10.42919
10.30-11 am	24.84862	27.18759	8.87799	9.713666
11-11.30 am	22.86695	25.48562	8.169976	9.105582
11.30-12 pm	20.72407	21.63952	7.404358	7.731436
12-12.30 pm	18.52651	18.63512	6.619208	6.658012
12.30- 1 pm	20.33453	18.25718	7.265183	6.522983
1-1.30 pm	16.92388	16.44335	6.046617	5.874931
1.30-2 pm	14.14041	15.49673	5.05213	5.536719
2-2.30 pm	12.88877	14.20759	4.604939	5.076131

Table A.27 Experimental and simulated data for 0.1 Al_2O_3- H_2O –$C_2H_6O_2$ (60:40% by vol.) nanofluid as a working fluid at 80 LPH (15/5/2015)

Time	T_{in} (^oC)	T_{out}) (^oC). (Exp.)	T_{out} (^oc) (Sim.)	Exp. G_t (W/m^2)	Sim. G_t (W/m^2)
9.30-10am	41.9	47.7	47.898	818	838
10-10.30 am	47.6	53.5	53.619	853	863
10.30-11 am	53.5	59.1	59.629	884	889
11-11.30 am	59.1	64.4	64.863	928	916
11.30-12 pm	64.4	69.2	69.631	939	931
12-12.30 pm	69.2	73.6	73.951	954	948
12.30- 1 pm	73.6	77.3	77.61	926	925
1-1.30 pm	77.3	80.5	80.848	886	894
1.30-2 pm	80.5	83.1	83.699	861	877
2-2.30 pm	83.1	85.2	85.424	839	842

Time	η_i (Exp.)	η_i (Sim.)	η_t (Exp.)	η_t (Sim.)
9.30-10am	54.41909	54.93381	19.44302	19.62692
10-10.30 am	53.08594	53.52921	18.96671	19.12508
10.30-11 am	48.6197	52.91334	17.371	18.90504
11-11.30 am	43.83333	48.28703	15.66091	17.25214
11.30-12 pm	39.23306	43.12334	14.01731	15.40724
12-12.30 pm	35.39817	38.46396	12.64717	13.74252
12.30- 1 pm	30.66672	33.27208	10.9567	11.88755
1-1.30 pm	27.71997	30.45954	9.903877	10.88268
1.30-2 pm	23.17644	27.99574	8.28055	10.0024
2-2.30 pm	19.21029	21.18368	6.863511	7.568569

APPENDIX J

Table A.28 Experimental and simulated data for 0.125 Al_2O_3- H_2O –$C_2H_6O_2$ (60:40% by vol.) nanofluid as a working fluid at 30 LPH (16/5/2015)

Time	T_{in} (^oC)	T_{out}) (^oC). (Exp.)	T_{out} (^oc) (Sim.)	Exp. G_t (W/m^2)	Sim. G_t (W/m^2)
9.30-10am	42.5	47.7	47.964	812	829
10-10.30 am	47.6	52.4	52.878	841	859
10.30-11 am	52.4	57	57.472	862	883
11-11.30 am	57	61.3	61.762	887	909
11.30-12 pm	61.3	65.1	65.589	915	927
12-12.30 pm	65.1	68.8	68.719	937	948
12.30- 1 pm	68.8	72.2	72.399	908	914
1-1.30 pm	72.2	75.1	75.219	875	880
1.30-2 pm	75.1	77.6	77.888	859	868
2-2.30 pm	77.6	79.4	79.785	837	843

Time	η_i (Exp.)	η_i (Sim.)	η_t (Exp.)	η_t (Sim.)
9.30-10am	18.3316	18.86728	6.54957	6.740958
10-10.30 am	16.33798	17.58852	5.837282	6.28408
10.30-11 am	15.27579	16.44264	5.45778	5.874677
11-11.30 am	13.87707	14.99611	4.958043	5.357855
11.30-12 pm	11.88818	13.24431	4.247447	4.731968
12-12.30 pm	11.30356	10.92781	4.03857	3.904323
12.30- 1 pm	10.7188	11.27168	3.829645	4.027181
1-1.30 pm	9.487307	9.820497	3.389654	3.508698
1.30-2 pm	8.331052	9.194457	2.976544	3.285024
2-2.30 pm	6.156021	7.419539	2.199442	2.650876

Table A.29 Experimental and simulated data for 0.1 Al_2O_3- H_2O –$C_2H_6O_2$ (60:40% by vol.) nanofluid as a working fluid at 50 LPH (17/52015)

Time	T_{in} (^oC)	T_{out}) (^oC). (Exp.)	T_{out} (^oc) (Sim.)	Exp. G_t (W/m^2)	Sim. G_t (W/m^2)
9.30-10am	42.5	48	48.178	824	833
10-10.30 am	47.9	52.9	53.112	839	846
10.30-11 am	52.8	58.4	58.013	892	899
11-11.30 am	58.4	63.2	63.415	929	923
11.30-12 pm	63.2	67.6	68.063	942	949
12-12.30 pm	67.6	71.8	71.72	954	962
12.30- 1 pm	71.8	75.4	75.589	912	938
1-1.30 pm	75.4	78.5	78.714	903	922
1.30-2 pm	78.5	81.2	81.054	871	878
2-2.30 pm	81.1	83.4	83.239	867	861

Time	η_i (Exp.)	η_i (Sim.)	η_t (Exp.)	η_t (Sim.)
9.30-10am	31.84471	32.52012	11.37757	11.61889
10-10.30 am	30.13809	31.08426	10.76783	11.10588
10.30-11 am	29.95194	27.66494	10.70132	9.884215
11-11.30 am	24.65059	25.92215	8.807238	9.261544
11.30-12 pm	22.28453	24.4478	7.961886	8.734785
12-12.30 pm	21.00403	20.43261	7.504385	7.300226
12.30- 1 pm	18.83256	19.27185	6.728556	6.885507
1-1.30 pm	16.37856	17.14839	5.851782	6.126829
1.30-2 pm	14.78929	13.87804	5.283964	4.958388
2-2.30 pm	12.65641	11.85248	4.521921	4.234692

Table A.30 Experimental and simulated data for 0.125% alumina- water – ethylene glycol mixture (60:40% by vol.) nanofluid as a working fluid at 80 LPH

(18/5/2015)

Time	T_{in} (^oC)	T_{out}) (^oC). (Exp.)	T_{out} (^{o}c) (Sim.)	Exp. G_t (W/m^2)	Sim. G_t (W/m^2)
9.30-10am	41.3	47	47.335	802	832
10-10.30 am	46.9	52.8	53.051	844	867
10.30-11 am	52.8	58.6	58.801	881	894
11-11.30 am	58.6	64.2	64.474	923	911
11.30-12 pm	64.2	69.3	69.548	933	927
12-12.30 pm	69.3	74	74.283	957	944
12.30- 1 pm	74	78.1	78.613	932	920
1-1.30 pm	78.1	81.7	81.972	897	905
1.30-2 pm	81.7	84.4	84.898	875	881
2-2.30 pm	84.4	86.6	86.924	853	845

Time	η_i (Exp.)%	η_i (Sim.)%	η_t (Exp.)%	η_t (Sim.)%
9.30-10am	55.20461	55.37016	19.72367	19.78282
10-10.30 am	53.3619	54.15623	19.0653	19.34911
10.30-11 am	50.25437	51.23986	17.95504	18.30713
11-11.30 am	46.31355	49.21952	16.54705	17.5853
11.30-12 pm	41.72634	44.0386	14.90811	15.73425
12-12.30 pm	37.48933	40.29403	13.3943	14.39638
12.30- 1 pm	33.5807	38.2752	11.99781	13.67508
1-1.30 pm	30.63598	32.65943	10.94572	11.66866
1.30-2 pm	23.55469	27.70922	8.415693	9.900037
2-2.30 pm	19.68772	22.80103	7.034089	8.146422